Title of thesis	A parametric study on the effects of the variations in line width on the circuit model parameters of a planar spiral inductor on GaAs

I, SELMA ABDELBAGI IBRAHIM MOHMED,

hereby allow my thesis to be placed at the Information Resource Center (IRC) of

University Teknologi PETRONAS (UTP) with the following conditions:

1. The thesis becomes the property of UTP

2. The IRC of UTP may make copies of the thesis for academic purposes only.

3. This thesis is classified as

☐	Confidential
✓	Non-confidential

If this thesis is confidential, please state the reason:

_____

The content of the thesis will remain confidential for_____years.

Remarks on disclosure:

_____

Endorsed by

_____   _____

Signature of Author   Signature of Supervisor

Prof. Dr. Grant .A. Ellis

Electrical and Electronic Department

Univeristi Teknologi PETRONAS

Tronoh, Bandar Seri Iskandar

Perak-Malaysia

Date: _____   Date: _____

UNIVERSITI TEKNOLOGI PETRONAS

Approval by Supervisor (s)

The undersigned certify that they have read, and recommend to The postgraduate Studies programme for acceptance, a thesis entitled "**A parametric study on the effects of the variations in conductor line width on the circuit model parameters of a planar spiral inductor on GaAs**" submitted by (**SELMA ABD ELBAGI**) for the fulfillment of the requirements for the DEGREE OF MASTER OF SCIENCE IN ELECTRICAL AND ELECTRONIC ENGINEERING.

_____

Date

Main Supervisor   : …Prof. Grant Andrew Ellis………………

Signature   : ……………………………………………

Date   : ……………………………………………

Co- Supervisor   : ……………………………………………

Signature   : ……………………………………………

Date   : ……………………………………………

UNIVERSITI TEKNOLOGI PETRONAS

A parametric study on the effects of the variations in line width on the circuit model parameters of a planar spiral inductor on GaAs

By

Selma Abdelbagi

A THESIS

SUBMITTED TO THE POSTGRADUATE STUDIES PROGRAMME

AS A REQUIREMENT FOR THE

DEGREE OF MASTER OF SCIENCE IN

ELECTRICAL AND ELECTRONIC ENGINEERING PROGRAMME

BANDAR SERI ISKANDAR

PERAK

September -2009

DECLARATION

I hereby declare that the thesis is based on my original work except for quotations and citations which have been duly acknowledged. I also declare that it has not been previously or concurrently submitted for any other degree at UTP or other institutions.

Signature: _____

Name   :   <u>Selma Abdelbagi Ibrahim</u>_____

Date   :   _____

ACKNOWLEDGEMENT

DEDICATION

To my brother Mustafa

ABSTRACT

The increasing demands for low cost radio frequency integrated circuits (RFIC's) has generated great attention in on-chip passive components. A spiral inductor is an important passive component for many radio frequency circuits such as low noise amplifiers, mixers, switches, and voltage controlled oscillators. Considerable effort has gone into the design and modeling of the spiral inductor, however, very little research has investigated the effects due to the errors introduced into the spiral inductor modeling. This research investigates the effects of variations in conductor line width on equivalent circuit model of planar rectangular spiral inductors. A parametric study is performed where a full wave electromagnetic simulator, Sonnet ^{TM}, is used to simulate several sets of inductors on Gallium Arsenide (GaAs) substrate having different dimensions. The scattering parameters of a particular inductor were simulated over the desired frequency range. These simulated scattering parameters are used to extract the equivalent circuit model parameters using optimization process. The extracted inductor model parameters are validated through the existing physics based formulae. the simulation results reveals that variations in the conductor line width affect every parameters in the equivalent circuit model of the inductor i.e. the series inductance, the series resistance, the capacitance between the inductor turns. Change in series inductance due to the variations in the conductor line width is nearly a linear function of the nominal inductance. Variation in series resistance is an exponential function of nominal conductor width. Change in line to line capacitance due to variations in conductor line width is an exponential function of nominal spacing between conductors. Finally, variations in conductor line width have no or little effects on substrate capacitance.

Curve fitting techniques are utilized to extract simple equations useful for estimating the changes in the circuit model parameters with respect to the variation in conductor line width. These equations advantageous to the RFIC's designer since the inductor equivalent circuit model parameters can easily be modified to account for variations in conductor line width and also they can be used during circuit design optimization to explore inductor space.

ABSTRAK

Permintaan yang tinggi terhadap litar bersepadu berfrekuensi tinggi yang berkos rendah telah menjana perhatian yang mendalam terhadap komponen pasif "on chip". Induktor berbentuk lingkaran merupakan komponen pasif yang penting untuk kebanyakan litar frekuensi radio seperti "low-noise amplifier", "mixer", suis, dan juga "VCO". Pelbagai kajian telah dijalankan untuk merekabentuk dan membina model induktor berbentuk lingkaran, namun kurang penyelidikan yang dibuat terhadap berlakunya ralat semasa membina model induktor berbentuk lingkaran. Penyelidikan ini menyiasat kesan perbezaan-perbezaan dalam lebar garis konduktor pada model litar setaraf induktor berbentuk lingkaran bersatah segiempat tepat. Satu kajian berparameter dijalankan dengan menggunakan simulasi elektromagnetik gelombang lengkap, SONNET ^{TM} untuk mensimulasi beberapa set induktor pada substrat " (GaAs)" berlainan dimensi. "S-parameters" pada induktor tertentu disimulasikan pada julat frekuensi yang diinginkan. "S-parameter" ini akan digunakan untuk mengekstrak model litar setaraf dengan menggunakan proses pengoptimuman. Model induktor yang sudah diekstrak akan disahkan dengan formula berasaskan fizik. Hasil simulasi mendedahkan bahawa perbezaan-perbezaan dalam lebar garis konduktor mendatangkan kesan kepada model litar setaraf induktor seperti aruhan bersiri, rintangan bersiri, dan juga kapasitan diantara lingkaran induktor. Perubahan dalam aruhan bersiri disebabkan perbezaan lebar garis konduktor adalah hampir kepada fungsi linear aruhan nominal. Perbezaan dalam rintangan bersiri adalah satu fungsi eksponen kelebaran konduktor nominal. Perubahan sejajar dalam kapasitan disebabkan perbezaan dalam kelebaran garisan konduktor adalah satu fungsi eksponen jarak nominal diantara konduktor. Akhir sekali, perbezaan dalam kelebaran garisan konduktor tidak mempunyai kesan atau memberikan kesan yang kecil terhadap substrat kapasitan.Teknik penyuaian lengkung digunakan untuk mengekstrak persamaan-persamaan mudah yang boleh digunakan untuk menganggarkan perubahan yang berlaku pada parameter model litar terhadap perbezaan kelebaran garisan konduktor. Persamaan-persamaan ini amat menguntungkan kepada perekabentuk RFIC kerana parameter model litar setaraf induktor dengan mudah dapat diubah suai untuk menjelaskan perbezaan dalam kelebaran garisan konduktor dan juga ia boleh digunakan semasa pengoptimuman rekabentuk litar bagi meneroka ruang induktor.

TABLE OF CONTENT

LIST OF TABLES

LIST OF FIGURES

xvi

ABREVIATION

nH	Nano Hennery
μm	Micrometer
pF	Pico farad
w	Conductor line width
w_n	Nominal conductor line width
s	Spacing between the inductor turns
s_n	Nominal spacing between the inductor turns
t	Conductor thickness
n	Number of turns
h	Substrate height
ε_r	relative dielectric permittivity
L	Series Inductance
R	Series Resistance
C	Line to line Capacitance
C_G	Substrate capacitance

CHAPTER 1

INTRODUCTION

1.1 Background

A great deal of research has been conducted on planar spiral inductors and these research activities have been mostly directed towards spiral inductor design and inductor modeling using electro-magnetic field solvers and equivalent circuit models [1, 2, 3, 4]. One field that is important in this area is the investigation of the errors introduced to planar spiral inductor equivalent circuit models due to variations in inductor dimensions during its fabrication process. This project investigates the effects of variations in inductor line width on the equivalent circuit model of planar spiral inductors.

There are two ways to implement inductors. Firstly, bond wire or off chip inductors which are made by winding metal around a core and secondly, on-chip or on-die planar spiral inductors made of embedded metal track on a planar substrate [5]. According to its shape, the planar spiral inductor is classified as rectangular, square, circular, hexagonal, or octagonal [6].

The structure of a planar spiral inductor can be described using several dimensions such as the number of turns (n), the conductor line width (w), the spacing between turns (s), the total area covered which can be expressed using the inner diameter (d_i) and the outer diameter (d_o), conductor thickness (t) and substrate height (h) as shown

Figure 2-4. Once these variables are defined, the main characteristics of the spiral inductor can be uniquely determined at a given frequency [7].

The rapid development of wireless communications requires low cost, high frequency operation and low power dissipation circuits and these criteria can be met with the use of the spiral inductor. The spiral inductor is used in many radio frequency integrated circuits (RFICs), such as voltage controlled oscillators and low noise amplifiers, In voltage controlled oscillators the spiral inductor is used to achieve low phase noise in high Q tank circuits, while it used to match the input impedance and improve the gain capability in low noise amplifiers [8, 9, 10].

There are two major techniques for the spiral inductor characterization: Electromagnetic field solvers and analytical models, Field solvers provide the most accurate means for modeling spiral inductors; however, they consume a great deal of memory and processing time. Analytical models are not as accurate as field solvers but are fast and useful during the optimization of radio frequency circuit design [11].

Analytical models are further grouped into segmented and equivalent circuit model or compact models. Segmented models treat the inductor as several transmission line segments, with each segment modeled using a separate π circuit model. By contrast, the equivalent circuit model or compact models represents the spiral inductor by a single π circuit model. A π circuit model is a model that consists of series elements to model the inductance and resistance and shunt elements to model the substrate capacitance as shown in Figure 2-2 [5].

Modeling errors can be introduced to planar spiral inductors. These errors affect the inductor's key characteristics and consequently impact the overall design performance and circuit yields, the most common sources of modeling error are: coupling to a nearby structure on the same die, thermal coefficient of the expansion, errors in the model itself, and variations in geometry during the actual fabrication process. Processing and mask imperfections e.g. mask misalignment introduce variations in conductor line width [12]. Chemical mechanical polishing of the conductors can cause conductor thickness variations [11].

1.2 Problem statement

Variations in conductor geometry can be introduced during the processing of planar spiral inductors. Chemical-mechanical polishing of the conductor leads to conductor thickness variations because erosion and dishing can be introduced to the conductor during the processing [11]. The etching process can also have an impact on variations in conductor line width and these variations are affected by the etch rate control process and mask preparation [10]. The two most general conductor line width variations are over etching and under-etching of the inductor width. In over-etching, the resultant conductor line width is less than the desired width. In under-etching, the resultant conductor line width is greater than the desired width. Conductor line width variations also can be introduced due to resist thickness variations during GaAs MMIC processing [13].

Equivalent circuit or compact models are the most commonly used models for implementing inductors because of their simplicity and capability to be integrated into tools such as Cadence, Agilent ADS or Microwave Office. In addition, these models have sufficient accuracy at least up to the first parallel self-resonant frequency of the inductor, which is usually the frequency range of interest for most RF designs. These advantages of the equivalent circuit inductor model make them excellent for use in circuit design and optimization tools [14].

Variations in conductor line width affect each element in the equivalent circuit [11]. This can affect the inductor's key characteristics and consequently the overall circuit design performance and yield. The effects of variations in conductor line width on the equivalent circuit model parameters must be accounted for. Defining simple models to account for these variations is advantageous to the circuit designer as the nominal inductor model can be easily modified to account for these variations. This is especially helpful during circuit design optimization.

1.3 Objectives of study

1. To investigate the effects of variations in conductor line width on the equivalent circuit model parameters of the planar spiral inductor.

2. To extract the equivalent circuit model parameters of the rectangular spiral inductor using electromagnetic simulator Sonnet[TM] and Agilent Advanced Design System (ADS) simulator.

3. To identify simple models to account for the variations in the equivalent circuit model parameters of spiral inductor due to the variations in the conductor line width using curve fitting.

1.4   Scope of Study

To fulfill the objectives of this study, a parametric study is performed to investigate the variations in the inductor circuit model parameters due to the variations in the conductor line width. This parametric study is performed in five steps. Firstly, the electromagnetic (EM) simulator Sonnet[tm] is used to simulate the scattering parameters of several sets of inductors over the desired frequency range, roughly up the first self resonance frequency (SRF). After the SRF point, the inductor has a negative reactance value, thus behaves as a capacitor. Secondly, the Agilent Advanced Design System (ADS) [15] is used to fit the simulated S-parameter data to the equivalent circuit model and extract the model parameters values. The substrate parasitics for Gallium Arsenide are neglected due to its high resistivity, consequently, the circuit model considered doesn't account for these parasitics. The model parameters are extracted using random followed by gradient optimization. In the third step, the simulation results are validated using the existing physics-based models. In the fourth step of this study the extracted circuit model parameters are curve fitted to new empirical equations that vary with inductor parameters such as nominal conductor line width (w_n), nominal spacing between the conductors (S_n), number of turns (n) and conductor thickness (t). Finally the proposed empirical equations are validated through the existing models.

CHAPTER 2

LITERATURE REVIEW

2.1 Basic concepts of the inductor

An inductor is a passive electrical component that can store electrical energy in a magnetic field. The generation of this field is due to the current passing through the inductor loops. The inductor is made by winding an electrical conductor into a coil or spiral as shown in Figure 2-1.
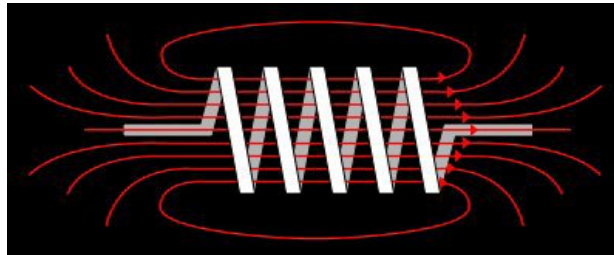
Figure 2- 1: Magnetic field in Conductor

The flow of the current through the inductor introduces a magnetic field and hence a magnetic flux. The ratio of the magnetic flux to the current is called the self inductance of the inductor. In the various inductor conductors, the magnetic flux lines interact with each other, this affects the inductance of each conductor. The mutual inductance is the change introduced to the isolated conductor's inductance when in proximity to another conductor. The inductance of a particular inductor consists of the self and the mutual inductance between all of its windings.

In theory an ideal inductor has inductance L which stores and releases magnetic energy but does not have capacitance. It does not dissipate any power and the phase of the time varying electrical current lags the phase of the voltage across its terminals by 90^0. In practice, a real inductor is equivalent to a combination of inductance, some

resistance due to the resistivity of the conductors, and some capacitance between its loops [16], This is modeled by a circuit consisting of series inductance connected in series to resistance and shunt capacitance [17] as shown in Figure 2 -2 [16].
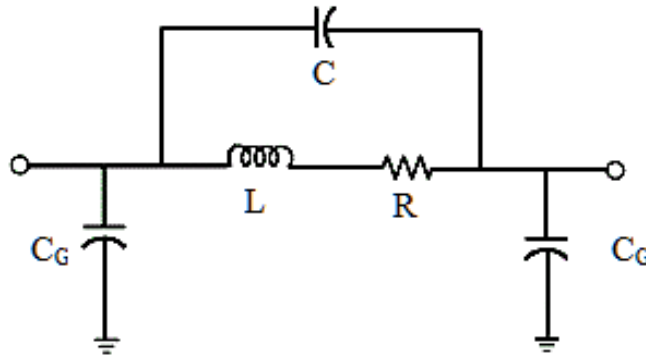
Figure 2- 2: Equivalent circuit model of spiral inductor

2.2 Methods of creating the inductor

The two main methods of creating inductors for wireless application are: rolling a conductor around a core, a ferrite or air, this type of inductors is called bond-wire inductors as shown in Figure 2-3a . The alternative method to create inductors is implementing one or more planar metal layer on a planar substrate [6]. This type is called Planar Spiral inductor as shown by Figure 2-3b [18]. There are at least six categories of planar spiral inductor based on its shape i.e. meander, rectangular or square, hexagonal, octagonal or circular [16].
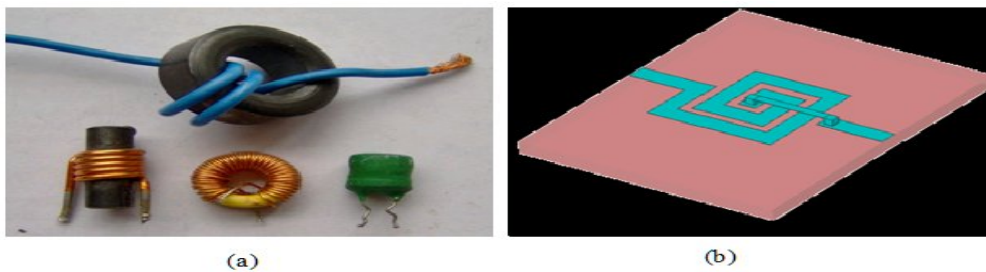
Figure 2- 3 (a): Bond wire inductors (b): Planar spiral inductors

A planar spiral inductor is vitally important for realization of the small inductance values required in wireless applications. Their inductance is well defined over a broad range of process variations. However, they have a limited quality factor [19]. By contrast, Bond wire inductors possess high quality factors and realize large values of inductance, however, their inductance values are sensitive to manufacturing

6

fluctuations. Additionally, they have a limited range of realizable inductances [1]. The quality factor of the spiral inductor can be improved using a lower conductivity substrate, wider, thicker and lower resistance metal conductor, a thicker and low permittivity and low-loss insulator layer between the substrate and the corresponding conductor [20].

2.3   Planar spiral inductor

The planar spiral inductor is an essential component for many circuit blocks such as low noise amplifiers and high dynamic range filters. The realization of voltage controlled oscillators is not feasible without the planar spiral inductor. Bond wire or off-chip inductors can be used, however, due to some restrictions there is   an upper limit on the frequency at which these components can be utilized [1]. The structure of an on chip spiral inductor is defined using several parameters e.g. the number of turns (n), the conductor line width (w), the spacing between conductors (s), total area covered which can be expressed using the inner diameter (d_i) and the outer diameter (d_o)   conductor thickness (t), and substrate height (h) [21] as shown in Figure 2-4 [22].Once these variables are defined the main characteristics of a particular spiral inductor are uniquely determined at a given frequency.
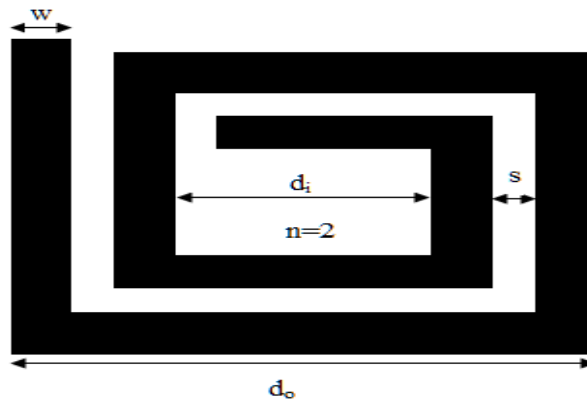
Figure 2- 4 : Spiral inductor dimensions

2.4   Characterization of planar spiral inductor

To characterize a spiral inductor, three parameters are considered. They are the quality factor (Q); inductance (L); and self resonant frequency (SRF). These

parameters determine the performance of a spiral inductor. Thus, they must be extracted accurately [23].

2.4.1 *Quality factor*

The quality factor or Q-factor is a figure of merit used to qualify the energy storage elements. The quality factor for the inductor can be defined in different ways based on the application for which the inductor is used. The most common definition is the criteria of an inductor's storage efficiency since it represents the ratio of the amount of energy stored to the amount of energy dissipated in a device as shown by the following equation [2].

$$Q = 2\pi \frac{E_{stored}}{E_{dissipated}} \qquad (2\text{-}1)$$

2.4.2 *Self- resonance frequency*

At a certain frequency, parallel resonance occurs due to the parasitic effects of the substrate and the distribution characteristic of metal tracks. At the Self resonance frequency the capacitive reactance equals but opposes the inductive reactance [23]. After the SRF point, the inductor has a negative reactance value, thus behaves as a capacitor. Usually, the inductors are required to operate at frequencies far below its SRF. Key performance goals of spiral inductors include high quality factor, high self-resonance frequency [23].

2.5 Operational properties of planar spiral inductor at high frequency

The performance of the spiral inductor at high frequency region is degraded by a variety of mechanisms: skin effect, proximity effect and the substrate losses [24].

2.5.1 *Skin effect*

The electric current is evenly distributed across the conductor at direct current (DC) and at low frequency. By contrast, the current distribution is uneven across the conductor at higher frequencies. Skin effect is the propensity of an alternating current (AC) to distribute itself within a conductor such that the current density near the surface of the conductor is greater than that at its core. In other words, the current has a great tendency to flow at the skin of the conductor [24, 25].

The skin depth is defined as the depth at which current density is 1/e or approximately 37% of the current density at the conductor's surface [26]. This is represented in the following equation [27].

$$\delta = \sqrt{\frac{2\rho}{\omega\mu}} \qquad (2\text{-}2)$$

Where δ is the skin depth in m, ρ is the bulk resistivity of the conductor in ohm-m, ω is the radian frequency of the signal in Hz, and μ is the permeability of the conductor. At low frequencies, the skin depth is comparable or greater than the thickness of the conductor, therefore the conductor resistance in this instance is the DC resistance. At higher frequencies, the skin depth can become significantly less than the conductor thickness, causing the effective resistance of the conductor to increase with the frequency, this degrades the quality factor of the inductor [28].

2.5.2 *Proximity effects*

The alternating current flows across a conductor form an associated alternating magnetic field. The alternating magnetic field induces eddy currents within adjacent conductors varying the overall distribution of current flowing through them. The resulting current crowding is termed the proximity effect. The proximity effects Resulting in resistance increases at a higher than linear rate and a function that is concave downward, as shown in Fig. 1 [29]. [William B. Kuhn].
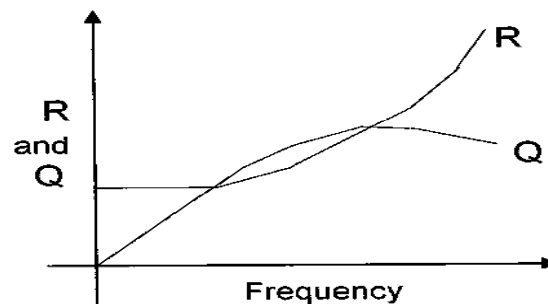
Figure 2- 5: General form of R and Q for spiral inductor

2.5.3 *Substrate parasitic effects*

The penetration of magnetic field into the substrate can induce a current in that substrate. This current affects the inductance and the resistance of the inductor, particularly in high conductive substrates e.g. CMOS. The capacitive coupling

between the spiral and substrate reduces the energy stored in the inductor [30]. As the frequency increases the substrate parasitic effects increase, thus the Q factor of the spiral inductor degrades. Substrate parasitic restricts the frequency range of operation by causing the inductor self-resonance. To minimize the Substrate parasitic a physical separation between the spiral and the substrate is increased by employing thick dielectric layers or removing the substrate underneath the spiral [20].

2.6   Planar spiral inductor on Gallium Arsenide technology

There are two main substrate technologies for implementing spiral inductors, Gallium Arsenide (GaAs) and Silicon (Si). Although the Silicon technology is full-grown and has lower cost compared to GaAs, the use of Gallium Arsenide so more popular than Silicon, because of superior electronic and physical properties of GaAs. Compared to Silicon, GaAs has higher electron mobility, higher saturated electron velocity and lower noise at high frequencies [31].

GaAs is a better insulator compare to Si, Consequently, substrate losses of GaAs are negligible and the inductor modeling becomes simpler. Also insulating properties of GaAs make the quality factor values of inductors fabricated using GaAs higher than Si based inductors, so GaAs based inductor are more suitable for high frequency applications than Si based inductors [16].

2.7   Planar spiral inductor modeling

Modeling is important for inductor design because it can assist to forecast the inductor performance without fabricating the inductor, so, an enormous amount of time and effort has been spent in developing and improving modeling techniques. Numerous tools have been developed to aid in the modeling of an inductor. A model that can accurately predict the behavior of inductors with different structural parameters over a broad frequency range would be a useful RF IC design tool. A measurement based approach has typically been used to characterize the spiral inductors, whereby, a large number of spirals are designed, fabricated, and measured. This is followed by an extraction procedure where the measured data is fitted to an equivalent circuit model. This approach doesn't allow predictive design because larger number of spirals is

characterized when only a small selection of the spirals can be used in practical designs [32]. The modeling schemes currently used to model spiral inductors includes full wave electromagnetic simulators, where Maxwell's equations are solved numerically, and compact circuit models [5].

2.7.1   *Field solver*

Field solvers or electromagnetic simulators are used to determine the network behavior of an inductor such as its 1- or 2-port S-parameters. By fitting these parameters to the inductor equivalent circuit model, the parameters of this circuit model can be extracted. Several field solvers have been introduced to model microstrip structures in multilayer dielectric, and they have been based on various methods such as Finite Elements (FE), Finite Difference Time Domain (FDTD) and Method of Moments (MoM) to solve numerically Maxwell's equations [23]. These techniques can vary extensively in how the electromagnetic interactions within an inductor are transformed into mathematical relations, and in the computational resources required to solve these relations. MoM does not require the meshing of the entire volume containing the structure, so, it is mostly employed for the modeling of planar geometries [4]. The method of moment significantly reduces the computational complexity of the model because it considers only the metal surfaces in formulating field quantities for solution. However, at the same time, MoM can fail to take into account some three-dimensional effects occurring within the conductors due to the limited modeling of the vertical dimension. This approach is usually called "2.5-dimension" simulation [33]. There are many electromagnetic simulators available such as Sonnet and Advanced Design System (ADS) [34, 35].

2.7.2   *Compact planar spiral Inductor Models*

A compact model is a mathematical description of an electrical component used by circuit designers to mimic the electrical device behavior [36]. The compact models for the inductor are extracted from measurement data and /or simulation data as well as physics based and imperial formulae. The main advantages of this model over EM solvers are in its model simplicity, rapid simulation analysis, and reasonable accuracy. The ability to quickly extract parameters using this model allows us to use them in circuits design optimization [14]. This model fails at higher frequencies. However, the models have an adequate precision up to the first self-resonant frequency of the spiral,

which is the frequency range of interest as it represents the region where the spiral acts as an inductor [37].

2.7.3 *The proposed compact models of planar spiral inductor on GaAs*

Al though many studies based on Silicon have been reported, the characteristics of inductors based on GaAs are still lacking [16]. Figure 2-5 shows a variety of compact models employed for GaAs inductors.

Figure 2-5a is the simplest inductor model. This model contains of series inductance L and resistance R of the inductor and doesn't account for the substrate effects. A frequently used model is shown in Figure 2-5b. An accurate model that accounts for substrate losses is shown in Figure 2-5c. While inclusive model for larger inductance value is shown in Figure 2-5d. In all of these models the series inductance is represented by L, R accounts for the total loss in the inductor, C is the line to line capacitance, R_{sb1} and R_{sb2} and $C_{G1 \text{ and }} C_{G2}$ represents the shunt resistance and capacitance between the metal trace and the substrate [16].
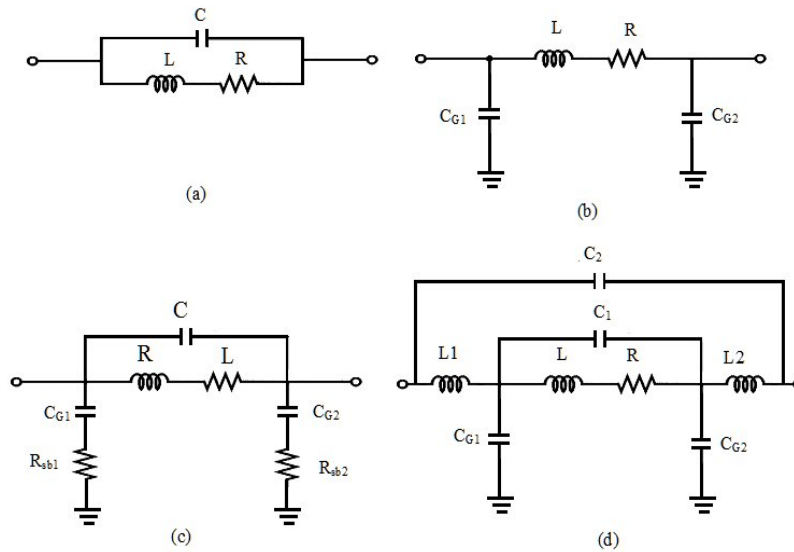
Figure 2- 6 : Proposed circuit models for inductor on GaAs technology [16].

2.7.4 *Proposed lumped element models for Silicon based spiral inductors*

The first compact model reported in the literature was introduced by Jan Crols. He introduced a lumped element model for planar inductors on Silicon for high frequency analog design, shown in Figure 2-6 [38].
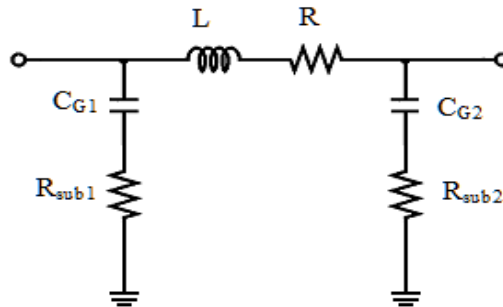
Figure 2- 7: Crols inductor model

In this model, L and R represent the inductance and the resistance of spiral metal, the capacitance C_{G1} and C_{G2} is relative to metal area. Analytical formulas were introduced to extract the model parameters. The skin effects are considered in R modeling. Another lumped element model for silicon planar inductor is reported by Yue [3] shown in Figure 2-7. Like the Crols model, the Yue model represents the inductance and resistance of the spiral with the inductance L connected in series to the resistance R. Yue models the capacitive coupling between the spiral and the air bridge by the parallel capacitance C. The oxide capacitance between the spiral and the silicon substrate is modeled by the capacitance C_{ox}, and resistance of the silicon substrate is modeled by R_{sb1} and R_{sb2} and capacitance between the spiral and the substrate is model by C_{G1} and C_{G2}. This model calculates the inductance based on the concepts of the self inductance of a conductor and the mutual inductance between a pair of conductors. Analytical formulae to calculate the series resistance are also introduced in this work. The effects of eddy currents i.e. the skin depth and the proximity effects are included in the resistance R.

13
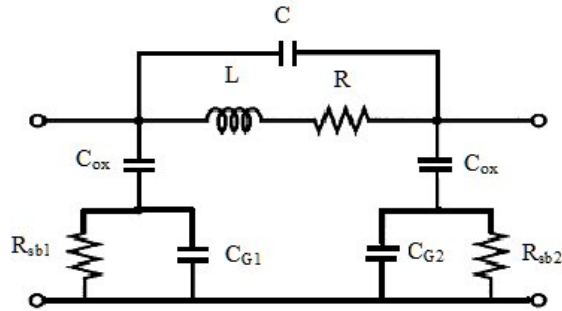
Figure 2- 8 : Yue inductor model

Another lumped element model for silicon planar inductor is reported in [39] and is given in Figure 2-8.
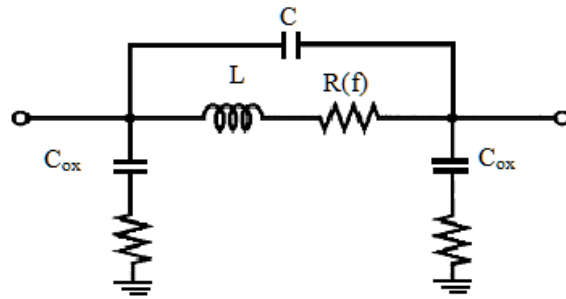
Figure 2- 9: Christensen inductor model

Christensen model is similar to Crols model except that the series resistance in Christensen model is a frequency dependent resistance R (f) whereas it is not in Crols model. Christensen proposed an empirical formula to estimate the frequency dependent resistance. CAE tools like Advanced Design System ADS, APLAC or Fast Henry in addition to empirical formulae were proposed to estimate the inductance L and the capacitance C_{ox}.

2.7.5 *Analytical expressions to calculate the inductance of spiral inductor*

Many expressions have been proposed to calculate the lumped model parameters of the spiral inductor. The following are some proposed analytical formulas for calculating the inductance of the spiral inductor.

2.7.5.1   Greenhouse's formula

Based on Grover formulas, Greenhouse proposed an expression to calculate the inductance of rectangular spiral inductor [40]. The Greenhouse method divides the inductor into straight segments and calculates the inductance by summing the self inductance of the individual segment and mutual inductance between any two parallel segments as follows:

$$L_t = L_s + M_+ - M_-$$

(2-3)

L_t is the total inductance of the spiral , L_s is the sum of the self inductance of all the straight spiral segments. M_+ is the sum of the positive mutual inductances and M_- is the sum of the negative mutual inductances. The self inductance for a straight segment is given by the following formula:

$$L_s = 0.002l \left[\ln(\frac{2l}{w+t}) + 0.50049 + \frac{w+t}{3l} \right]$$

(2-4)

L_s is given in microhenries, w and t are the rectangular dimensions of the cross section in cm, and l is the segment length in cm. The mutual inductance between any two parallel segments is calculated as:

$$M = 2lQ$$

(2-5)

Where M is the mutual inductance in nanohenries, l is the conductor length in centimeters, and Q is the mutual-inductance parameter, calculated from Equation (2-6).

$$Q = \ln \left[\frac{l}{GMD} + \sqrt{1 + \left(\frac{l}{GMD}\right)^2} \right] - \sqrt{1 + \left(\frac{l}{GMD}\right)^2} + \frac{l}{GMD}$$

(2-6)

In the Equation (2-6), l is the line length corresponding to the subscript of Q, and GMD is the geometric mean distance between the two conductors which is approximately equal to the distance d between the track centers. The exact value of the GMD can be calculated as:

$$\ln GMD = \ln d - \frac{w^2}{12d^2} + \frac{w^4}{60d^4} - \frac{w^6}{168d^6} + \frac{w^8}{360d^8} - \frac{w^{10}}{660d^{10}} + ... \qquad (2\text{-}7)$$

Although the above expressions seem simple, the real challenge is determining the L_S and M. As the number of segments increases, the calculation complexity is increased considerably. Another drawback of the model is its limitation to only square shaped inductors.

2.7.5.2 Jenei's expression

Jenei, et. *al* developed analytical models to extract the inductance of the spiral inductor, Their approach also divides the inductor into straight segments and calculate the inductance as the sum of self inductance, positive mutual inductance and negative mutual inductance [41]. The self inductance of a straight segment with length $L_{self,\,seg}$ is given by:

$$L_{self,seg} = \frac{\mu_0}{2\pi} l_{seg} \left[\ln(\frac{2l_{seg}}{w+t}) + 0.5 \right] \qquad (2\text{-}8)$$

Note the similarity with Equation (2-4).

μ_0 is the permeability of free space which is given by $4\pi \times 10^{-7}$ H/m, w and t is the segment width and thickness respectively. In this approach the length of the spiral for square inductor is estimated as follow: l_{total} is the average length of the spiral

$$\text{where } l_{ave} = \frac{l_{total}}{4n} \qquad (2\text{-}9)$$

$$\text{and } l_{total} = (4n+1)d_{in} + N_i(4N_i+1)(w+s) \qquad (2\text{-}10)$$

n is the number of turns, N_i is the integer part of n (i.e. If n =3.5, N_i = 3), d_{in} is the inner diameter of the inductor, and s is the spacing between turns. Considering the total spiral length the self inductance can also be estimated using the following equation:

$$L_{self} = \frac{\mu_0}{2\pi} l_{total} \left[\ln(\frac{l_{total}}{n(w+t)}) - 0.2 \right]$$

(2-11)

Negative mutual inductance arises from the anti-parallel segments i.e. the segments on the opposite side of the square. An average segments length is used in addition to an average distance to obtain the negative mutual inductance expression:

$$M_- = 4n^2 (\frac{\mu_0}{2\pi} \frac{l_{total}}{4n} 0.47)$$

(2-12)

The positive mutual inductance which is the third term of the total inductance arises from parallel segments i.e. the segments on the same side of the square. The average distance, d^+, between these segments is calculated using the following closed form

$$d^+ = (w+s) \frac{(3n - 2N_i - 1)(N_i + 1)}{3(2n - N_i - 1)}$$

The positive mutual inductance can be expressed as

$$M^+ = \frac{\mu_0}{2\pi} l_{total} (n-1)(\ln(\sqrt{1 + (\frac{l_{total}}{4nd^+})^2} + \frac{l_{total}}{4nd^+}) - \sqrt{1 + (\frac{4nd^+}{l_{total}})^2} +$$

$$\frac{4nd^+}{l_{total}})$$

(2-13)

Finally the total inductance can be calculated as the sum of self ,positive and negative inductances:

$$L = \frac{\mu_0}{2\pi} l_{total} (\ln(\frac{l_{total}}{n(w+t)}) - 0.2 - 0.47n + (n-1)(\ln(\sqrt{1 + (\frac{l_{total}}{4nd^+})^2} + \frac{l_{total}}{4nd^+}) -$$

$$\sqrt{1 + (\frac{4nd^+}{l_{total}})^2} + \frac{4nd^+}{l_{total}}))$$

(2-14)

2.7.6 *Empirical expressions to calculate the inductance of spiral inductor*

Empirical formulas are developed based on the measurements or simulation of a particular inductor layout. They offer a high degree of accuracy for inductors within the envelope for which the model was calibrated. However they are time consuming to develop due to the large number of inductors needed and they are only valid within the inductor sample set. The following is a discussion of some of the proposed empirical formulas to calculate the inductance of the spiral inductor.

2.7.6.1 The modified Wheeler formula

Mohan, et. *al* published a formula that accounts for the inductance of the spiral inductor having different geometries. This formula is a modified version of a formula proposed by Wheeler to calculate the inductance of radio coils [20]:

$$L = K_1 \mu_0 \frac{n^2 d_{avg}}{1 + K_2 \rho} \tag{2-15}$$

Where $\qquad\qquad\qquad\qquad \rho = (d_o - d_{in})/(d_o + d_{in})$

And $\qquad\qquad\qquad\qquad d_{avg} = 0.5(d_o - d_{in})$

K_1 and K_2 are numerical coefficients that are geometry dependent given in Table 2-1, μ_0 is the free space permeability and n is the number of turns, d_o the outer diameter, d_{in} is the inner diameter, d_{avg} is the average diameter and ρ is the fill ratio.

Table 2- 1: Coefficients for modified wheeler expression

Layout	K_1	K_2
square	2.34	2.75
Hexagonal	2.33	3.82
Octagonal	2.25	3.55

2.7.6.2 Current sheet expression

Mohan, et. *al* developed [20] another formula based on the current Sheet Approximation .In this method, inductance can be obtained by approximating the spirals by symmetrical current sheets of equivalent current densities. The concepts of

geometric mean distance (GMD), arithmetic mean distance (AMD), and arithmetic mean square distance (AMSD) are used to evaluate the self and the mutual inductances of the spiral. Their formula is given below:

$$L = \frac{\mu n^2 d_{avg} \, c_1}{2}\left(\ln\left(\frac{c_2}{\rho}\right) + c_3\rho + c_4\rho^2 \right)$$ (2-16)

where $\rho = (d_o - d_{in})/(d_o + d_{in})$

and $d_{avg} = 0.5(d_o - d_{in})$

Where C_1, C_2, C_3 and C_4 are layout dependent coefficients and are given in Table 2-2, d_{avg}, d_o and d_{in} is average, inner and outer diameter respectively.

Table 2- 2: Coefficients for current sheet expression

Layout	C_1	C_2	C_3	C_4
square	1.27	2.07	0.18	0.13
Hexagonal	1.09	2.23	0.00	0.17
Octagonal	1.07	2.29	0.00	0.19
Circular	1.00	2.46	0.00	0.20

2.7.6.3   Data Fitted Expression

The data fitted expression also developed by [20] is based on a data fitting technique:

$$L = \beta d_o^{\alpha_1} w^{\alpha_2} d_{avg}^{\alpha_3} n^{\alpha_4} s^{\alpha_5}$$ (2-17)

$$d_{avg} = 0.5(d_o - d_{in})$$

Where d_o is the outer diameter of the inductor, d_{avg} is the average diameter of the inductor, w is the inductor's trace width, s is the spacing between turns, n is the number of turns and $\beta, \alpha_1, \alpha_2, \alpha_3, \alpha_4$ and α_5 are fitting coefficients which are given in Table 2-3 for different layout types.

Table 2- 3: Coefficients for data-fitted expression.

Layout	β	$\alpha_1(d_o)$	$\alpha_2(w)$	$\alpha_3(d_{avg})$	$\alpha_4(n)$	$\alpha_5(s)$
Square	1.62×10^{-3}	-1.21	-0.147	2.40	1.78	-0.030
Hexagonal	1.28×10^{-3}	-1.24	-0.174	2.47	1.77	-0.049
Octagonal	1.33×10^{-3}	-1.21	-0.163	2.43	1.75	-0.049

2.7.6.4 H. Ronkanien's formula

In [42] a semi-empirical formula to calculate the inductance of rectangular inductor is introduced:

$$L = 1.5 \mu_0 N^2 D^{\frac{-3.7(N-1)(w+s)}{D}} \left(\frac{D}{w}\right)^{0.1} \qquad (2\text{-}18)$$

where μ_0 is the free space permeability, N the number of inductor turns, D the length of the side of the rectangular inductor, and s and w are the spacing and the width of the inductor traces, respectively.

2.7.6.5 Crols's expression

Crols proposed another empirical formula to estimate the inductance of rectangular and circular inductors [38].

$$L = K_L \frac{Ar^{\frac{3}{2}}}{w^2} \eta_{Ar}^{5/3} \eta_w^{\alpha} \qquad (2\text{-}19)$$

Where η_{Ar} is the ratio of wire area to total area, η_w is the ratio of wire width to turns pitch, A_r is the metal area, K_L is 1.3×10^{-7} H/m and $\alpha=114$ for square and $\alpha=117$ for circular inductor.

2.7.7 *Proposed expressions to calculate the resistance of a spiral inductor*

At low frequency, the skin depth, δ, is in the order of the conductor thickness, and the current distribution is almost uniform across the thickness of the conductor [43]. The AC resistance of the conductor per unit length can be calculated as given by Equation (2-20) [44].

$$R = R_{dc} = \frac{1}{\sigma w t} \qquad (2\text{-}20)$$

$$\text{where} \quad t \geq 2\delta$$

In Equation (2-20) σ is the metal conductivity, and w and t are the conductor line width and thickness, respectively. At high frequencies, however, when the skin depth is much smaller than the strip thickness ($t > 4\delta$), a nearly exponential penetration of the electric field distribution in the conductor can be observed. For microstrip conductors at high frequencies the effective thickness can then be approximated by [44].

$$t_{eff} = \delta(1 - e^{-t/\delta}) \tag{2-21}$$

$$\text{where} \quad \delta = \sqrt{\frac{2\rho}{\omega\mu}}$$

High frequency resistance of microstrip inductor can then be estimated as [39, 44]:

$$R_s = \frac{\rho.l}{wt_{eff}} \tag{2-22}$$

Based on Equation (2-22) resistance of a microstrip line does not decrease by increasing its thickness in excess of $5 \times$ skin depths [45] at high frequencies.

2.7.8 *Proposed expressions for the capacitance of a spiral inductor*

In general, there are essentially three equivalent capacitances in spiral planar inductor models, the line to line capacitance C between metal lines, the oxide capacitance C_{ox} associated with the oxide layer, and the coupling capacitance, C_{Si} associated with the Si substrate. Commonly, they are modeled using the parallel-plate capacitance concept as follows [46]:

$$C = nw^2 \frac{\varepsilon_{ox}}{t_{0xM_1 - M_2}} \tag{2-23}$$

$$C_{0x} = \frac{1}{2}l_T w \frac{\varepsilon_{0x}}{t_{0x}} \tag{2-24}$$

$$C_{si} = \frac{1}{2} l_T w C_{sub} \qquad\qquad (2\text{-}25)$$

where w is the line width, t_{ox} is the oxide thickness underneath the metal, l_T is the overall length of the inductor, n is number of crossovers between the two metal layers, $t_{0xm1\text{-}m2}$ is the thickness between the metal layers, C_{sub} is the capacitance of the substrate, t_{ox} is the oxide thickness between metal layer and substrate and ε_{ox} is the oxide Permittivity. The oxide capacitance is present in inductor fabricated using CMOS substrates. For this project, Gallium Arsenide substrate is assumed .Thus there is no oxide capacitance present. $C_{ox} = 0$. C_{Si} is also neglected.

2.8   Fabrication of planar spiral inductor

In monolithic microwave integrated circuit all components such as FETs, inductors, resistors and capacitors are fabricated on the same Gallium Arsenide substrate through the same process flow [13]. The first step of GaAs MMIC processing is growth of large crystals that are cut into high resistive wafers. This is followed by preparing a doped region to define the devices [31]. The devices are defined based on lithography process. This process is used to transfer patterns of geometric shapes on energy - sensitive chemical substances called resist covering the surface of the GaAs wafer [31]. The resist photo are applied to the wafer as thin film coatings and selectively exposed to energy patterns such as light and electrons. In GaAs MMIC processing, light is usually used and the lithography process called photolithography [13]. In the photolithography the light causes a chemical change in the exposed regions that alters the solubility of the photoresist film in a solution called a developer. When the exposed regions have become more soluble the resist is called a positive resist, in contrast, when the exposed region have become less soluble the resist is called a negative resist. Positive resist is preferred for most aspects of GaAs processing [13, 31]. The spinning procedure can coat a flat wafer to a highly uniform thickness, but substantial local variations in the thickness of the resist film can occur if the wafer have topographical feature such as metal patterns. Resist thickness variations can thus translate directly into line width variations. [13, 31]. There are different lithography techniques used for MMIC processing. Lithography based on etch process and lithography based on lift-off process, both of these techniques can be used in GaAs MMIC processing, but the technique that is usually used is the

lithography based on lift-off process [13, 31, 47]. Etching process consists of applying metal over the wafer, spinning resist over the metal, exposing and developing the resist to define the metal pattern, etching away all exposed metal and finally removing the left behind resist. Figure 2-9 shows the steps of etching process [47].

i.   Deposit metal and photoresist

ii.   Define features

iii.   Etch metal

iv.   Remove resist
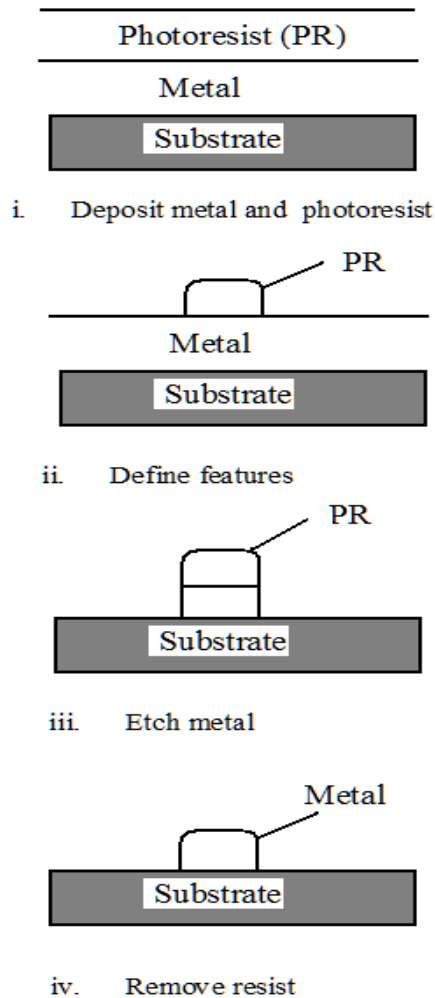
Figure 2- 10: Etching process [31].

In the lift-off process, first, resist is applied to the wafer, then exposed and developed to define the desired pattern. Second, the metal is applied to the wafer, usually by evaporation followed by application of a solvent to dissolve the resist. Finally the desired metal pattern is exposed [13]. Figure 2-10 shows the lift -off process.

Photoresist (PR)

Substrate

i.   Deposit photoresist

PR

Substrate

ii.   Define features in photoresist

Metal

PR

Substrate

iii.   Deposit metal

Metal

Substrate

iv.   Lift-off by removing photoresist
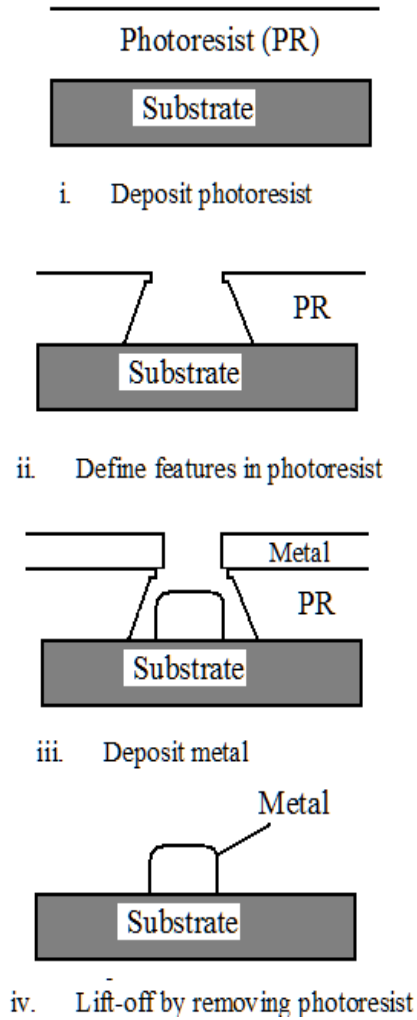
Figure 2- 11:lift-off process [31].

2.8.1   *Process variations*

Faster and denser circuits with increasing functionalities are produced due to the
advances in integrated circuit (IC) design. The continued down-scaling of the devices
and high level of integration of functional blocks into the system-on-a-chip (SoC),
have traditionally driven down the cost of these chips [48], however, the complexity
of design and manufacturing throughput has continued to increase. The integrated
circuit fabrication process has imperfections and fluctuations that result in ever-
growing systematic and random variations in the electrical parameters of fabricated
active and passive devices [49].

There are two primary sources of variations that can impact the electrical performance of an integrated circuit, firstly, environmental factors which include variations in power supply voltage and temperature. Second, physical factors which include variations in the electrical and physical parameter characterizing the behavior of active and passive devices. These variations are caused by processing and mask imperfection [50]. The impact of variability on circuit design is increasing as we scale technology further. During the spiral inductor fabrication, variation in conductor geometry can be introduced. Chemical-mechanical polishing can have a significant impact on conductor thickness by introducing erosion and dishing to the conductor as shown in Figure 2-11 [33].
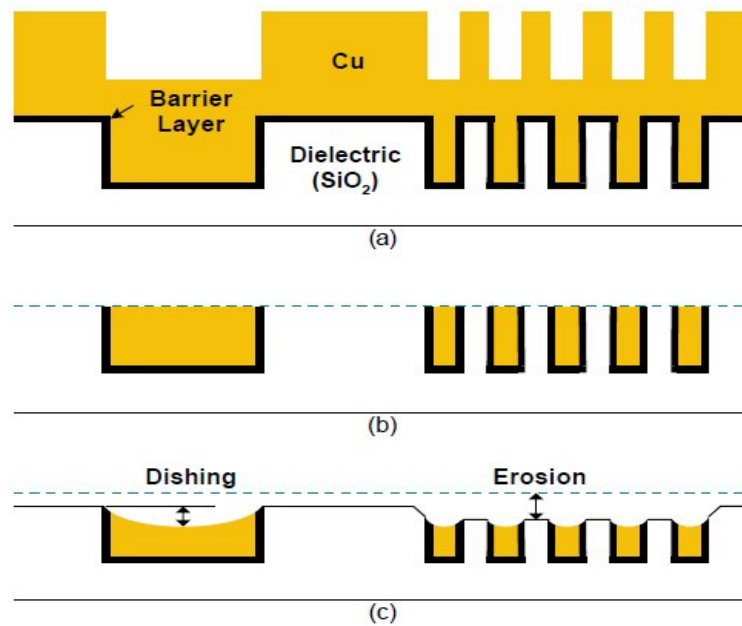
Figure 2- 12:cross sectional view of a single Cu interconnect layer (a) before polishing   (b) ideal case (after polishing) (c) actual case (after polishing) [10].

Line width can vary over a small range [33], especially for conductors having narrow line, line width variation is introduced due to photolithographic process and mask preparation [10]. Lithography based on etch process can introduce variations to the conductor line width due to etching process control. Conductor line width over etching occurs when the exposed metal sidewalls beneath the masking photoresist are chemically or reactively etched for a long enough period of time [33]. Consequently the resulting conductor line width is less than the required line width as shown in

Figure 2-12. Conductor under etch occurs when etching is for a shorter period of time, so, the resulting conductor line width is greater than the required width.
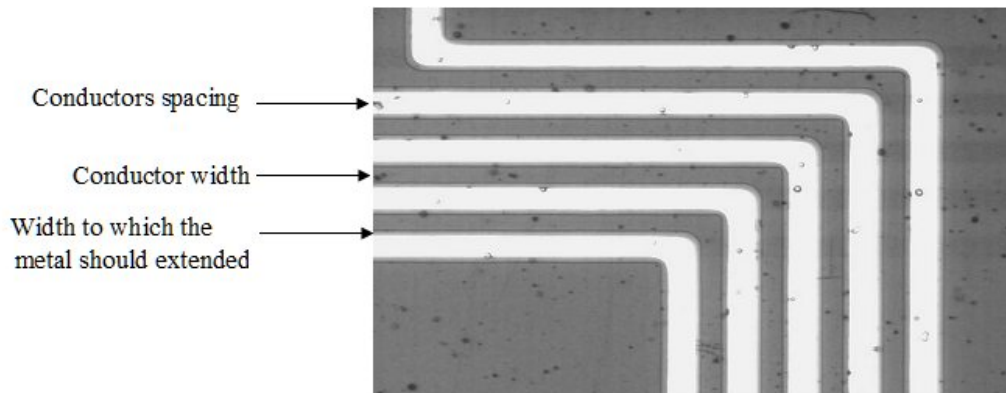
Figure 2- 13: Over etched conductor [33]

In Figure 2-12, the white lines are the metal traces of a spiral inductor, while the faint darker outlines show the width to which the metal should extend [33]. Conductor under etch means that etching occurred for a shorter period of time so the resulting line width is greater than the required width. Conductor line width variations can also be introduced due to resist thickness variations during lift- off process of the inductor metallization [13]. Stefan and Thomson reported that a track of 0.25mm width may be reduced to 75% in the worst case due to tolerances caused by the PCB manufacturing. [51].This variation in conductor width affects all characteristics of planar spiral inductor. C.K Liu, P.L. has conducted study to investigate the effects of geometric variation on the inductance for inductor fabricated on FR4 substrate. They developed a normalizing procedure is developed to relate the inductor structure, inductance and inductance tolerance to fabrication process precision [52]

CHAPTER 3

RESEARCH METHODOLOGY

3.1   Introduction

During the fabrication process of planar spiral inductors, the conductor line width can vary over a small range due to the photolithographic process [33]. Etching rate control and mask imperfections have significant impact on these variations [10]. Resist thickness variations during lift-off process of the inductor metallization can also introduce variations to conductor line width [33]. The variations in conductor line width affects the equivalent circuit model parameters of the inductor i.e. inductance, resistance and line to line capacitance .The goal of this research is to investigate how the inductor model parameters vary due to the changes introduced to conductor line width.

A parametric study is performed whereby a simulation process is used to extract the circuit model parameters of several sets of rectangular inductors on Gallium Arsenide (GaAs) substrate having different dimensions. The simulation results are validated by contrasting the extracted circuit model parameters to the existing physics based formulae. Curve fitting techniques are utilized to fit the extracted model parameters to equations useful for determining the variations in the inductor circuit model parameters with respect to the conductor line width variations.

3.2   Parametric study

This parametric study is performed in five steps. First, the electromagnetic (EM) solver Sonnet ^{tm} [34] is used to simulate the scattering parameters of a particular inductor over the desired frequency range. Second, Agilent Advanced Design System

(ADS) is used to fit the simulated S-parameter data to the equivalent circuit model of the inductor and extract the model parameters values i.e. series inductance (L), series resistance (R), line to line capacitance (C), and coupling capacitance between the substrate and the spiral (C_G). The substrate parasitics for Gallium Arsenide can be neglected due to it high resistivity, consequently, circuit model used doesn't account for these parasitics. The third step in this study is the simulation validation through the existing physics based formulae. Then the extracted model parameters are curve fitted, and finally the equations of these curves used to identify simple formulae to estimate the variations in the inductor model parameters due to the variations in the conductor line width. Figure 3-1 shows the process flow of this parametric study.
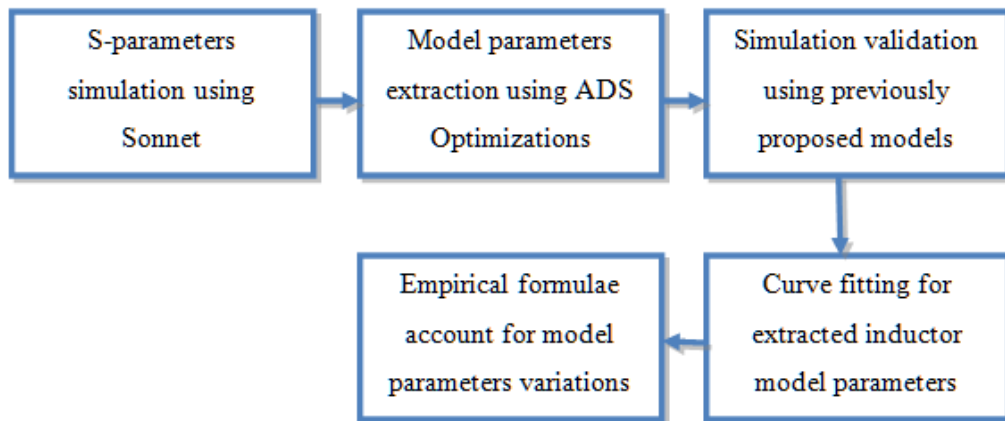
Figure 3- 1: The process flow of conducted parametric study.

3.2.1   *Sonnet* [tm]

Sonnet is an electromagnetic simulation package for design and analysis of planar microwave circuits. It is utilized to develop radio frequency models for the structures that consist of metal layers embedded in dielectric material i.e. Microstrip, strip line, and coplanar waveguide.

Sonnet uses an FFT -based method of moment analysis technique to solve Maxwell's equations for simulated structures. In this method, Sonnet first meshes the metal of a circuit into small subsections. It then takes one of these subsections and, ignoring all other subsections, calculates the voltage everywhere due to the current on that one subsection. Sonnet repeats this process for each subsection in turn. Then Sonnet places current on all subsections simultaneously and adjusts those currents such that the total voltage (due to current on all subsections) is zero everywhere that there is

conductor. This is called a "boundary condition". The current that gives us zero voltage across all conductors is the solution to the problem (for lossless metal). Not quite all subsection voltages are set to zero. There must be at least one voltage source, or excitation, to make current flow. A voltage source is created by setting the voltage on one or more subsections to 1.0 Volts. Such a subsection is called a 'port'. Metal loss is included by setting the voltage on each subsection (except ports), not to zero, but to a value proportional to the current flowing through it. The calculation of the voltage everywhere due to current on a given subsection is done by a 2-D Fast Fourier Transform (FFT). The current-to-voltage coupling for every possible pair of subsections is stored in an NxN matrix, where N is the number of subsections. The "adjustment" of the current on each subsection is done by a matrix inversion. By determining surface currents S-parameters can be calculated [53].

Many tools are used in this simulator to allow the user to insert, modify, supervise, and evaluate his /her circuit as shown by the Figure 3-2 [34].

Figure 3- 2 Sonnet ^{TM} task bar

3.2.2 *Agilent Advanced Design System (ADS)*

ADS is linear and nonlinear microwave circuit simulator. In addition to em simulations, ADS performs optimization which uses a set of parameters values to satisfy predetermined performance goals. Optimizers compare computed and desired responses and modify design parameter values to bring the computed response closer to that desired response over the entire desired frequency range. There are many optimizations available in ADS such as Random Optimizer, Gradient Optimizer, Random Minimax Optimizer, Gradient Minimax Optimizer and Quasi-Newton. The circuit type and the performance requirement decide which optimizer should be used. Each optimizer uses a different error-function (EF) and search methods in order to accomplish the required results. Random optimization or Monte Carlo uses random search method while the gradient optimizer uses gradient search method, however,

both random and gradient optimization use least squares error function [15]. This error function estimates the error for each optimized goal at each frequency point, then, squares the magnitude of these errors and averages the squared magnitudes over frequency [15].

The ith frequency dependent error contribution on specified "jth" frequency range e_{ij} (f) is calculated as follows:

$$e_{ij}(f) = (|R_{ij} - g_{ij}|^2)$$ (3-1)

Where R_{ij} is "ith" frequency dependent response that is being optimized over the "jth" Frequency range and g_{ij} is the "ith" goal value within the "jth" frequency range that is the optimization criterion corresponding to the R_{ij} response.

The total error function from response R_{ij} (f) over the set of frequencies Fj in the j_{th} range is then given by:

$$E_{ij} = W_{ij} \bullet \sum_{f \in F_j} e_{ij}(f)$$ (3-2)

where W_{ij} is weighting factor which is a measure of the significance of a particular goal comparing to other goals. The contribution from all responses within the frequency range E_j is expressed as follows:

$$E_j = \frac{\sum_i E_{ij}}{N_j}$$ (3-3)

where N_j is the number of frequencies in frequency range Fj. The final step in the error function calculation is to sum over all frequency ranges. [15]

$$E = \sum_j E_j$$ (3-4)

3.3 S-parameters simulation using Sonnet

The inductor simulated using Sonnet is drawn inside a rectangular box using the project editor. The side walls of this box are defined as perfect electrical conductor

PEC (lossless). The size of the box is 512 x 512 μm. The box is snapped into small cells with cell size 1x1 μm, the cell size is selected based on the wavelength of the circuit at highest frequency of analysis, therefore, cell size smaller than 1/20 of a wavelength is recommended. The wavelength of the circuit at the highest frequency (20 GHz) is 15 millimeters, the selected cell size is small comparing to 1/20 of a wavelength of the circuit because extremely high accuracy and smooth current density are required. Different dielectric layers are defined for the simulated structure. Top or first dielectric layer is set to be free space with thickness t of 100,000 μm, relative permittivity (ε_r) of 1.0, bulk conductivity (σ) of 0 S/m and loss tangent (δ) of 0. This layer is to simulate the open space above the inductor. The second dielectric layer is Silicon Nitride (Si_3N_4) with thickness of 5.0 μm, relative permittivity of 6.3, bulk conductivity, of 0 S/m and loss tangent of 0.This layer is passivation layer typically used in GaAs circuits. The third layer is the Gallium Arsenide (GaAs) with thickness of 100 μm, relative permittivity of 12.9, and bulk conductivity of 0 S/m and loss tangent of 0. The loss tangent for Gallium Arsenide is normally 10^{-4}, however, for this study tanδ for GaAs is assumed to zero for simplicity. These dielectric layers shown in Figure 3-3.
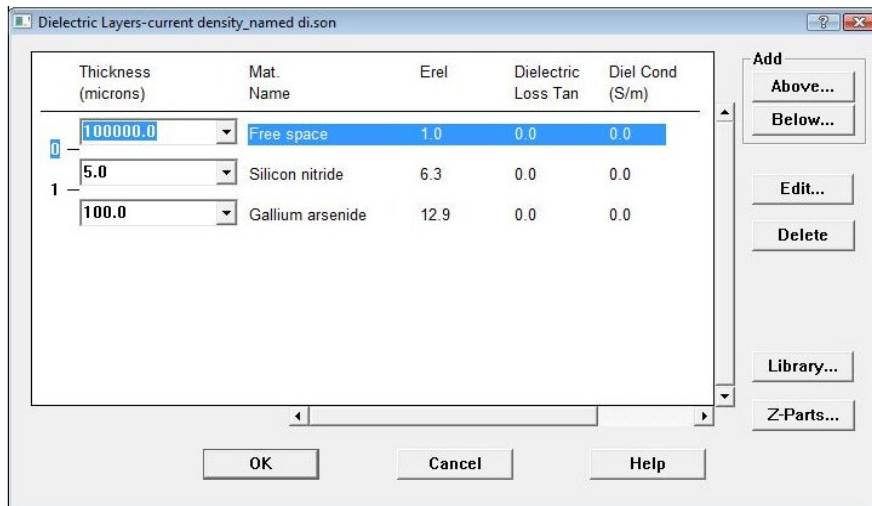
Figure 3- 3: Dielectric layers used for the simulated inductors [34].

The spiral metallization is placed at the top of the GaAs layer. An Air Bridge metallization is located at the top of the Silicon Nitride layer in order to connect the inner and outer lines of the inductor. Top vias were formed on the top of spiral

metallization through the Silicon Nitride layer to support the airbridge metal. Figure 3-4 shows a cross sectional view of the simulated structure.
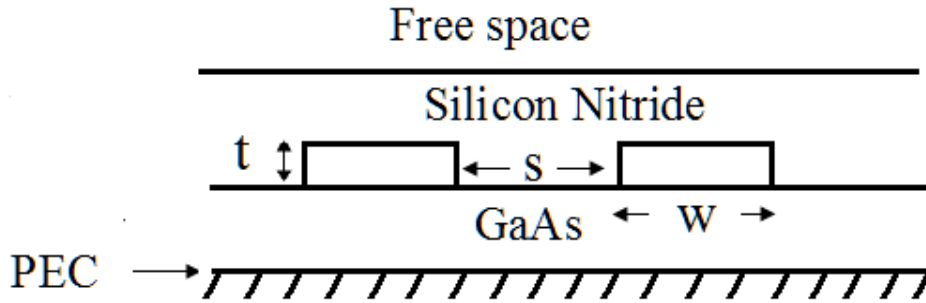
Figure 3- 4: Cross sectional of the simulated structure.

The metallization is defined to be gold with conductivity (σ) of 4 x 10^7s/m. The conductor losses are modeled assuming a thick metal model which allows accurate modeling of three dimensional (3D) characteristics of the metal conductors as well as the calculation the electromagnetic effects of conductor thickness. The thick metal model is also necessary for accurately simulating the capacitance effects between the adjacent conductors. The Sonnet thick metal model divides the conductor thickness into many infinitely thin sheets of metal having zero thickness in order to accurately represent the current distribution. The current flows between these sheets through the top or front vias located. Figure 3-5 shows thick metal model consisting of two metal sheets.
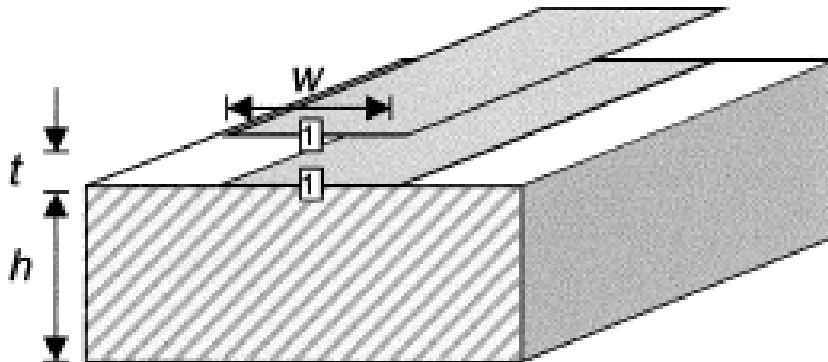
Figure 3- 5: Thick metal model consisting of two metal sheets [43].

In order to study the convergence behavior of the simulation results, the number of sheets per unit length and the cell size are varied, different numbers of sheets and cell

size were used until the simulation results converge as shown in Appendices E,F,G, and H. This test is used to determine the cell size and number of sheets per unit length for all the inductors simulated. See section 4.3.

To complete the circuit two ports were added, boxwall port is used. Figure 3-6 shows the simulated structure using Sonnet[tm].
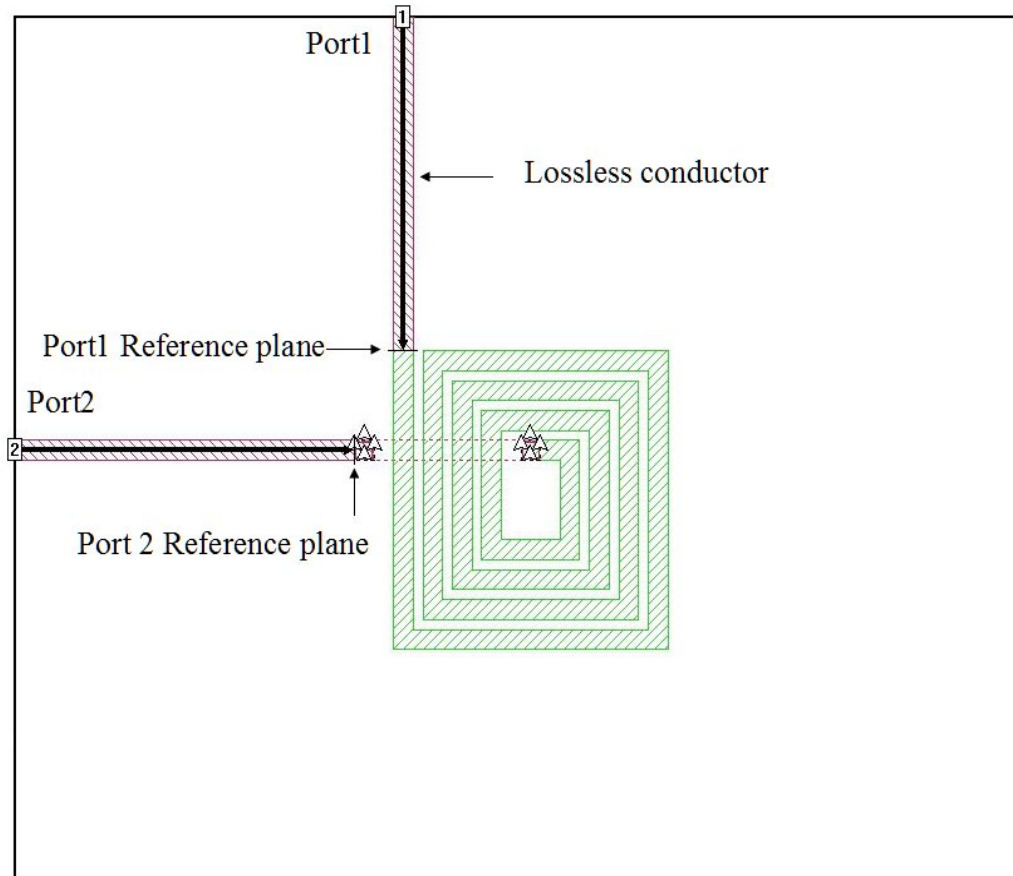
Figure 3- 6: The simulated inductor with boxwall ports [34]

To calculate the circuit response, Sonnet [tm] divides inductor metallization into small subsections based on the cell size of the box .This process is called metal fill .There are different fill types in Sonnet which are Staircase, Diagonal and Conformal. Staircase can be used for the simulated structure because it divides the metal area into rectangular subsections. Figure 3-7 shows the circuit sub sectioning for a two turn inductor. As can be observed from Figure 3-7, Sonnet places smaller subsections in the areas where the current density varies quickly, i.e. the conductor corners,

33

however, large subsections are placed in the areas where current density varies slowly.
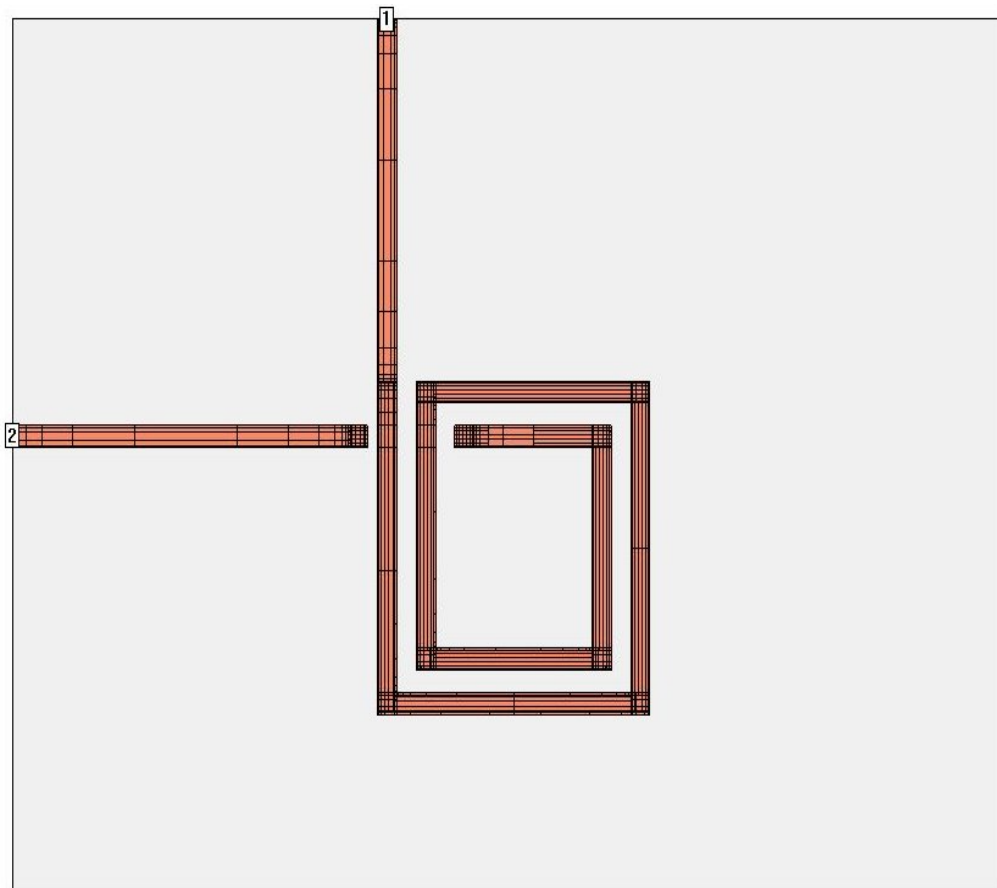
Figure 3- 7: Sonnet circuit subsectioning [34].

Many rectangular inductors are simulated to study the effects of the variations in the equivalent circuit model parameters due to the variations in the conductor line width of the spiral inductor. The simulated inductors were grouped into several sets, each set consists of five inductors. The first inductor of each set has nominal conductor line width (no conductor line width variations introduced), for the second and the third inductor in the set the nominal conductor line width is decreased by 1 μm and 2 μm, respectively. However, the nominal conductor line width is increased by 1 μm and 3 μm for the fourth and the fifth inductors in the set. Figure 3-8 shows the procedures of the inductor circuit model parameter extraction using Sonnet [tm] and Advanced Design System (ADS).
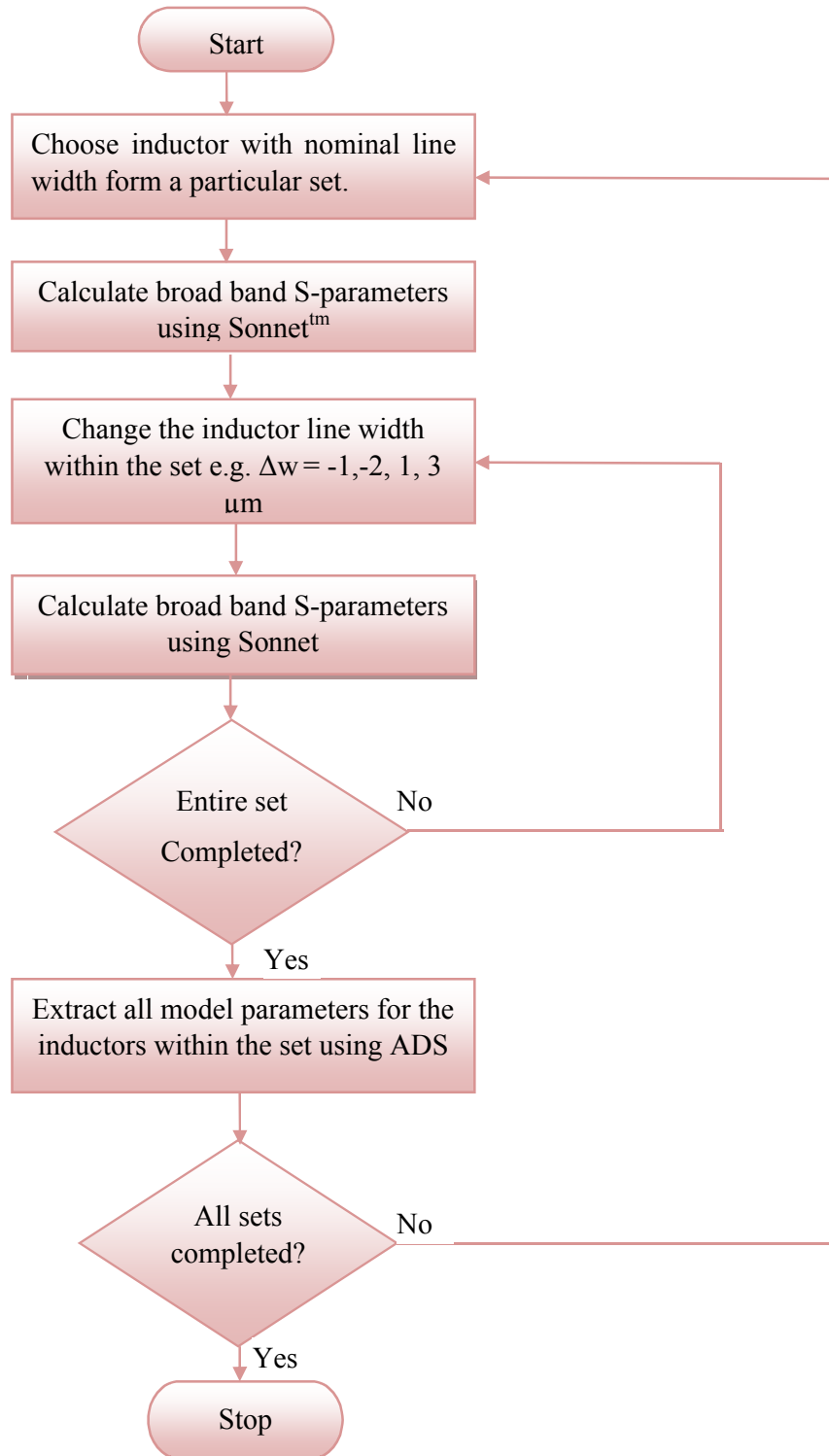
Figure 3- 8: Steps of model parameters extraction using Sonnet and ADS for simulated inductors sets.

Table 3-1 shows four main sets of inductor simulated. Additional sets of simulated inductors are given in the Appendix A.

Table 3- 1: Simulated rectangular inductors dimensions.

No. of turns (n)	Conductor Width (w μm)	Side1 Length (L1 μm)	Side2 Length (L2 μm)	Conductor thickness (t μm)	Spacing (S μm)	Width variations	Set .No
1	5	120	110	1	5	Nominal	
1	4	120	110	1	6	Δw= -1 μm	
1	3	120	110	1	7	Δw= -2 μm	Set1
1	6	120	110	1	4	Δw= +1 μm	
1	8	120	110	1	2	Δw= +3 μm	
2	5	120	110	1	5	Nominal	
2	4	120	110	1	6	Δw= -1 μm	
2	3	120	110	1	7	Δw= -2 μm	Set2
2	6	120	110	1	4	Δw= +1 μm	
2	8	120	110	1	2	Δw= +3 μm	
3	5	120	110	1	5	Nominal	
3	4	120	110	1	6	Δw= -1 μm	
3	3	120	110	1	7	Δw= -2 μm	Set3
3	6	120	110	1	4	Δw= +1 μm	
3	8	120	110	1	2	Δw= +3 μm	
4	5	120	110	1	5	Nominal	
4	4	120	110	1	6	Δw= -1 μm	
4	3	120	110	1	7	Δw= -2 μm	Set4
4	6	120	110	1	4	Δw= +1 μm	
4	8	120	110	1	2	Δw= +3 μm	

For each inductor the pitch is assumed to be constant i.e. if the nominal conductor line width is changed by a particular amount (Δw) the nominal spacing should change by the same amount. This is shown in Figure 3-9.

Each inductor was simulated using the Sonnet linear frequency sweep analysis for frequency range from 0.1 GHz to 20 GHz (roughly up to it is first resonant frequency) with steps of 2 GHz. While running electromagnetic simulations using Sonnet, Touchstone data files were generated that contain magnitude and phase angle of the scattering parameter data for each frequency. The CPU time for each inductor simulated is shown in Appendix A.
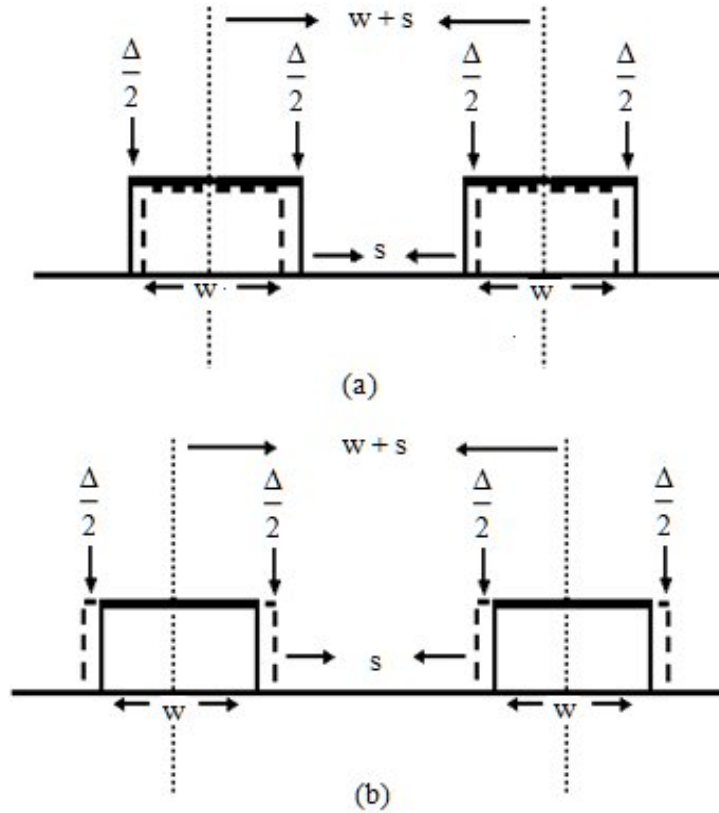
Figure 3- 9 a: over etched conductor line width, b: under etched conductor line width.

3.4 Model parameter extraction using ADS

After em simulation accomplished for a particular inductor, the touchstone file containing the S-parameter data for this inductor is used with ADS to extract the values of circuit model parameters. The model parameters were extracted using random optimization followed by gradient optimization. Sequencing Random optimization with gradient optimization achieves robust and fast solution. Random optimizer locates the solution space around local/global minimum then the gradient optimizer find solution with the global minimum i.e. the gradient optimizer can reach the solution fast. This in shown in Figure 3-10. Many optimization tools in ADS were used to perform model parameter extraction, the following is a brief introduction for these tools [ADS].
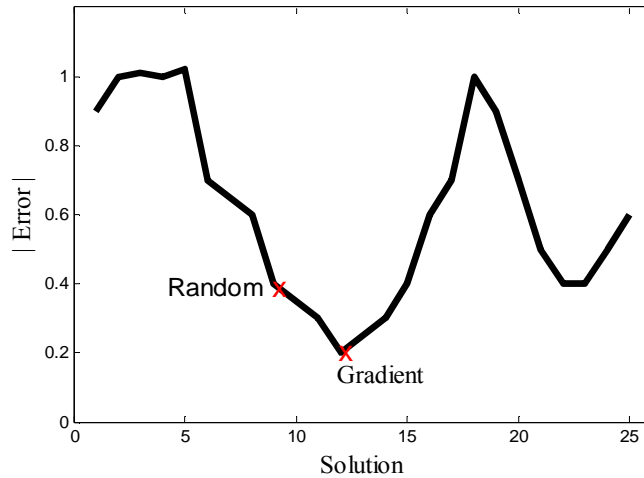
Figure 3- 10: How to find the solution using Random and Gradient optimization

Before applying random and gradient optimization, the following tools were first set up [15].

3.4.1 *Optimization variables*

The variables to be optimized are the inductor model parameters shown in Figure 3-11. L represents the total inductance of the inductor which is consists of the self inductance and the mutual inductance between the different turns. R is the resistance of inductor metal trace, C is the line to line capacitance which is the capacitance between the different inductor turns in addition to the capacitance between the air bridge and the spiral, and C_G represents the capacitance between the spiral and the substrate.
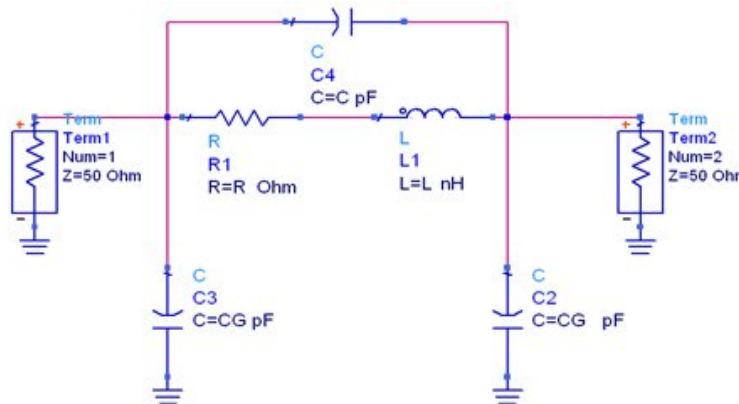
Figure 3- 11: Inductor model parameters [15].

3.4.2 *Data Access Component*

The data access component (DAC) is used to enable the optimizer to gain access to the simulated data (S-Parameters simulated using Sonnet.) by defining the file name and the file type. The DAC is shown by Figure 3-12.

Figure 3- 12: ADS Data Access Component [15].

3.4.3 *Simulation control component*

Different analysis types are available in ADS such as S-Parameter, AC, DC and Harmonic Balance. Each analysis has simulation control components. A fitting Simulation control component for this optimization is S-Parameter as shown by Figure 3-13.
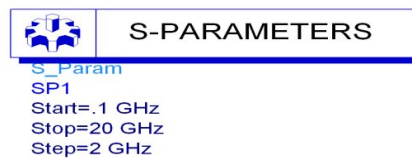
Figure 3- 13: ADS S-parameters control component [15]

3.4.4 *Optimization goals*

The goal of this optimization is to minimize the magnitudes of the differences between the simulated S-parameters using Sonnet and the model S-parameters shown in Figure 3-10. Four goal components were used. One goal for each S-parameter, these are shown in Figure 3-14. For each goal component, the goal expression (Expr)

was set to be the difference between the simulated and the modeled data referring to Measurement Equation (MeasEqn). The minimum goal magnitude (Min) and the maximum goal magnitude (Max) were set to zero.

GOAL
Goal
OptimGoal2
Expr="s22dp"
SimInstanceName="SP1"
Min=0
Max=0
Weight=1
RangeVar[1]=
RangeMin[1]=
RangeMax[1]=

GOAL
Goal
OptimGoal1
Expr="s11dp"
SimInstanceName="SP1"
Min=0
Max=0
Weight=1
RangeVar[1]=
RangeMin[1]=
RangeMax[1]=

GOAL
Goal
OptimGoal4
Expr="s12dp"
SimInstanceName="SP1"
Min=0
Max=0
Weight=1
RangeVar[1]=
RangeMin[1]=
RangeMax[1]=

GOAL
Goal
OptimGoal3
Expr="s21dp"
SimInstanceName="SP1"
Min=0
Max=0
Weight=1
RangeVar[1]=
RangeMin[1]=
RangeMax[1]=

Meas Eqn MeasEqn
s11_quo
s12dp = mag((Smeas(1,2) - Smodel(1,2))/Smeas(1,2))
s21dp = mag((Smeas(2,1) - Smodel(2,1))/Smeas(2,1))
s11dp = mag((Smeas(1,1) - Smodel(1,1)) /Smeas(1,1))
s22dp = mag((Smeas(2,2) - Smodel(2,2))/Smeas(2,2))

Figure 3- 14 ADS Optimization goals component [15]

3.4.5 *Nominal optimization component:*

One nominal optimization component (Optim) was used to define the optimization type (Optim Type), e.g. Random or Gradient, and the maximum number of iterations (maxIters). The Optim is shown in Figure 3-15.

OPTIM
Optim
Optim1
OptimType=Gradient
MaxIters=300
DesiredError=0.0

Figure 3- 15: ADS Nominal optimization component [15].

Subsequent to setting the nominal optimization tools, the optimization is accomplished over a frequency range of 0.1 GHz to 20 GHz and the model

parameters extracted for all simulated inductors. The variations in the inductance L, the resistance R and the capacitances C and C_G due to the variations in the conductor line width were investigated separately. The curve fitting for the extracted data is used to help to derive empirical formulae to estimate the amount of variations in the inductor model parameters due to introduced conductor line width variations.

CHAPTER 4

RESULTS AND DISCUSSION

4.1 Introduction

In this chapter, the results of electromagnetic simulation are presented and validated using comparison with existing models. The changes in the inductor model parameters i.e. series inductance L, series resistance R, substrate capacitance C_G, and line to line capacitance C, with respect to the variation in the conductor line width are individually investigated. Curve fitting is used to derive empirical equations to account for these changes.

4.2 ADS optimization results

The EM simulation results for Sonnet are stored on Touchstone format files. The Touchstone files contain S-parameter data for the inductors are used by ADS to extract the inductor model parameters. Model parameters extraction is performed using Random optimization followed by Gradient optimization. Figures 4-1 to 4-3 show the results of the ADS optimization process for inductor with n = 4 turns, w_n = 10 μm, s_n = 5 μm and t = 3 μm. Figure 4-1 shows S_{11} in Smith chart. Figure 4-2 and Figure 4-3 shows s_{11} in dB and s_{11} in phase respectively. From these Figures, ADS optimizations match the simulated data and the circuit model S-parameters very well. The rest of S-parameters for this inductor are shown in appendix B, C and D.

freq (100.0MHz to 20.00GHz)
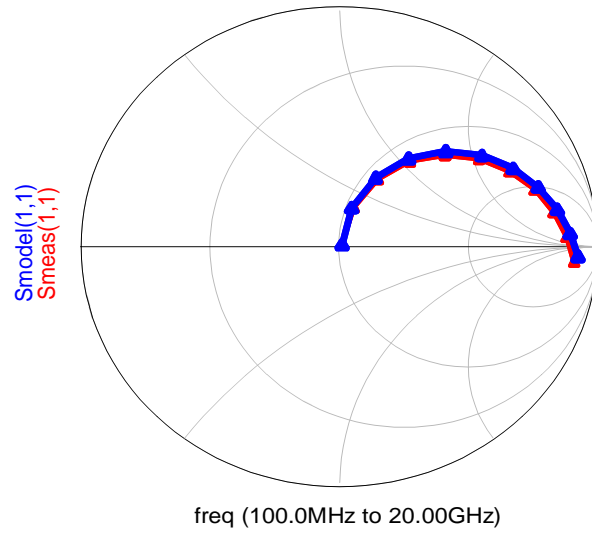
Figure 4- 1: s₁₁ in smith chart
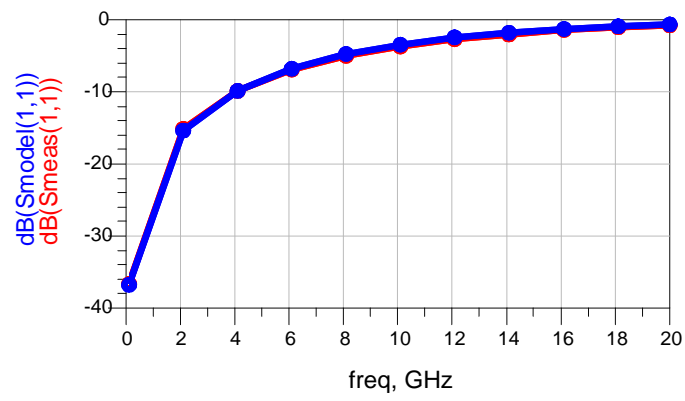
Figure 4- 2 : s₁₁ in dB
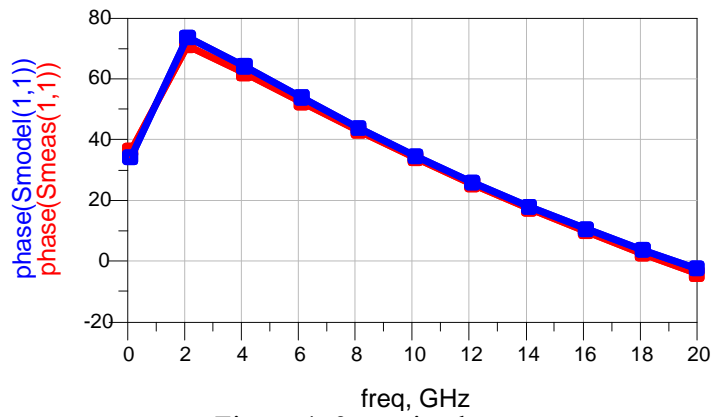
Figure 4- 3 : s₁₁ in phase

4.3   Convergence test for simulation results

The convergence behavior of the inductor model parameters extracted using electromagnetic simulation is investigated to study the effect of the grid size and the number of sheets on the accuracy of the simulation results. The convergence test is based on the ratio test proposed by [54,55]. To study the convergence of extracted inductance L, first consider a function L(x), with values L_1, L_2 and L_3 corresponding to the number of sheets or grid size of n_1, n_2 and n_3 respectively, with $n_1 > n_2 > n_3$. The convergence of L(x) can be qualified as follows:

$$R = \frac{b_2 L_2 - b_1 L_1}{b_3 L_3}$$

(4-1)

Where $b_1 = n_1^2(n_3^2 - n_2^2), \quad b_2 = n_2^2(n_3^2 - n_1^2), \quad b_3 = n_3^2(n_2^2 - n_1^2)$

For correct monotonic convergence $R = 1$, and the closeness of R to unity is a measurement of the actual convergence. L_1, L_2 and L_3 can also be used to predict the asymptotic value L_0 without attempting a very fine grid size or large number of sheets as follow:

$$L_0 = \sum_{r=1}^{3} L_r a_r$$

(4-2)

$$a_1 = \frac{n_1^4(n_3^2 - n_2^2)}{D}, \quad a_2 = \frac{n_2^4(n_1^2 - n_3^2)}{D}, \quad a_3 = \frac{n_3^4(n_2^2 - n_1^2)}{D}$$

$$D = n_1^2 n_2^2(n_2^2 - n_1^2) + n_2^2 n_3^2(n_3^2 - n_2^2) + n_3^2 n_1^2(n_1^2 - n_3^2)$$

The same convergence test and predicted asymptotic values are also carried out for extracted resistance and capacitance values. Tables 4-1, 4-2, 4 - 3 show extrapolated values   and   convergence test results for the extracted inductance, resistance and capacitance respectively calculated using Equations (4-1) and (4-2)   for inductor having n=3- turns , w_n =10 μm, s_n = 5 μm, t = 1μm . As shown by these Tables the

extracted inductor model parameters show a true monotonic convergence. The number of sheets and the grid size to be used for all simulated inductors are determined based on this test. For each of the inductor simulations a 1μm x 1 μm grid size and 4 sheets per skin depth at 20 GHz are found to be sufficient.

Table 4 - 1: Monotonic convergence Extrapolated values for inductance of 3-turns inductor with w=10 μm, s=5μm, t=1μm.

Grid size / number of sheets	2μm	1μm	0.5μm	Extrapolated value	Convergence test
4	1.32368	1.31953	1.32574	1.289492	0.98
8	1.32408	1.32016	1.33037	1.289762	0.98
12	1.32476	1.32449	1.33387	1.289025	0.99
Extrapolated value	1.32330	1.31974	1.32114	-	-
Convergence test	0.99	0.99	0.98	-	-

Table 4 - 2: Monotonic convergence Extrapolated values for resistance of 3-turns inductor with w=10 μm, s=5μm, t=1μm.

Grid size / number of sheets	2μm	1μm	0.5μm	Extrapolated value	Convergence test
4	3.00076	3.02644	3.03937	2.90889703	1.0
8	3.02086	3.09951	3.1187	2.90694644	0.99
12	3.0326	3.10553	3.13304	2.92088251	1.0
Extrapolated value	2.98066	2.95181	2.95867	-	-
Convergence test	0.98	1.01	1.01	-	-

Table 4 - 3: Monotonic convergence Extrapolated values for line to line capacitance of 3-turns inductor with w=10 μm, s=5μm, t=1μm.

Grid size / number of sheets	2μm	1μm	0.5μm	Extrapolated value	Convergence test
4	0.0103751	0.0107745	0.0107495	0.00992910	1.1
8	0.0103615	0.0107568	0.0107005	0.009916873	1.1
12	0.0103645	0.0105613	0.0106686	0.010004396	1.0
Extrapolated value	0.010389	0.010784	0.010798	-	-
Convergence test	0.99	1.0	1.0	-	-

The circuit model parameters are extracted for all the sets of inductors simulated as shown in Appendix E. The changes in these parameters due to variations in the conductor line width are individually investigated.

4.4 **Variation in inductance versus conductor width**

The electromagnetic simulation results show that the variations in the conductor line width of a planar spiral inductor affects its inductance. Figure 4-4 shows the electromagnetic simulation results for sets of inductors with n = 1 - 4 turns, w_n= 5 μm, S_n = 5 μm and t = 1 μm.
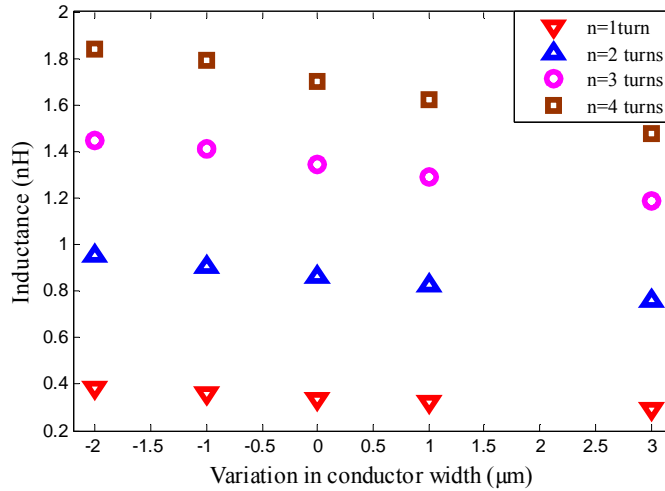
Figure 4- 4: Inductance versus the conductor line width extracted using EM simulation.

From Figure 4-4, the inductance values are shown to decrease nearly linearly with increasing the conductor line width i.e. the variation in the inductance is inversely proportional to the conductor line width. The simulation results show good agreement with Equation (2-14) [41]. Figure 4-5 shows inductance extracted from electromagnetic simulation and Equation (2-14) for sets of inductors having n = 1 - 4 turns, w_n = 5 μm, s_n = 5 μm and t = 1 μm. It can also be observed from Figure 4-5 that the inductance extracted using the electromagnetic simulation and Equation (2-14) vary roughly in the same manner versus the conductor line width. This becomes obvious by curve fitting the inductance extracted using these two methods to the following linear equation:

$$L = L_0 + a\Delta w \qquad\qquad (4-3)$$

where *L*, *L₀* and *Δw* are the inductance including the effects of the variations in the conductor line width, nominal inductance (no conductor line width variations introduced) and the amounts of the variations in the conductor line width respectively.
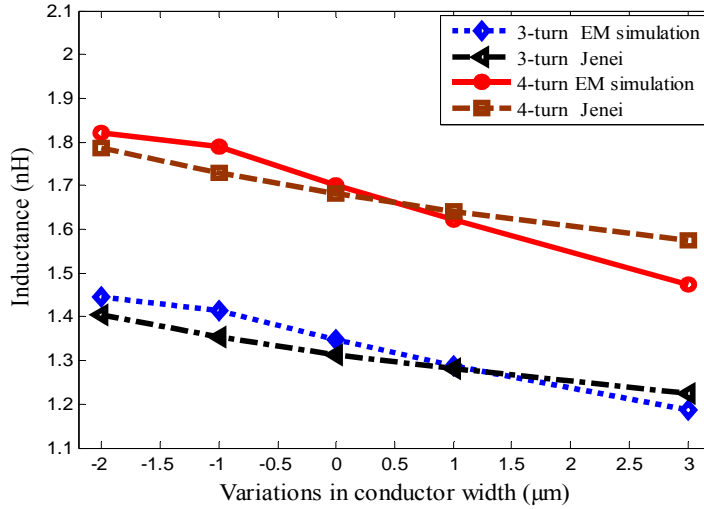
Figure 4- 5 : Inductance versus the conductor line width extracted using the EM simulation and the Jenei model.

Table 4 - 4 compares the coefficients of Equation (4-3) for inductance extracted using EM simulation and [41] for sets of inductors with n = 3 and 4 turns, w_n = 5 μm, s_n = 5 μm and t = 1 μm.

Table 4 - 4: coefficients of Equation(4-3) for inductance extracted using EM simulation and equation proposed by Jenei.

No of turns	EM Simulation		Equation proposed by Jenei	
	L_0	a	L_0	a
1turn	0.334	0.017	0.317	0.014
2turns	0.859	0.038	0.839	0.026
3turns	1.347	0.053	1.314	0.035
4turns	1.702	0.071	1.680	0.041

From Table 4-4 the inductance extracted versus the conductor width using EM simulation and [41] varies in the same manner suggesting that the simulation results follow a known physical model. The inductance extracted using EM simulations is greater than the inductance calculated using Equation (2-14) because Equation (2-14) doesn't take into account the effects of skin depth, the proximity effect and the effects of the inductor corners. These effects increase the resistance and consequently the change in the inductance as suggested by [56].

The change in the inductance due to the variation in the conductor line width for inductors with different dimensions is investigated by varying only one of the dimensions while keeping the others fixed. This allows the investigation of the dependency of the change in the inductance with respect to the conductor line width on each inductor dimension and also to identify new empirical formula to account for the change in the inductance with respect to the conductor line width.

4.4.1 *Effects of Variation in number of turns*

The change in the inductance due to the variation in the conductor line width for sets of inductors having different numbers of turns and fixed conductor width, conductor spacing and conductor thickness is first investigated. This is performed to study the dependency of this change on the number of turns. Figure 4-6 shows the inductance versus the variations in the conductor line width for sets of inductors having different n = 1 - 4 turns and fixed w_n = 5 μm, s_n = 5 μm and t = 3 μm. Figure 4-6, also shows the curve fit using least squares for the simulated inductance. A linear type fit is used with the Equation (4-3).
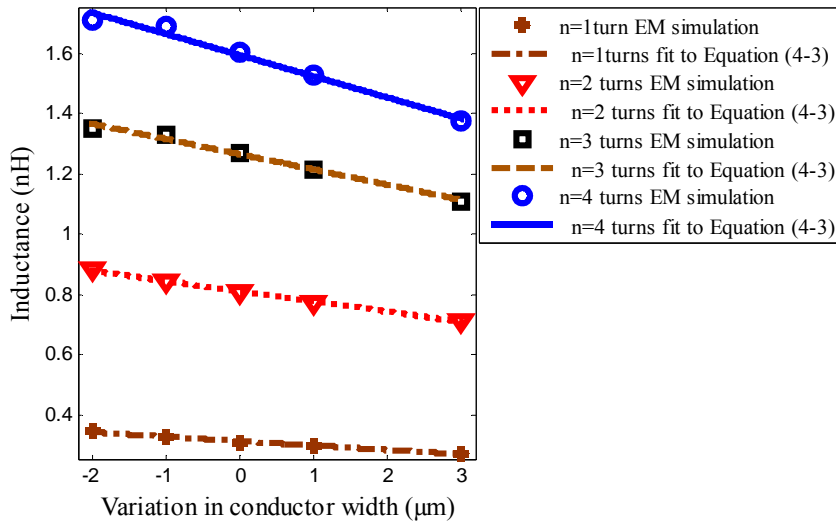
Figure 4- 6: inductance versus conductor line width for inductors having different n and fixed w_n, t and s_n.

Table 4-5 shows the coefficients extracted from Equation (4-3) for the inductance versus the variation in the conductor line width shown in Figure 4-6.

Table 4 - 5: Coefficients of Equation (4-3) for inductors having n = 1- 4 turns, w_n = 5 μm, s_n = 5 μm and t = 3 μm

inductors Set	R-square	Equation coefficients		Nominal inductance (nH) from EM simulation
		L_0 (nH)	a	
n =1turn	0.98	0.3149	-0.01459	0.35
n=2turns	0.99	0.8123	-0.03369	0.87
n=3turns	0.98	1.267	-0.05044	1.28
n= 4turns	0.98	1.591	-0.07014	1.48

From Table 4-5, L_0 values match the nominal inductance from EM simulation for each set of inductors and the amount of the inductance variation, a, is proportional to the nominal inductance and the number of inductor turns.

4.4.2 *Effects of variation in conductor line width*

Figure 4 -7 shows the inductance versus the conductor line width for four sets of inductors having different and fixed s_n =5 µm, n = 3-turns and t = 3 µm. Table 4-6 shows the coefficients extracted from Equation (4-3) for inductance versus the conductor line width shown in Figure 4-7. From Table 4-6, the magnitude coefficient "a" decrease with increasing the nominal conductor line width. This shows that the variation in the inductance versus the conductor line width is inversely proportional to the nominal conductor width w_n.

Table 4 - 6: coefficients of Equation (4-3) for inductors with different w_n and fixed s_n =5 µm, n=3-turns and t= 3 µm.

Data Set	R-square	Equation coefficients		Nominal inductance (nH) from EM simulation
		L_0	a	
w_n=5 µm	0.9800	1.267	-0.05044	1.27173
w_n = 7µm	0.9434	1.046	-0.05026	1.0272
w_n = 9µm	0.9990	0.8346	-0.04052	0.833819
w_n=10 µm	0.9990	0.7443	-0.03808	0.7460609
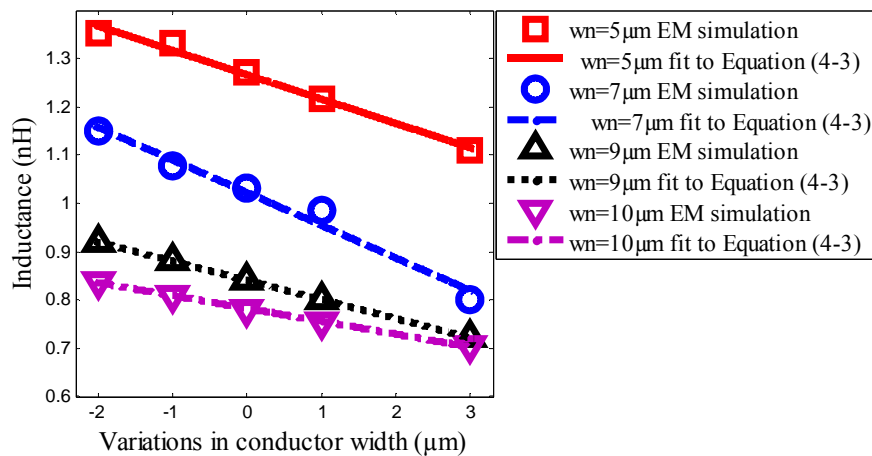
Figure 4- 7: Inductance versus conductor line width for different w_n and fixed s_n, n and t.

4.4.3 *Effects of variation in conductor thickness*

Figure 4-8 shows the extracted inductance versus the variation in the conductor line width for three sets of inductors having fixed $w_n = 5$ μm, n = 4-turns, $s_n = 5$μm and different t = 1 μm, 2 μm and 3 μm.
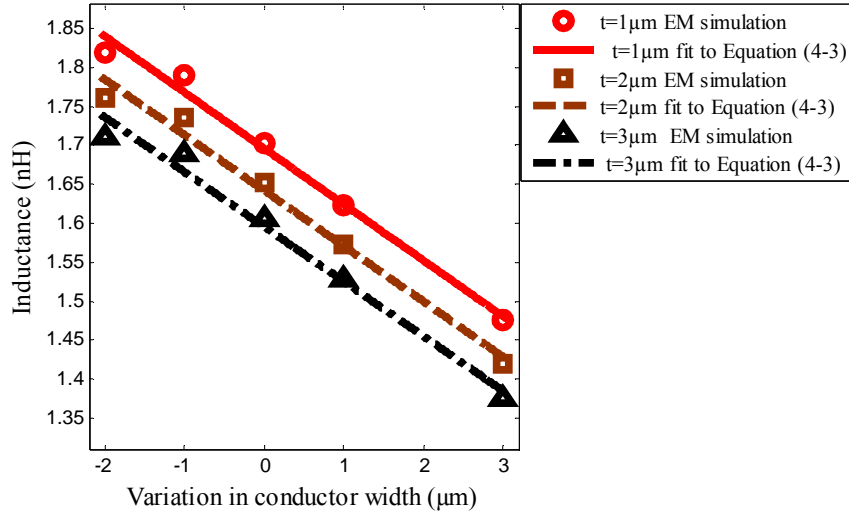
Figure 4- 8 : Inductance versus conductor line width for inductors having different t= 1 μm, 2μm and 3μm and fixed. w_n, S_n, and t.

Table 4-7 shows the coefficients extracted from Equation (4-3) for the inductance versus the conductor line width shown in Figure 4-8. This table shows that the variations in the conductor thickness have very little effect on the coefficient "a" of Equation (4-3).

Table 4 - 7: coefficients of Equation (4-3) for inductors having $w_n = 5$ μm, n=4-turns, $s_n = 5$μm and 1 μm, 2 μm and 3 μm.

Data Set	R-square	Equation coefficients		Nominal inductance (nH) from EM simulation
		L_0 (nH)	a	
t=1 μm	0.981	1.69	-0.071	1.70
t=2 μm	0.98	1.64	-0.070	1.65
t=3 μm	0.98	1.596	-0.070	1.60

4.4.4 *Effects of variation in conductors spacing*

Figure 4-9 shows the inductance versus the conductor line width for four inductors sets with fixed w_n =10 μm, t= 2 μm, n = 2-turns and different s_n. Table 4-8 shows the coefficients of Equation (4-3) for the inductance of these sets of inductors.
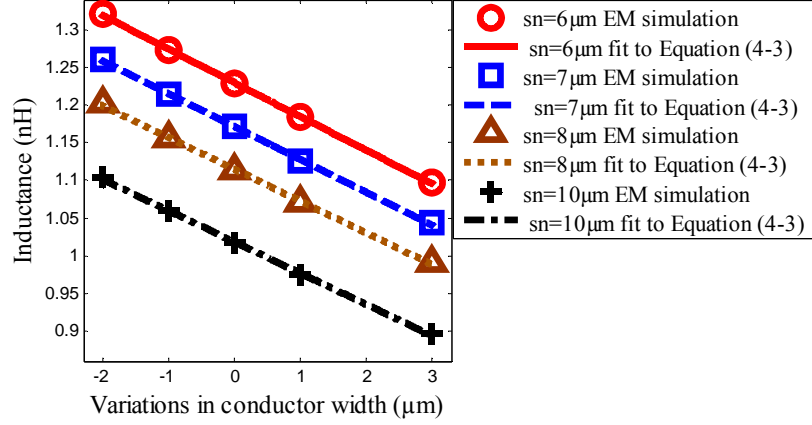
Figure 4- 9: Inductance versus conductor line width for inductors having different s_n and fixed t, w_n and n.

Table 4 - 8: Coefficients of Equation (4-3) for inductors w_n = 10 µm, t = 2 µm, n = 3-turns and different s_n .

Data Set	R-square	Equation coefficients		Nominal inductance (nH)
		L_0	a	
Sn=6µm	0.9997	1.23	-0.04465	1.2287
Sn=7µm	0.9992	1.172	-0.04349	1.17137
Sn=8µm	0.9992	1.115	-0.04209	1.11361
Sn=10µm	0.998	1.021	-0.04028	1.01646

From Table 4-8 the coefficient "a" is nearly same for all inductor sets. This suggests that different nominal spacing have similar effects on the variation in the inductance with respect to the conductor line width.

The amount of variation on inductance due to variations in conductor line width, a, was extracted for several sets of inductance .dependency of a on variations on w_n ,s_n ,n and t was studied as shown on Tables 4-5 to 4-8. From these tables a is strongly dependent on w_n and n whereas it is weekly dependent on t and s_n , consequently, *a* can be written as follows:

$$a = \frac{\partial L}{\partial w} = \frac{bn}{w_n} \tag{4-4a}$$

The nominal inductance, L_0, is proportional to the number of turns, n

$$L_0 \alpha n$$

Consequently Equation (4-4a) can be written as

$$a = \frac{\partial L}{\partial w} = \frac{bL_0}{w_n} \tag{4-4b}$$

Coefficient *b* is found to be about 0.3. Using Equation (4-3) and (4-4a), the inductance including the effects of the variations in the conductor line width can be estimated as follow:

$$L = L_O(1 - \frac{0.3}{w_n}\Delta w) \tag{4-5}$$

In Equation (4-5) L is the total inductance including the effects of variation in the conductor line width, L_0 is the nominal Inductance, and Δw is the amount of variation (from nominal) in the conductor line width.

Equation (4-5) gives a good agreement with Equation by [57]. From equation proposed by [57] the amount of the variations in the inductance with respect to the conductor line width is given by the following equation:

$$\frac{\partial L}{\partial w} = -\frac{\mu_0 l}{2\pi}(\frac{1}{w}) \tag{4-6}$$

Where *l* is the total length of metallization. Table 4-9 shows the comparison between the amount of inductance variation due to the change in the conductor line width calculated using Equation(4-4) and Equation(4-6) for sets of inductors with n = 3 and 4 turns , $w_n = 5$ µm ,$S_n = 5$µm, and t = 1 µm.

Table 4 - 9: Amount of inductance variation versus conductor line width calculated using Equation (4-4) and Equation (4-6).

Conductor line width variations	Change in the inductance (∂w) in nH/µm	
	Equation (4-6)	Equation (4-4)
w=5µm ,s=5 µm, t=1 n=1	-0.0172	-0.0167
w=5µm , s=5 µm, t=1 n=2	-0.0318	-0.042
w=5µm , s=5 µm, t=1 n=3	-0.043	-0.067
w=5µm , s=5 µm, t=1 n=4	-0.051	-0.085
w=10µm , s=5 µm, t=1 n=1	-0.0107	-0.0091
w=10µm , s=5 µm, t=1 n=2	-0.0191	-0.0220
w=10µm , s=5 µm, t=1 n=3	-0.0251	-0.033
w=10µm , s=5 µm, t=1 n=4	-0.0287	-0.038
w=10µm, s=10µm, t=1 n=3	-0.017	-0.0195
w=10µm, s=10µm, t=1 n=4	-0.0224	-0.0254

From Table 4-9, Equation (4-4) shows a greater amount of inductance variation than Equation (4-6) for inductors with more than one turn. This is because Equation (4-6) only considers the inductance for a straight line and doesn't take into account the

current crowding and proximity effects for inductors. The proximity effect increases the resistance and according to the incremental inductance rule by Wheeler, the change in inductance increases with the higher resistance particularly in the corners [56]. For multi-turn inductors and $w_n = 5$ μm the disparity between the changes in inductance obtained in Equation (4-4) and Equation (4-6) is greatest. Also, for multi-turn inductors, the change in inductance using Equation (4-4) is always greater than the inductance using Equation (4-6).

Figures 4-10 to 4-12 show the change in inductance due to the variations in the conductor line width extracted using the EM simulation and Equation (4-5) for sets of inductors having $n = 1 - 4$ turns, $w_n = 5$ µm and $s_n = 5$ µm and $t = 1$µm, 2µm and 3µm.
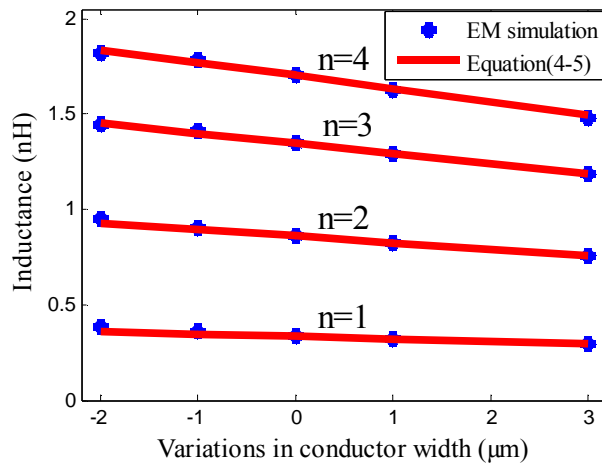
Figure 4- 10**:** Inductance versus conductor line width calculated using EM simulation and Equation (4-5) for 1-4 turns inductors with $w_n= 5$ µm, $s_n= 5$ µm and $t= 1$ µm.
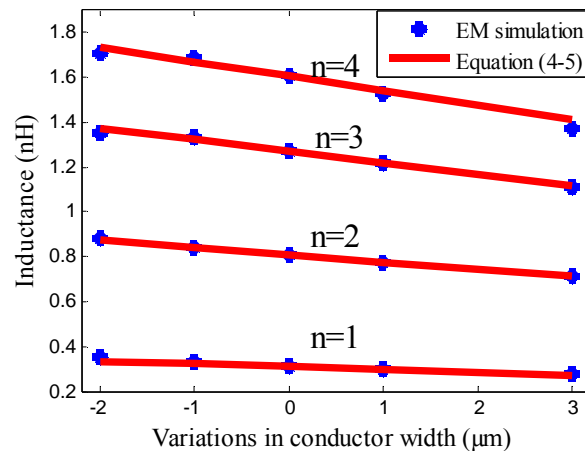
Figure 4- 11**:** Inductance versus conductor line width calculated using EM simulation and Equation (4-5) for 1-4 turns inductors with $w_n= 5$ µm , $s_n= 5$ µm and $t= 2$ µm.
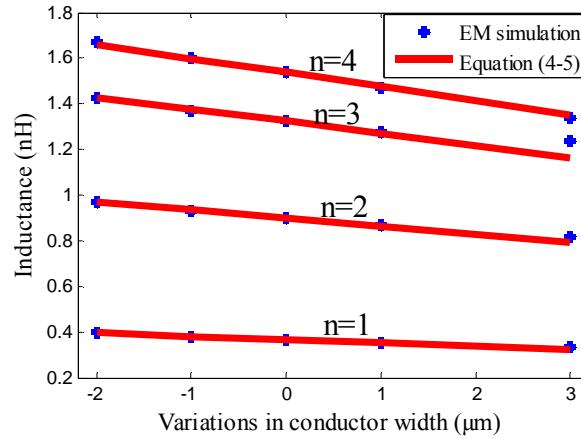
Figure 4- 12**:** Inductance versus conductor line width calculated using EM simulation and Equation (4-5) for 1-4 turns inductors with w_n= 5 µm   , s_n= 5 µm and t= 3 µm.

From Figure 4-10 to Figure 4 -12, the inductance extracted using the electromagnetic simulation shows good agreement with the inductance estimated using the proposed empirical Equation (4-5) with small percentage difference. The percentage difference is 2%, 5 % and 4%   for the simulated inductors shown in Figures 4 -10 to Figure 4 - 12 respectively. Figures 4-13 to 4-15 shows the variations in inductance due to the variations in the conductor line width for sets of inductors with n = 1 - 4 turns, w_n = 10 µm, s_n = 5 µm extracted using EM simulation and calculated using Equation (4-5) for t = 1µm, 2 µm and 3 µm respectively. From Figures 4-13 to 4-15 the difference between the inductance extracted using the EM   simulation and the inductance calculated using Equation (4-5) is only 6% for t = 1µm and 5% for t = 2 µm and 2 µm.
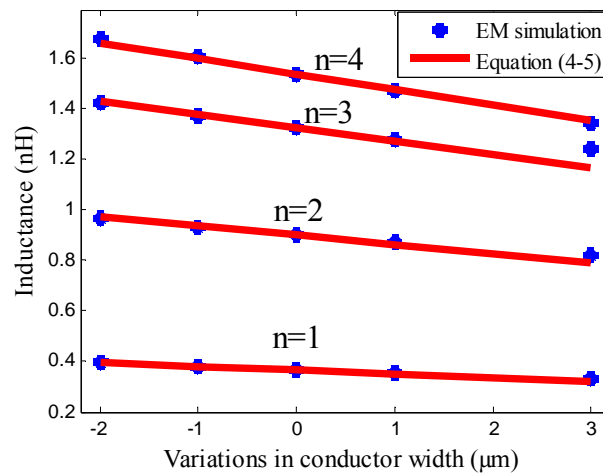
Figure 4- 13: Inductance versus conductor line width calculated using EM simulation and Equation (4-5) for 1-4 turns inductors with w_n = 10 µm   , s_n = 5 µm and t = 1 µm.
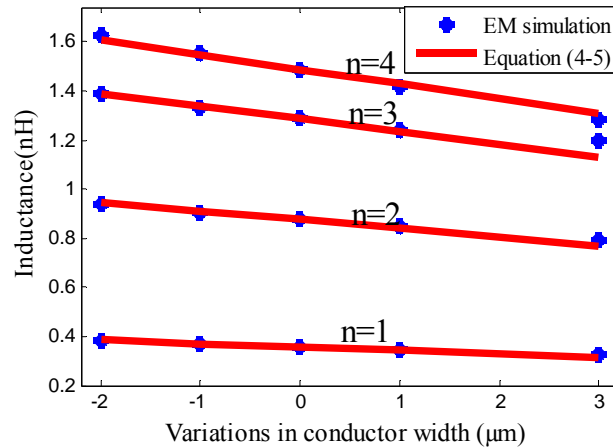
Figure 4- 14: Inductance versus conductor line width calculated using EM simulation and Equation (4-5) for 1 - 4 turns inductors with $w_n = 10$ µm , $s_n = 5$ µm and $t = 2$ µm.
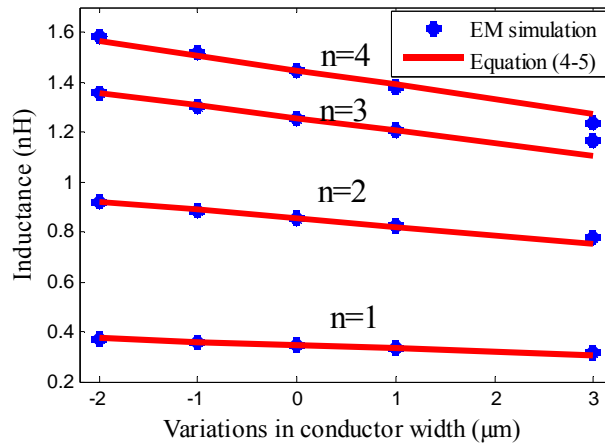
Figure 4- 15: Inductance versus conductor line width calculated using EM simulation and Equation (4-5) for 1 - 4 turns inductors with $w_n = 10$ µm, $s_n = 5$ µm and $t = 3$ µm.

The inductance versus the variations in the conductor line width for two sets of inductors with n = 2 and 3 turns, $w_n = 10$ µm, $t = 2$ µm and $s_n = 10$ µm extracted using the electromagnetic simulation and calculated Equation (4-5) is compared as shown in Figure 4-16.
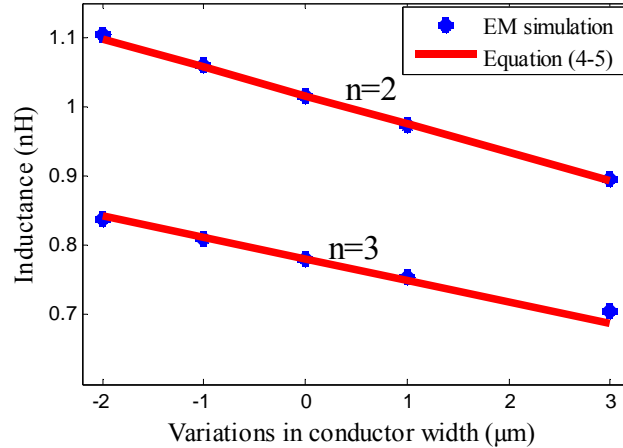
Figure 4- 16: inductance versus conductor line width calculated using EM simulation and Equation (4-5) for 1 - 4 turns inductors with $w_n = 10$ μm , $s_n = 10$ μm and $t = 2$ μm.

Figure 4-16 shows that Equation (4-5) has an excellent agreement with the simulation results. The percentage difference is still less than 6%.

It can be concluded from above figures that Equation (4-5) can be used to estimate the inductance including the effects of the conductor line width variations for Gallium Arsenide based inductors with gold conductor having nominal width 5μm,7 μm , 9 μm and 10 μm, and number of turns 1 - 4 turns, and conductor thickness of 1 to 3 μm and nominal conductor of spacing 5 μm, 6 μm, 7 μm, 8 μm and 10 μm.

4.5 Variations in resistance versus conductor width

The series resistance of the planar spiral inductor is a strong function of the conductor line width, consequently, the variations in the conductor line width lead to variations in this resistance. The simulation results illustrate that the variations in the resistance inversely proportional to the conductor line width. Figure 4-17 shows the variation in the resistance versus the conductor line width extracted using the electromagnetic simulation for sets of inductors having n=1-4 turns, wn = 5μm, s_n =5 μm and t= 2 μm. From Figure 4-17 extracted resistance values are shown to decrease exponentially with increasing conductor line width. This agrees with Equation (4-7) proposed by [16].

$$R = \frac{KR_{sh}l}{2(w+t)} \tag{4-7}$$

$$\text{where} \quad K = 1 + 0.333(1 + \frac{S}{w})$$

w, t, l and R_{sh} are the conductor line width, the conductor thickness, the length of the spiral and sheet resistance per square.
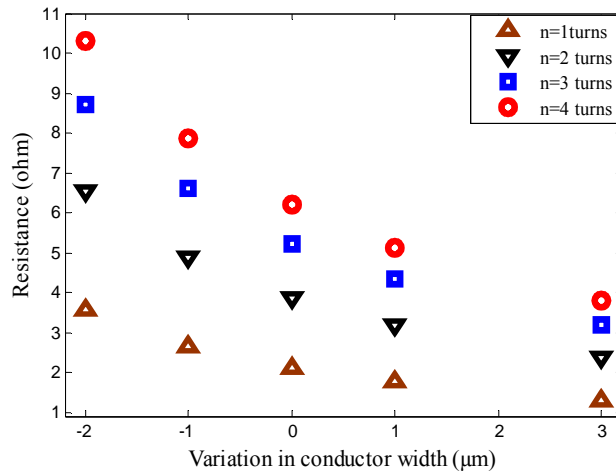
Figure 4- 17: Resistance versus the conductor line width extracted using EM simulation.

Figure 4-18 compares the inductance versus the conductor line width extracted using the electromagnetic simulation and Equation (4-7) for two sets of inductors with n =1 and 3 turns, w_n = 5µm, s_n =5 µm and t = 1 µm. As can be observed from Figure 4-18, the simulation results are fairly matching Equation (4-7) with small difference. This because Equation (4-7) doesn't take into account many factors that can affect the resistance of the spiral inductor such as the skin, proximity and effects while EM simulation accounts for all these effects. Figure 4-18 also shows that the resistance extracted using EM simulation and Equation (4-7) vary in the same manner with the conductor line width.
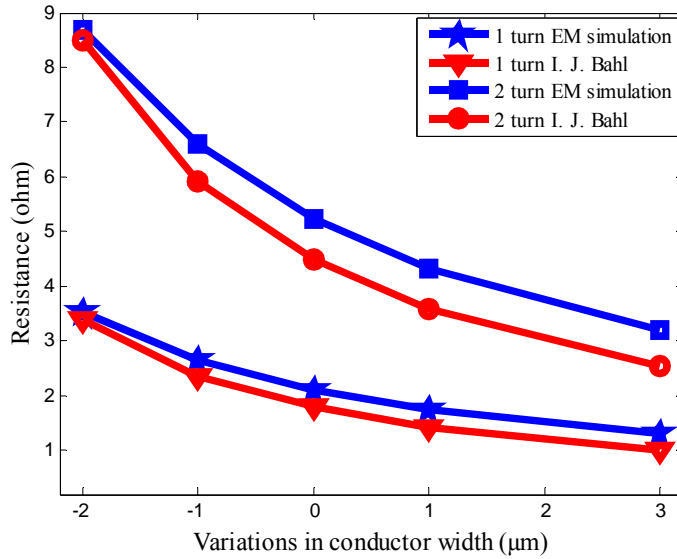
Figure 4- 18: Resistance versus the conductor line width extracted using the EM simulation and I. J. Bahl formula.

The relation between the resistance and the conductor line width for several inductors with different dimensions is investigated. This is used to identify the equation parameters for estimating the change in the resistance due to the variation in the conductor line width

4.5.1 *Effects of variation in number of turns*

The relationship between the resistance and the conductor line width for inductors having different number of turns but with the same nominal conductor line width, conductor thickness, and nominal spacing between the conductors is investigated using curve fit to Equation (4-8). Figure 4-19 shows the variations in the resistance versus the conductor line width for sets of inductors with different n =1 - 4 turns and fixed w_n = 5 µm, s_n =5 µm t= 3 µm.

$$R(\Delta w) = R_0 \exp(b\Delta w) \qquad (4-8)$$
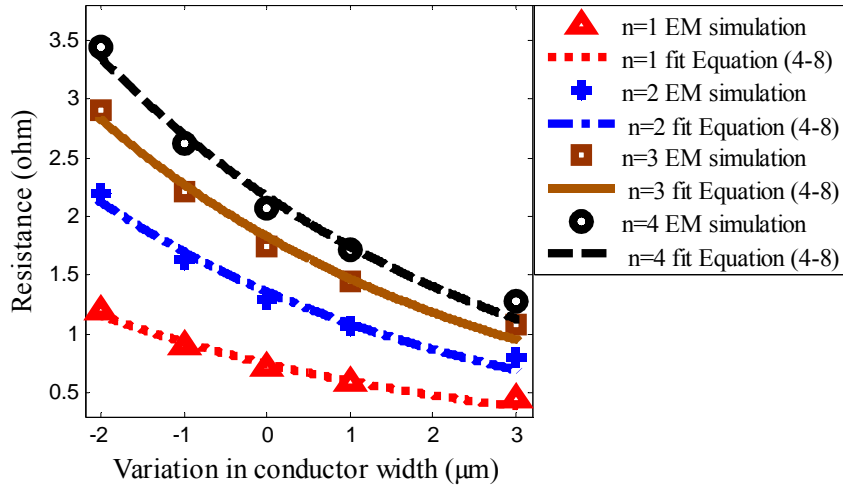
Figure 4- 19: Resistance versus conductor line width for inductors having n=1-4 turns and fixed t, w_n and s.

Table 4-10 shows the coefficients extracted from Equation (4-8) for the resistance versus the conductor line width shown in Figure 4-19 .

Table 4 - 10: Coefficients of Equation (4-8) for inductors n=1-4 turns w_n =5µm, s_n =5 µm t= 3 µm.

Data Set	R-square	Equation coefficients		Simulated nominal Resistance (ohm)
		R_0	b	
n=1turn	0.97	0.75	-0.21	0.714707
n=2turns	0.97	1.36	-0.22	1.2966
n=3turns	0.98	1.832	-0.21	1.74962
n=4turns	0.98	2.173	-0.21	2.07751

From Table 4-10, R_0 values match the nominal resistance extracted using EM simulation for each set of inductors and the coefficient b is constant, about 0.20. This suggests that variation in the resistance with the conductor line width is nearly independent of the number of turns

4.5.2 *Effects of Variation in conductor line width*

The variation in the resistance versus the conductor line width for inductors having different nominal conductor line width is investigated. Figure 4-20 shows the resistance versus the conductor line width for two sets of inductors with different w_n =5µm and 10µm and fixed t= 1 µm, n=4turns, s_n =5µm. Figure 4-20 also shows the curve fit the resistance using Equation (4-8). Coefficients of this equation are shown by Table 4-11.
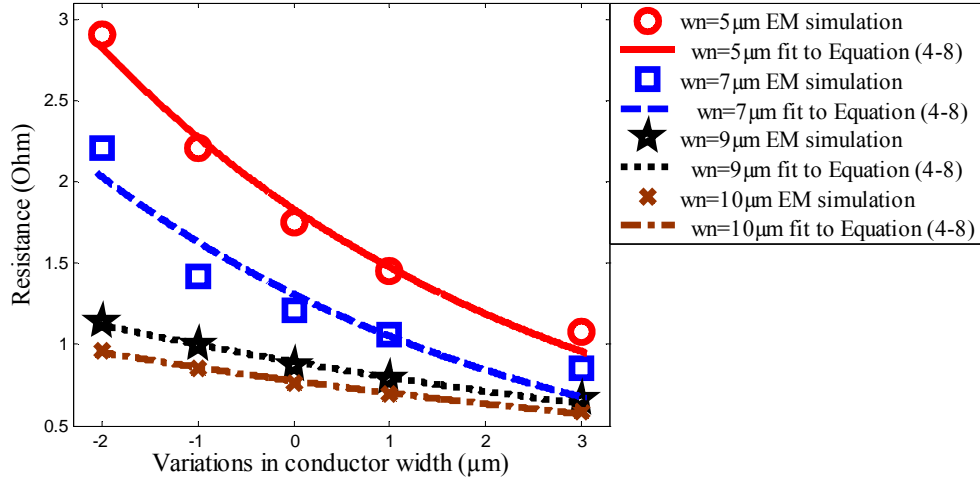
Figure 4- 20: Resistance versus conductor line width for inductors having different w_n=5µm and 10 µm and fixed t, n and s_n.

Table 4 - 11: Coefficients of the Equation (4-8) for inductors with different w_n and fixed t= 3 µm, n=3turns, s_n =5µm.

Data Set	R-square	Equation coefficients		Nominal Resistance
		R0	b	(ohm)
wn=5µm	0.9924	1.832	1.74962	1.74962
wn=7µm	0.9272	1.29	1.20964	1.20964
wn=9µm	0.9924	0.8942	0.872502	0.872502
wn=10µm	0.9924	0.7789	0.766072	0.766072

From Table 4-11 the coefficient "b" varies with the nominal conductor line width. b is equal to the reciporacl of nominal conductor width.

4.5.3   *Effects of Variation in conductor thickness*

Figure 4-21 shows the resistance versus the conductor line width for three sets of inductors having fixed w_n =5µm and s_n = 5µm, n=4 turns and different t= 1µm, 2µm and 3µm and curve fit this resistance using Equation (4-8). Table 4-13 shows coefficients of Equation (4-8) for these sets. From Table 4-13, the relation between the change in resistance and the conductor line width is independent of the conductor thickness.
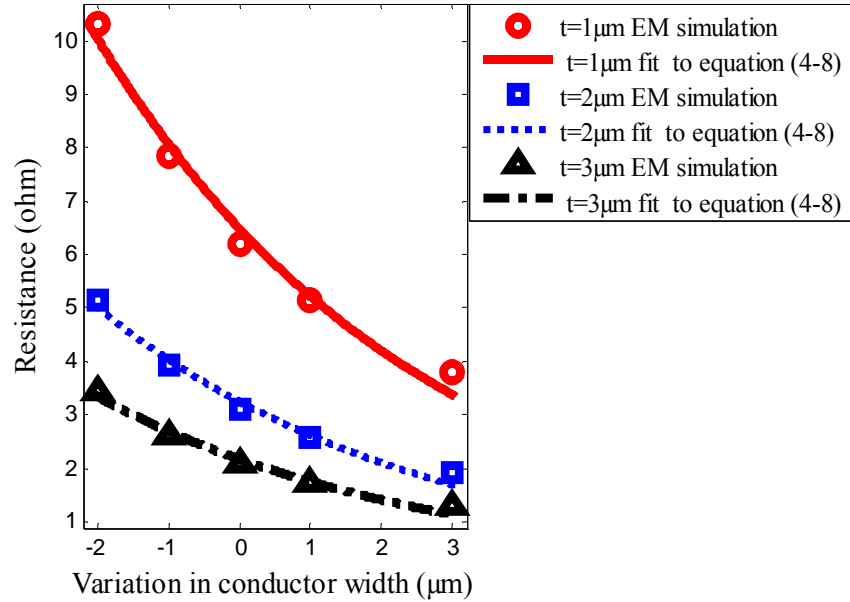
Figure 4- 21: Resistance versus conductor line width for inductors having different t=1µm, 2 µm and 3 µm and fixed w_n, n and s_n.

Table 4 - 12: coefficients of Equation (4-18) for inductors with w_n =5µm and s_n = 5µm, n=4 turns and t= 1µm, 2µm and 3µm.

| Data Set | R-square | Equation coefficients | | Nominal Resistance |
		R_0	b	(ohm)
t=1µm	0.981	6.499	-0.21	6.21503
t=2µm	0.98	3.252	-0.21	3.10719
t=3µm	0.98	2.173	-0.21	2.07751

4.5.4 *Effects of variation in conductors spacing*

Figure 4-22 shows the resistance versus the conductor line width for two sets of inductors with fixed w_n =10 µm, t=2 µm, n=3-turns, and different s_n =5 µm and 10 µm. From Figure 4-22, Although the sets of the inductors have different nominal spacing, cofficient "b" of Equation (4-8) has the same value as can observed from Table 4-14. This suggest that the relation between the change in resistance and the conductor line width is independent of the conductor spacing.
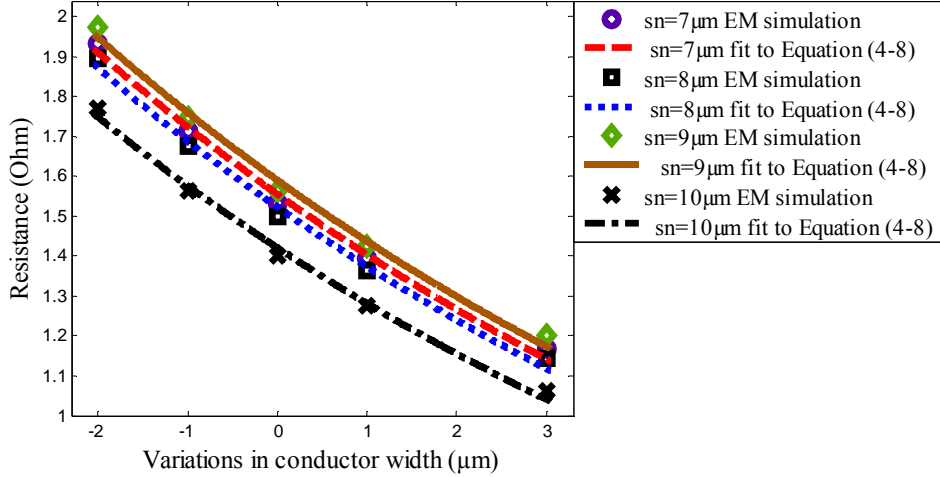
Figure 4- 22: Resistance versus conductor line width for inductors having different s_n=5µm and 10 µm and fixed 3 µm and fixed w_n, n and s_n.

Table 4 - 13: Coefficients of Equation (4-8) for inductors with w_n =10 µm, t=2 µm, n=3-turns, and different s_n.

Data Set	R-square	Equation coefficients		Nominal Resistance
		R_0	b	(ohm)
S_n=6µm	0.9931	1.591	-0.1012	1.56458
S_n=7µm	0.9925	1.556	-0.1027	1.53305
S_n=8µm	0.9941	1.524	-0.1029	1.49977
S_n=10µm	0.9931	1.422	-0.1035	1.40098

From Tales 4-11 to 4-13 it can be concluded the amount of variations in the resistance with respect to the conductor line width ,b, is only affected by the nomnal conductor width and it can estimated as follows:

$$b = \frac{1}{w}$$ (4-8b)

Using Equations (4-8a) and (4-8b) that the resistance including the effects of the variations in the conductor line width can be estimated as follows:

$$R = R_0 \exp(-\frac{\Delta w}{w})$$ (4-9a)

Equation (4-9) has been validated by the compersion to (4-7). Considering resistance variations with respect to conductor line width variations, Equation (4-9b) can be written as follow:

$$R = R_0 + \frac{\partial R}{\partial w}\Delta w + \frac{1}{2!}\frac{\partial^2 R}{\partial w^2}\Delta w^2 .....]$$ (4-9b)

$$\frac{\partial R}{\partial w} = -\frac{KR_{sh}l}{2(w+t)^2}$$

$$\frac{\partial^2 R}{\partial w^2} = \frac{KR_{sh}l}{(w+t)^3}$$

$$R = R_0 + C_1\Delta w + C_2\Delta w^2 \qquad\qquad (4\text{-}9c)$$

Where $C_1 = -\dfrac{KR_{sh}l}{2(w+t)^2}$ $\qquad$ $C_2 = \dfrac{KR_{sh}l}{2(w+t)^3}$

Resistance extracted using Equation (4-9a) can fitted to Equation (4-9e)

$$R = R_0 + C_1\Delta w + C_2\Delta w^2 \qquad\qquad (4\text{-}9d)$$

Table 4-15 shows the coefficients C1 and C2 from Equations (4-9c) and (4-9d)

Table 4 - 14: coefficients C1 and C2 from Equations (4-9c) and (4-9d)

Inductor dimensions	Equation(4-9d)			Equation(4-9c)		
	C_1 ohm/m	C_2 ohm/m^2	R_0	C_1 ohm/m	C_2 ohm/m^2	R_0
w=5 , t=1, n=3	-1.274	0.198	5.271	-1.395	0.119	3.4
w=5 , t=1, n=4	-1.5	0.23	6.2	-0.85	0.141	5.1
w=10 , t=1 n=3	-0.331	0.035	3.071	-0.231	0.0140	2.54
w=10 ,t=1, n=4	-0.394	-0.035	3.52	-0.264	0.024	3.042

From Table 4-10 the values of C_1 and C_2 extracted from (4-9c) Shows a good agreement (4-9d).

Figure 4-23 to Figure 4-25 show the comparison of the resistance for sets of inductors having n=1 - 4 turns, w_n =5 µm, s_n =5 µm extracted using EM simulation and calcultaed using Equation(4-9) for t = 1 µm, 2µm and 3µm respectively.
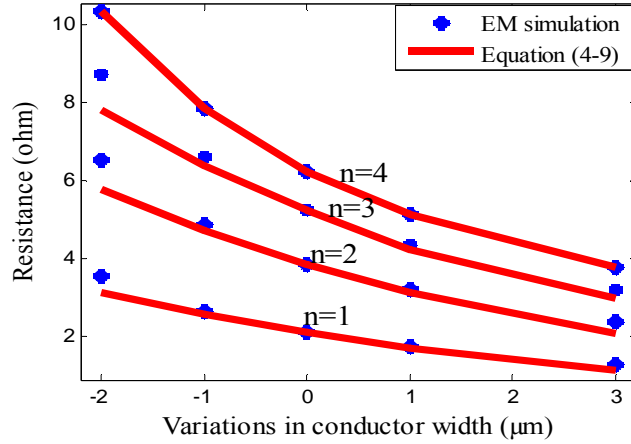
Figure 4- 23: Resistance versus conductor width calculated using EM simulation and Equation (4-9) for sets of inductors with n=1-4 turns, w_n= 5 µm, s_n= 5 µm and t= 1 µm.
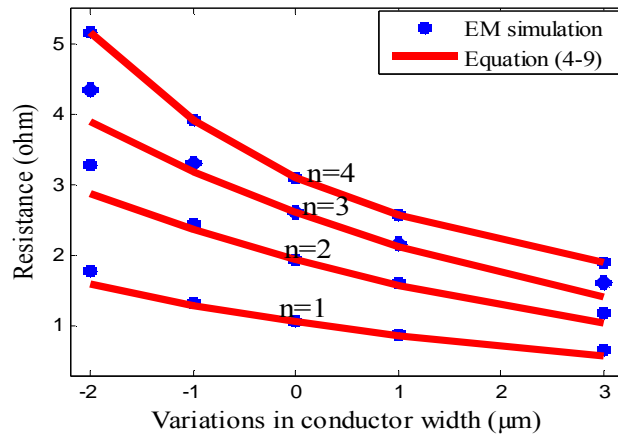
Figure 4- 24: Resistance versus conductor width calculated using EM simulation and Equation (4-9) for sets of inductors with n=1-4 turns, w_n= 5 µm , s_n= 5 µm and t= 2 µm.
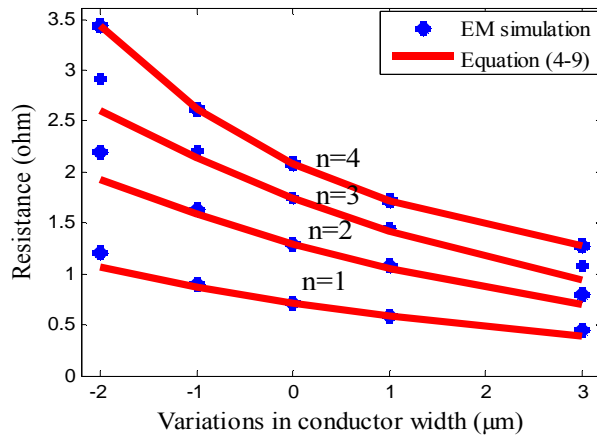
Figure 4- 25: Resistance versus conductor width calculated using EM simulation and Equation (4-9) for sets of inductors with n=1-4 turns, w_n= 5 µm , s_n= 5 µm and t= 3 µm.

Figure 4-26 to Figure 4-28 show the comparison between the resistance versus conductor line width for sets of inductors with n=1- 4 turns , w_n =10 μm, and s_n =5 μm extracted using EM simulation and calculated using Equation (4-9) for t= 1 μm, 2μm and 3μm respectively.
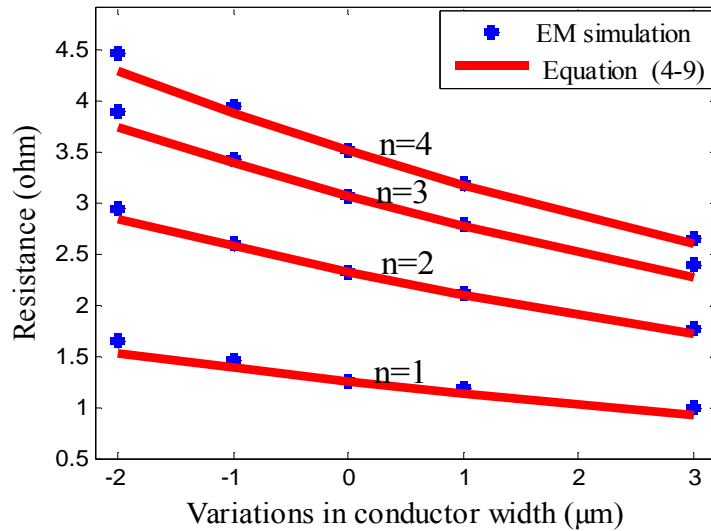
Figure 4- 26: Resistance versus conductor width calculated using EM simulation and Equation (4-9) for sets of inductors with n=1-4 turns, w_n= 10 μm , s_n= 5 μm and t= 1 μm.
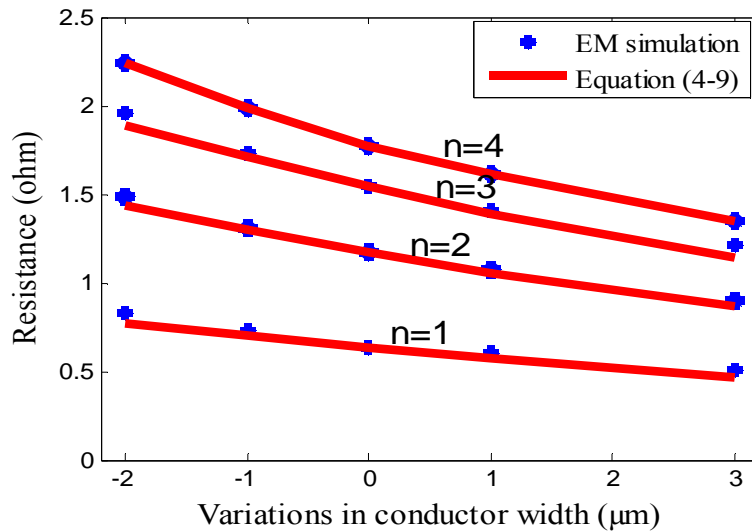
Figure 4- 27: Resistance versus conductor width calculated using EM simulation and Equation (4-9) for sets of inductors with n=1-4 turns, w_n= 10 μm , s_n= 5 μm and t= 2 μm.
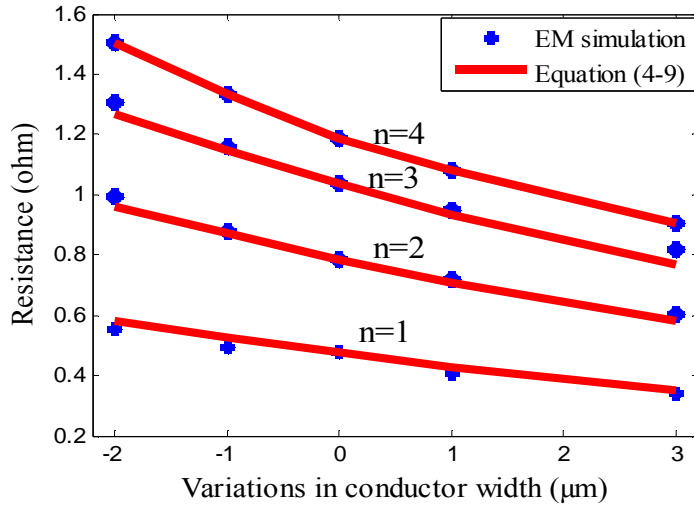
Figure 4- 28: Resistance versus conductor width calculated using EM simulation and Equation (4-9) for sets of inductors with n=1-4 turns, w_n= 10 µm , s_n= 5 µm and t= 3 µm.

The resistance versus conductor line width for sets of inductors having n=2 and 3turns, w_n =10 µm, t= 2 µm and s_n =10 µm extracted using electromagnetic simulation and estimated using Equation (4-9) is shown in Figure 4-29.
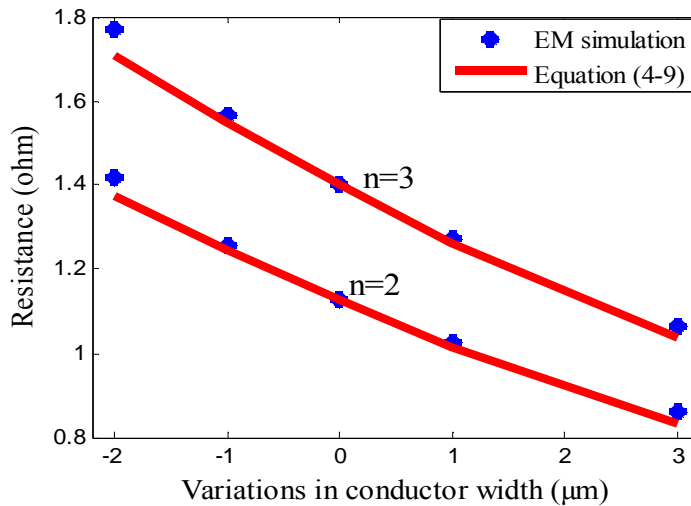
Figure 4- 29: resistance versus conductor line width calculated using EM simulation and Equation (4-9) for inductors with n=2 and 3 turn s_n = 10 µm , w_n= 10 µm and t= 2 µm.

From Figures 4-23 to 4-29 the resistance calculated using Equation (4-9) fairly matches the simulation results then this equation can be used to estimate the resistance including the effects of variations in the conductor line width for planar spiral inductors based Gallium Arsenide technology with gold conductors having w_n = 5µm ,7 µm , 9 µm and 10 µm, and n= 1- 4 turns, t= 1- 3 µm and s_n= 5 µm ,6 µm,7

μm, 8 μm and 10 μm with difference not more than 3% for the small conductor line width variations (-1μm and +1 μm) and 13% for the large conductor line width variations (-2μm and +3 μm).

4.6 Variation in line to line capacitance versus conductor width

Variations in the conductor line width result in variations in the spacing between the conductors affecting the line to line capacitance. The center to centre spacing is, however, usually fixed. If the conductor line width is increased by a certain amount during the fabrication process, then the spacing between the conductors will decrease by same amount and vice versa. Figure 4-30 shows the line to line capacitance versus the conductor line width extracted using the electromagnetic simulation for two sets of inductors with n=2 and 3 turn, w_n =5μm, t= 3 μm, s_n =5μm. From this figure, the line to line capacitance is shown to increase with increasing conductor line width.
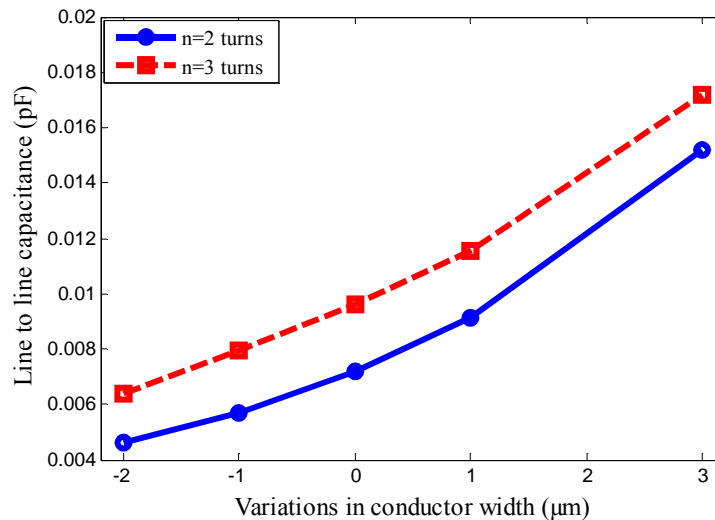
Figure 4- 30: Line to line capacitance versus the conductor line width extracted using EM simulation.

The simulation results are compared to the model proposed by Garg and Bahl [58]to calculate the capacitance of coupled microstrip lines. Due to differences in phase between the voltage on each conductor, the coupling capacitance for a coupled microstriplines can be calculated from the odd-mode capacitance in the substrate and air.

Figure 4-31 shows the odd mode capacitances for coupled microstripline. The interwinding Capacitance C_i is the summation of the capacitances c_{gd} the gap capacitances in the dielectric and c_{ga} the gap capacitances in the air [59].
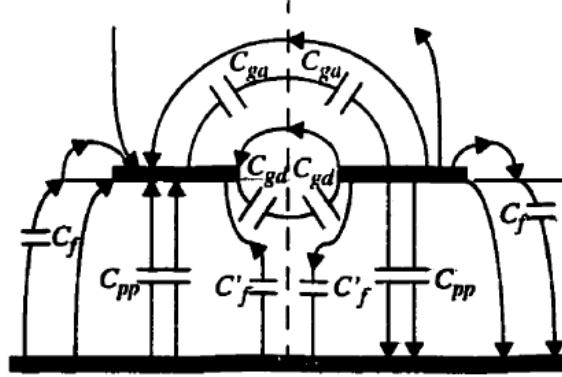
Figure 4- 31: capacitances of coupled microstriplines [59].

The proposed formulae by Garg and Bahl [58] calculate the c_{ga} and c_{gd} capacitance of coupled microstriplines as follow:

$$C_{ga} = \varepsilon_0 \frac{K(k')}{K(k)} \tag{4-10}$$

Where $K = \dfrac{s}{s + 2w_t}$ and $k' = \sqrt{1 - K^2}$

ε_0, s and w_e are permittivity of free space, spacing between the conductors and the conductor line width after the effects of conductor thickness. w_t can be estimated using the following formula which is valid only for $s \geq 2t$.

$$w_t = w + \Delta w \left[1 - 0.5 \exp(\frac{-0.69\Delta w}{\Delta t}) \right] \tag{4-11}$$

where $\Delta t = \dfrac{h}{\varepsilon_r} \dfrac{t}{s}$

h, t and ε_r are the substrate height, conductor thickness and relative dielectric constant. And Δw is the increase in strip width of single microstnpline due to strip thickness t, Δt the excess increase in effective width for the odd mode when compared

with the even mode, ratio of the complete elliptic function K (k) and its complement K (k') is given by:

$$\frac{K(K')}{K(K)} = \begin{cases} \left\{ \frac{1}{\pi} \ln\left[2\frac{1+\sqrt{K'}}{1-\sqrt{K'}} \right] \right\} & 0 \le K^2 \le 0.5 \\ \dfrac{\pi}{\ln\left[2\frac{1+\sqrt{K}}{1-\sqrt{K}} \right]} & 0.5 \le K^2 \le 1 \end{cases} \qquad (4\text{-}12)$$

The gap capacitances in the air can be estimated as follows:

$$gd = \frac{\varepsilon_0 \varepsilon_r}{\pi} \ln\left\{ \coth(\frac{\pi}{4}\frac{s}{h}) \right\} + 0.65 c_f \left[\frac{0.02}{s/h} \sqrt{\varepsilon_r} + 1 - \varepsilon_r^{-2} \right] \qquad (4\text{-}13)$$

Cf is the fringing capacitance of a microstripline of width w, impedance Z_0, and effective dielectric constant and is given by:

$$c_f = 0.5(\frac{\sqrt{\varepsilon_r}}{cZ_0 - c_p}) \quad c = 3\times10^8 \, m/s \qquad c_p = \frac{\varepsilon_0 \varepsilon_r w_e}{h}$$

$$z_0 = \begin{cases} \dfrac{60}{\sqrt{\varepsilon_{re}}} \ln(\frac{8h}{w_e} + 0.25\frac{w_e}{h}) & w/h \le 1 \\ \dfrac{376.7}{\sqrt{\varepsilon_{re}}} \left[\frac{w_e}{h} + 1.393 + 0.667 \ln(\frac{w_e}{h} + 1.4444) \right]^{-1} & w/h \ge 1 \end{cases}$$

Where ε_{re} is the effective dielectric constant of microstripline given by:

$$\varepsilon_{re} = \frac{\varepsilon_r + 1}{2} + \frac{\varepsilon_r - 1}{2} F(\frac{w_t}{h}) - C$$

$$F(\frac{w_t}{h}) = \begin{cases} \left[\left(1 + \frac{12h}{w}\right)^{-0.5} + 0.041\left(1 - \frac{w}{h}\right)^2 \right] & \frac{w}{h} \le 1 \\ \left(1 + \frac{12h}{w}\right)^{-0.5} & \frac{w}{h} \ge 1 \end{cases}$$

$$C = \frac{\varepsilon_r - 1}{4.6} \frac{t/h}{\sqrt{w_t/h}}$$

Using the above equations the interwinding capacitance C_i of coupled microstriplines is estimated as follow:

$$C_i = c_{gd} + c_{ga} \qquad (4\text{-}14)$$

Figure 4-32 shows a comparison between the variations in the coupling capacitance versus the conductor line width using Equation (4-14) for a pair of microstriplines with w_n =10 µm, h= 100 µm, ε_r =12.9 and l= 32 µm and the line to line capacitance of 2-turns inductor with w_n =10 µm, h= 100 µm and ε_r =12.9. As shown by Figure 4-32 the capacitance extracted using simulation results and Equation (4-14) exponentially increases with conductor width. The capacitance extracted from EM simulations show faster variations versus the conductor line width than the capacitance calculated using [58]. This is because the line to line capacitance extracted from EM simulation for a two turns inductor while the capacitance calculated using [58] for only one pair of lines.
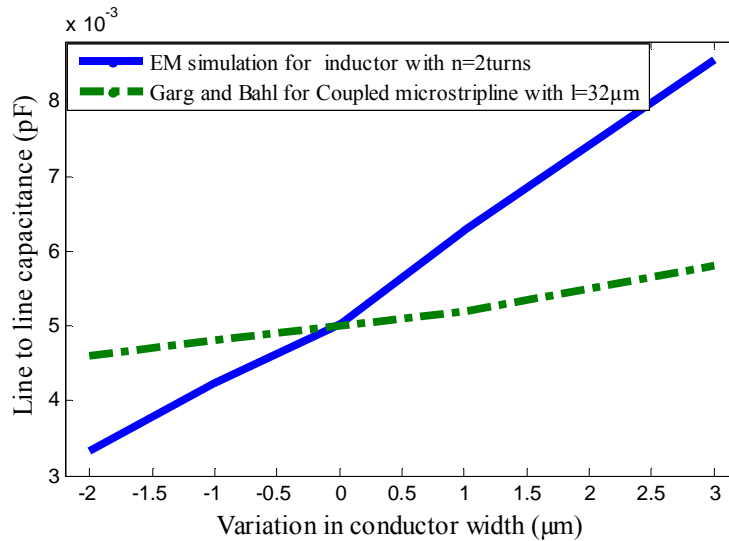
Figure 4- 32: Line to line capacitance versus conductor line width extracted using the EM simulation and Garg and Bahl model.

The variations in the line to line capacitance versus the conductor line width for sets of inductors having different dimensions are investigated. The dependency of these variations on the inductor dimensions is investigated by varying one of inductor dimensions while holding the others constant as follows:

4.6.1 *Effects of variation in conductors spacing*

The effects of variation in the nominal spacing on the relationship between the line to line capacitance and the conductor line width is first investigated by curve fitting sets of inductors having different spacing between the conductors and fixed nominal conductor line width, conductor thickness and number of turns. Figure 4-33 shows the line to line capacitance versus the conductor line width for two sets of inductors having different S_n = 5 µm and 10 µm same w_n = 10 µm, t = 2 µm, and n= 3 turns. Figure 4-33 also shows the curve fit this line to line capacitance. The coefficients extracted from Equation (4-15) shown in Table 4-15.

$$C = C_0 \exp(b\Delta w) \qquad\qquad (4\text{-}15)$$
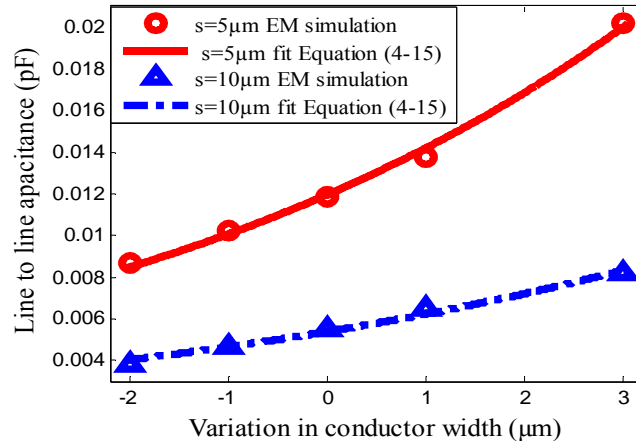
Figure 4- 33: line to line capacitance versus conductor line width for inductors having different s_n=5µm and 10 µm and fixed w_n, n and t.

Table 4- 15: Coefficients extracted from Equation (4-15) for inductors with n=3turns, t= 2 µm, wn =10 µm, s_n = 5µm and 10µm.

Data Set	R-square	Equation coefficients		Nominal line to line capacitance (pF)
		C_0	b	
s=5 µm	0.999	0.01195	0.1718	0.0118615
s=10 µm	0.996	0.00539	0.1454	0.0054936

From Table 4-15 the coefficient b extracted using eq. (5a) varies for different nominal spacing. The extracted value of b = 0.17 is obtained for s_n =5 µm and 0.14 for s_n = 10 µm. This suggests that the variation in the line to line capacitance with the conductor line width increases with decreasing the nominal spacing between the conductors.

4.6.2 *Effects of variation in number of turns*

Figure 4-34 shows the line to line capacitance for two sets of inductors having different n =1 and 2 turns and fixed w_n = 10µm, s_n = 5 µm and t = 3 µm as well as the curve fit this capacitance. Table 4-16 shown the coefficients extracted from Equation (4-15).
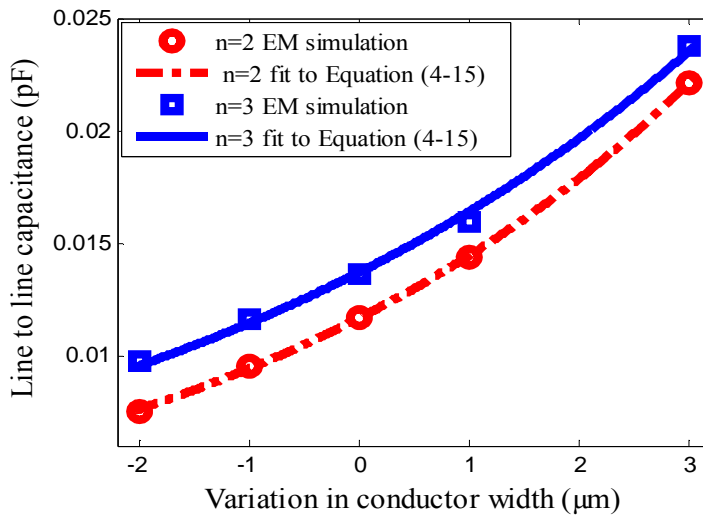
Figure 4- 34: line to line capacitance versus conductor line width for inductors having different n=2 and 3 turns and fixed w_n, n and t.

Table 4 - 16: Coefficients extracted from Equation (4-15) for inductors with n=1 and 2 turns, w_n = 10µm, s_n= 5 µm and t =3 µm.

inductors Set	R-square	Equation coefficients		Nominal line to line capacitance (pF)
		C_0	b	
n=1turn	0.999	0.01167	0.2132	0.0116829
n=2turns	0.996	0.0137	0.1803	0.0136049

From Table 4-16 the variation in the line to line capacitance due to the variation in the conductor line width, *b*, is independent of the number of turns.

4.6.3 *Effects of variation in conductor line width*

The variation in the line to line capacitance due to the variation in the conductor line width is independent of the nominal conductor line width. Figure 4-35 shows the

variations in line to line capacitance with the conductor line width for two sets of inductors having fixed n= 3- turns, $s_{n=}$ 5 µm, t= 2 µm and different w_n =5µm and 10 µm and the curve fit this capacitance . Table 4-17 shows the coefficients of Equation (4-15). As can be observed from this table the value of "b" is independent of the nominal conductor width.
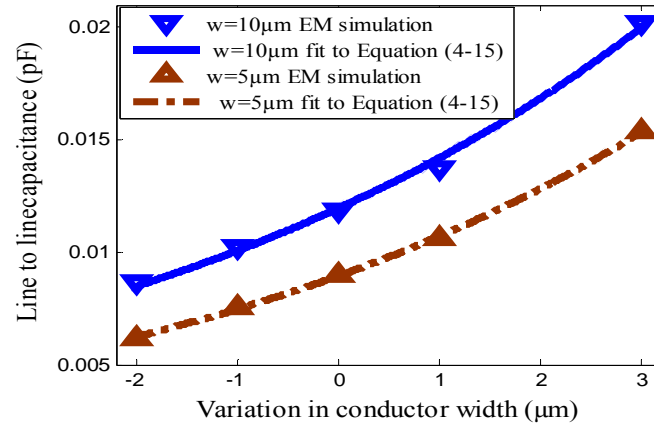
Figure 4- 35: line to line capacitance versus conductor line width for inductors having different w_n=5µm and 10 µm and fixed s_n, n and t.

Table 4 - 17: Coefficients extracted from Equation (4-15) for inductors with n= 3-turns, s_n= 5 µm, t= 2 µm and w_n =5µm and 10 µm.

Data Set	R-square	Equation coefficients		Nominal line to line capacitance (pF)
		C_0	b	
w=5 µm	0.99	0.008937	0.1803	0.0090
w=10 µm	0.99	0.01195	0.1718	0.0118615

4.6.4 *Effects of variation in conductor thickness*

Figure 4-36 shows the variation in the line to line capacitance due to the variations in the conductor line width for inductors having fixed n = 3 turns, w_n = 10µm,s_n =5 µm and different t= 1µm,2µm and 3µm and the curve fit this capacitance using Equation (4-15).
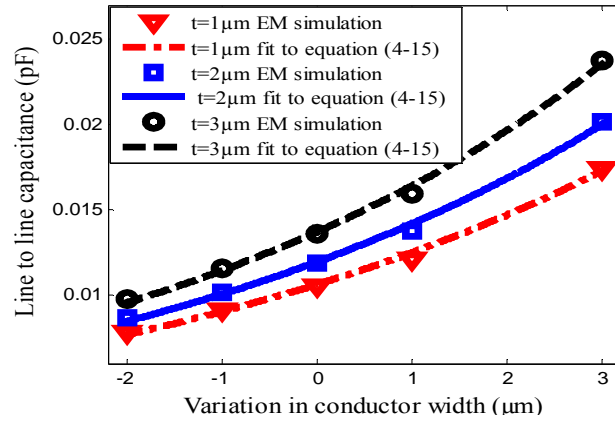
Figure 4- 36: Dependency of variations in the line to line capacitance with the conductor line width on the conductor line width.

Table 4-18 shows the coefficients of Equation (4-15) for line to line capacitance versus conductor line width shown in Figure 4-36. From Table 4-18 and Figure 4-36, the variation in the line to line capacitance due to the variations in the conductor line width is independent on the conductor thickness.

Table 4 - 18: coefficients extracted from Equation (4-15) for inductors with n=3 turns, $w_n = 10\mu m$; $s_n = 5$ µm, t= 1µm, 2µm and 3µm.

Data Set	R-square	Equation coefficients		Nominal line to line capacitance (pF)
		C_0	b	
t=1 µm	0.996	0.01063	0.1619	0.0105692
t=2 µm	0.996	0.01195	0.1718	0.0118515
t=3 µm	0.996	0.0137	0.1803	0.0136049

By invistigating the variations in the line to line capacitance due to the variations in the conductor line width for inductors having variuos dimensions , these variations are only dependent on the spacing between the condutors. line to line capacitance including the effects of the variation in the conductor line width can be estimated by rewriting Equation (4-15) as follows :

$$C = C_0 \exp(-\frac{\Delta w}{s}) \qquad (4-16)$$

Figure 4-37 to Figure 4-39 compare the line to line capacitance for sets of inductors having n=2 and 3 turns, w_n= 5 µm, s_n = 5 µm extracted from the electromagnetic

74

simulation and calculated from Equation (4-16) for t= 1 µm ,2 µm,3 µm respectively
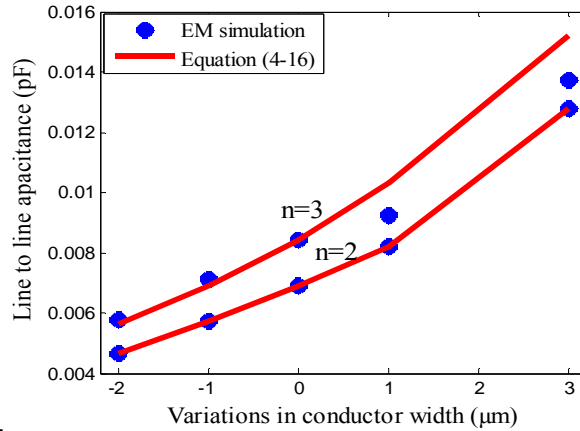
Figure 4- 37: Line to line capacitance versus conductor line width for inductors
having w_n= 5 µm, s= 5 µm and t= 1 µm calculated using EM simulation and Equation
(4-16).
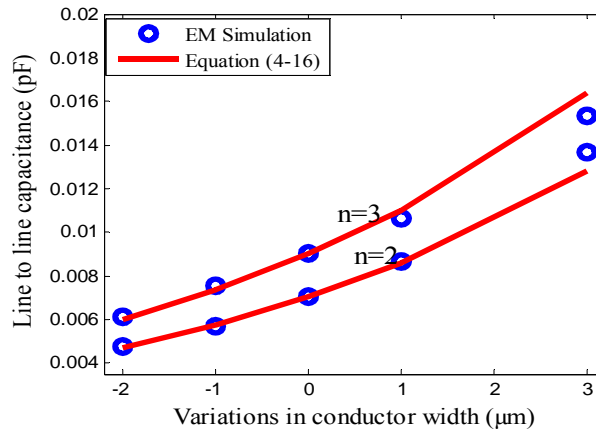
Figure 4- 38: Line to line capacitance versus conductor line width for inductors
having w_n= 5 µm, s= 5 µm and t= 2 µm calculated using EM simulation and Equation
(4-16).
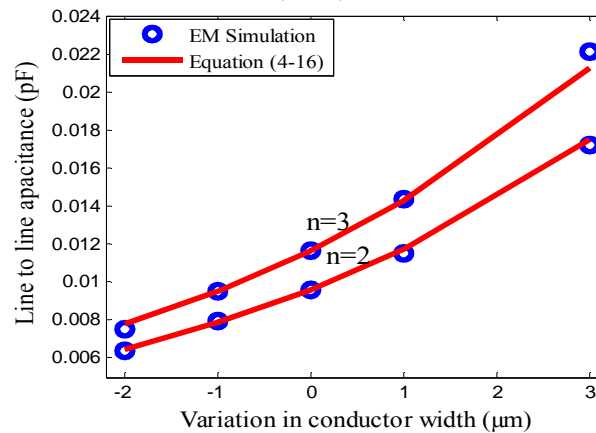
Figure 4- 39: Line to line capacitance versus conductor line width for inductors
having w_n= 5 µm, s= 5 µm and t= 3 µm calculated using EM simulation and Equation
(4-16).

Figures 4-40 to Figure 4-42 compare the line to line capacitance for sets of turns inductors having n=2 and 3turns, $w_n = 10$ μm, $s_n= 5$ μm extracted using the electromagnetic simulation and estimated using Equation (4-16) for t= 1 μm ,2 μm,3 μm respectively.
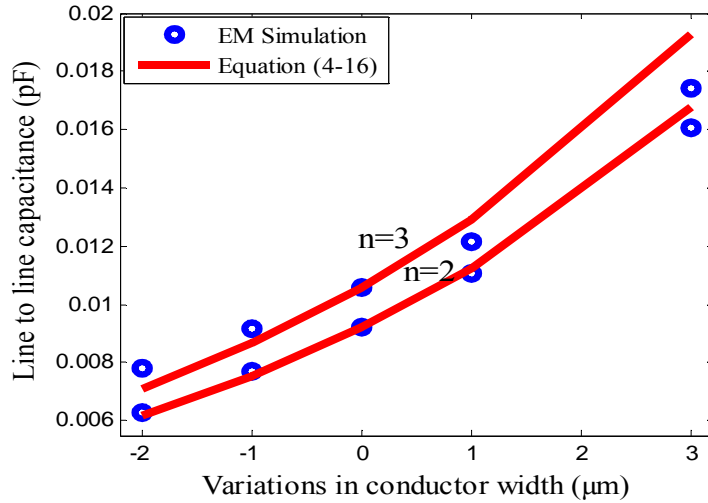
Figure 4- 40: Line to line capacitance versus conductor line width for inductors having w_n= 10μm, s= 5 μm and t= 1 μm calculated using EM simulation and Equation (4-16).
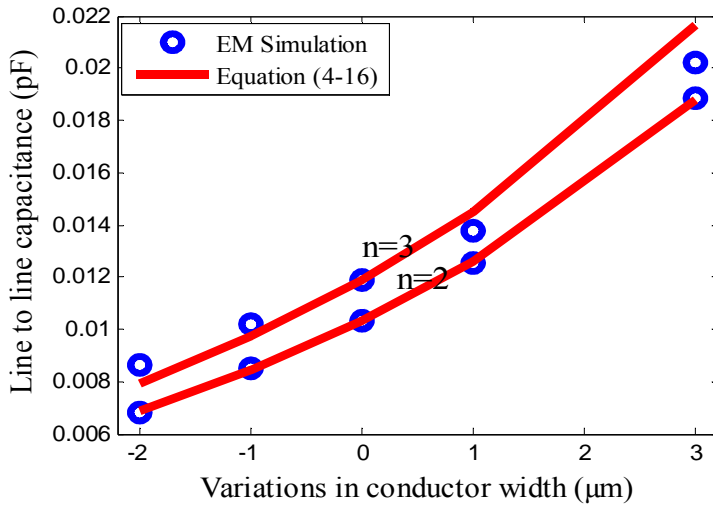
Figure 4- 41: Line to line capacitance versus conductor line width for inductors having w_n= 10 μm, s= 5 μm and t= 2 μm calculated using EM simulation and Equation (4-16).
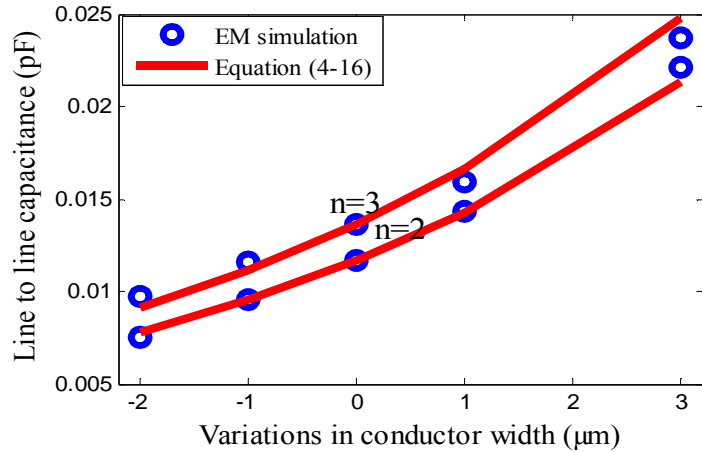
Figure 4- 42: Line to line capacitance versus conductor line width for inductors having w_n= 10 µm, s= 5 µm and t= 3 µm calculated using EM simulation and Equation (4-16).

Figure 4-43 displays the line to line capacitance extracted using the electromagnetic simulation and Equation (4-16) for sets of inductors having n=2 and 3 turns, w_n=10 µm, s_n 10 µm and t= 2 µm.
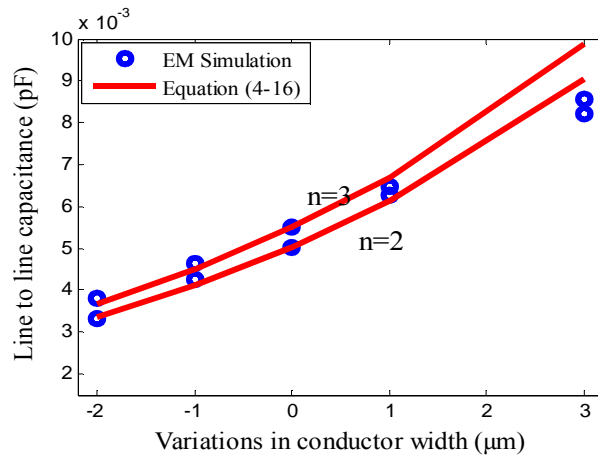
Figure 4- 43: Line to line capacitance versus conductor line width for inductors having w_n= 10 µm, s= 10 µm and t= 2 µm calculated using EM simulation and Equation (4-16).

4.7 Capacitance between the spiral in the substrate

The simulation results show that the variation in the conductor line width has little or no effect on the capacitance between the substrate and the spiral and this capacitance doesn't change when the conductor line width is varied. This can be observed from Figure 4-44 which shows the substrate capacitance versus conductor line width for some of sets of inductor simulated.
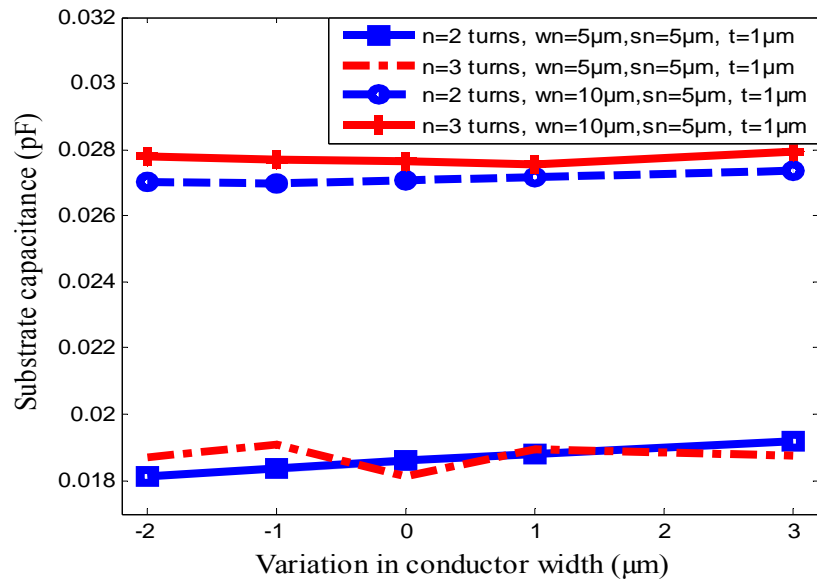
Figure 4- 44: substrate capacitance versus the conductor line width for inductors with different dimensions.

CHAPTER 5

CONCLUSION AND RECOMMENDATIONS

5.1   Conclusion

The dimensions of planar spiral inductor can vary the during its fabrication process. Variations in the conductor line width affect every element in the equivalent circuit model of the inductor i.e. the series inductance, the series resistance and the capacitance between the inductor turns. This research investigated these effects and the following are the main findings:

The change in the inductance due to the variations in the conductor line width is nearly a linear function of the nominal inductance and nominal conductor line width. Furthermore, this change is independent of the inductor dimensions such as nominal spacing between conductors, number of turns and conductor thickness.

An empirical formula to calculate the series inductance including the effects of conductor line width, Equation (4-5), is proposed with percentage error less than 10%,

The variation in the series resistance due to the variations in the conductor line width is an exponential function of the nominal resistance, nominal conductor line width. Furthermore, this variation is independent on nominal spacing between conductors, number of turns and conductor thickness.

An empirical formula to estimate the resistance including the effects of the variations in the conductor line width with , Equation (4-9), is proposed with percentage error not more than 3% for the small conductor line width variations (-1µm and +1 µm) and 13% for a large amount of conductor line width variations(-2µm and +3 µm).

The change in the line to line capacitance due to the variations in the conductor line width is an exponential function of the nominal line to line capacitance, nominal spacing. Furthermore, this change is independent on nominal conductor line width and number of turns and conductor thickness.

An empirical formula to calculate the series line to line capacitance including the effects of the variations in the conductor line width, Equation (4-16), is proposed with less than 10% for the small conductor line width variations (-1µm and +1 µm) and less than 20% for a large amount of conductor line width variations (-2µm and +3 µm).

Finally, the variations in the conductor line width have no or little effects on substrate capacitance.

The proposed empirical formulae has been validated for Gallium Arsenide based rectangular inductors with gold conductor having nominal conductor line width = 5µm ,7 µm , 9 µm and 10 µm, number of turns 1 - 4 turns, conductor thickness 1 - 3 µm and conductor spacing 5 µm ,6 µm,7 µm, 8 µm and 10 µm. These dimensions are typical for RFIC and MMIC applications.

The proposed formulae provide a quick estimation for the inductor model parameters including the effects of the variations in conductor line width if the nominal values are defined. This is advantageous to the RFIC's designer since the nominal inductor circuit model can easily be modified to account for these variations and especially helpful during circuit design optimization.

5.2 **Recommendations**

To investigate the effects of the variations in inductor geometry on the model parameters of silicon based planar spiral inductors.

To investigate the effects of the variations in inductor geometry on the model parameters of circular planar spiral inductors.

REFERENCES

[1] A. M Niknejad., M Chan , C Hu., B Brodersen., J. Xi, J He., S. Emami, C. Doan, Y. Cao, P Su., H. Wan, M. Dunga, C. H. Lin, " Compact Modeling for RF and Microwave Integrated Circuits", Technical Proceedings of the 2005 Workshop on Compact Modeling, pp. 339 – 342, 2005.

[2] Niknejad A. M., "Analysis Simulation, and Applications of Passive Devices on Conductive Substrates", PhD Thesis, University of California at Berkeley, 2000.

[3] Yue C. P., and S. S. Wong, "Physical Modeling of Spiral Inductors on Silicon", IEEE transactions on electron devices, Vol. 47, no. 3, March 2000, pp.560-568.

[4] K. Nikellis and N. Uzunoglu, "Full-wave modeling of stripline structures in multilayer dielectrics" Progress In Electromagnetics Research, PIER 57, 2006, pp.253–264.

[5] S. S. Mohan, "The design, modeling and optimization of on-chip inductor and transformer circuits", PhD dissertation, Bell & Howell information and Learning Company, 2000.

[6] C. S. Salimath, "Design of CMOS LC voltage controlled oscillators", Master Thesis, The Department of Electrical and Computer Engineering, Agricultural and Mechanical College, December 2006.

[7] S. Tang, Y. Shi, Tianxing, "A Novel Structure of Non-planar RF Spiral Inductor Based on Silicon", IEEE, Solid state and integrated circuit Technology 8th international conference, Oct. 2006, pp. 269-271.

[8] T. H., Bui "Design and Optimization of a 10 nH Square-Spiral Inductor for Si RF Ics", Master Thesis, department of Electrical and Computer Engineering, University of North Carolina at Charlotte,1999

[9]   Y. K. Koutsoyannopoulos and Y. Papananos, "Systematic Analysis and Modeling of Integrated Inductors and Transformers in RF IC Design" Analog and Digital Signal Processing, IEEE Transactions on Circuits and Systems II, Vol. 47, No, 8 August 2000, pp.699-711.

[10]   X. Qi, A. Gyure, Y. Luo, S. C. Lo, M. Shahram, and S. Kishore, "Measurement and Characterization of Pattern Dependent Process Variations of Interconnect Resistance, Capacitance and Inductance in Nanometer Technologies", Proceedings of the 16th ACM Great Lakes symposium on VLSI, Philadelphia, PA, USA, 2006, pp. 14 - 18.

[11]   Nieuwoudt, and Y. Massoud, "Variability-Aware Multilevel Integrated Spiral Inductor Synthesis," IEEE Transactions on Computer Aided Design of Integrated Circuits, vol. 25, No. 12, December 2006, pp. 2613-2625.

[12]   R. Nassif, "Modeling and Forecasting of Manufacturing Variations", 5th International Workshop on Statistical Metrology, Honolulu, HI, USA, 2000, pp.2-10.

[13]   R. William, modern GaAs processing technique, 2th ed. Artech House .Inc, 1990, pp.115-151.

[14]   Leong S., "Design, Optimization of RF Spiral Inductors Using Scalable Compact and Accurate Models", Analog Integrated Circuits and Signal Processing vol. 37, 2003, pp.165–177

[15]   ADS 2006A, Computer software, Agilent Technologies, Sept 28 2006.

[16]   I. Bahl, lumped element for RF and microwave circuits, Artech House, 2003, pp 17-87.

[17]   Yue C. P., Ryu C., Lau J., Lee T. H., Wong S. S., "A Physical Model for Planar Spiral Inductors on Silicon". IEEE International Electron Devices Meeting, 1996 ,pp. 155-158.

[18]   https://www.cst.com/Content/Applications/Article/Spiral+Inductor

[19]   L. F. Jr, N. P., and L. C. Kretly, "RF Integrated Inductor: Improving Q-Factor with Double Ground Shield for BiCMOS Technology", ICMMT 2008 International Conference on Microwave and Millimeter Wave Technology, Nanjing, April, 2008, PP. 580-583.

[20]   G. W. Dahlmann, E. M. Yeatman, P. Young , I. D. Robertson, S. Lucyszyn, "High Q Achieved in Microwave Inductors Fabricated by Parallel Self-Assembly" ,http://www.imperial.ac.uk/pls/portallive/docs/1/353904.PDF

[21]   S. S. Mohan, M. D. Hershenson, S. P. Boyd, and T. H. Lee, "Simple Accurate Expressions for Planar Spiral Inductances", IEEE Journal of solid-state circuits, Vol. 34, NO. 10, October 1999, pp.1419-1424.

[22]   M. J. Uddin, A. N. Nordin, M. I. Ibrahimy, M. B. I. Reaz, T. Z. A. Zulkifli, M. A. Hasan, "Design and Simulation of RF-CMOS Spiral Inductors for ISM Band RFID Reader Circuits", http://www.rmicusm.org/userfiles/file/Thesis/IIU_RFID.pdf

[23]   S. Pan J, L Li., W .Yin. and W. Y, "Performance trends of on-chip spiral Inductors for RFICS", Progress In Electromagnetic Research, PIER 45, 2004, pp.123–151

[24]   N. A. Talwalkar, C. P. Yue, and S. S. Wong, "Analysis and Synthesis of On-Chip Spiral Inductors", IEEE transactions on electron devices, Vol. 52, NO.2, February 2005, pp.176-182.

[25]   B. Fateh, "Modeling, Simulation and Optimization of a Microcoil for MRI-Cell Imaging", Master Thesis, Institute for Microsystem Technology IMTEK, Laboratory for Simulation, Albert-Ludwigs-University of Freiburg, Germany, 2006.

[26]   P. P. Shaha, R. K. Kamat, G. G. Tengashe., and S. R. Sawant, "Skin Effect Losses Calculations for Half Bridge Converter Using Fuzzy Logic", Old City Publishing, Inc, J. of Active and Passive Electronic Devices, Vol. 2, pp. 323–330, 2007.

[27]   H. Huang, "Depth of investigation for small broadband electromagnetic sensors", Geophysics", Vol. 70, NO. 6, November-December 2005, pp. G135–G142.

[28]   K. Rastogi and. Mishra .S, "Coplanar waveguide characterization with thick metal coating", International Journal of Infrared and Millimeter Waves, Vol. 20, No. 3, 1999.

[29]   W.B. Kuhn and N. M. Ibrahim, "Analysis of Current Crowding   Effects in Multi turn Spiral Inductors", Vol. 49, No. 1, January 2001,pp. 31-38.

[30]   A. Nieuwoudt and Y. Massoud, "Predicting the Performance of Low-Loss On-Chip Inductors Realized Using Carbon Nanotube Bundles" IEEE Transactions on electron devices, Vol. 55, No. 1, Jan 2008, pp.298-312.

[31]   S. J. Harrold, An introduction to GaAs IC design, New York: Prentice Hall Prentice Hall, 1993.

[32]   Jan Van Hese, "Accurate Modeling of Spiral Inductors on Silicon for Wireless RF IC designs", http://cp.literature.agilent.com/litweb/pdf/5989-9044EN.pdf

[33]   J. Peters, "Design of High Quality Factor Spiral Inductors in RF MCM-D", Master Thesis, Department of Electrical Engineering and Computer Science,

Massachusetts Institute of Technology, 2004.

[34]   Sonnet Software, Release 12, N. Syracuse, Computer software, NY 13212, 3 April 2009.

[35]   Kythakyapuzha S. R., "Modeling of spiral inductors and transformers" Master Thesis, Department of Electrical Engineering and Computer Engineering, Kansas state University, 1995.

[36]   R.Woltjer, L.Tiemeijer and D.Klaassen, "An industrial view on compact modeling, "IEEE Solid-State Device Research Conference, Vol 19, Sept. 2006,pp.41-48.

[37]   K.Obeidat, "Design and Characterization of Multi-Layer Coplanar Waveguide Baluns and Inductors", Master Thesis, Department of Electrical Engineering, University of South Florida, 2003.

[38]   J.Crols, P.Kinget, J.Craninckx and M.Steyaert., "An Analytical Model of Planar Inductors on Lowly Doped Silicon Substrates for High Frequency Analog Design up to 3 GHz", IEEE, VLSI Circuits Digest of Technical Papers Symposium, Vol . 13, Jun, 1996, PP.28 – 29.

[39]   K.Christensen and T.Jrgensen , "easy simulation and design of on-chips in standard CMOS processes", ISCAS '98. Proceedings of the 1998 IEEE International Symposium on Circuits and Systems, Monterey, CA, USA, May 1998, pp. 360 – 364.

[40]   H. M .Greenhouse., "Design of Planar Rectangular Microelectronic Inductor ", IEEE transactions on parts, hybrids, and packaging, Vol. php-10, no. 2, ,

June 1974, pp.101-109.

[41]   S Jenei,J. B. K, C. Nauwelaers., and S. Decoutere., "Physics-Based Closed-Form Inductance Expression for Compact Modeling of Integrated Spiral Inductors", IEEE Journal of solid-state circuits, Vol. 37, No. 1, January 2002,pp.71-80.

[42]   H..Ronkainen ,H.Kattelu, E.Tarvainen,T. Riihisaari , M.Andersson, P.Kuivalainen, "IC compatible planar inductors on silicon", IEE Proc.-Circuits Devices Syst., Vol. 144, No. 1,February 1997, pp.29-35.

[43]   J.C Rautio, and V. Demir, "Microstrip Conductor Loss Models for Electromagnetic Analysis", IEEE Transactions on Microwave theory and techniques, Vol. 51, No. 3, pp .915-921, MARCH 2003.

[44]   M. Raieszadeh, P. Monajemi, S.Yoon , J.Lash-ur, and F. Ayuzi , "High-Q Integrated inductors on trenched silicon islands", Master thesis , School of Electrical and Computer Engineering, Georgia Institute of Technology, April 2005.

[45]   M. Zadeh, J.R. Laskar, and ,F .Ayazi, "High Performance Inductors on CMOS-Grade Trenched Silicon Substrate", IEEE Transactions on components and packaging technologies, Vol. 31, no. 00, 2008, pp. 126-134.

[46]   C. Yue, C. Ryu, Jack Lau, T. H. Lee, and S. S. Wong, "A physical model for   planar   spiral   inductors   on   silicon",   http://www-smirc.stanford.edu/papers/IEDM96p-cpyue.pdf.

[47]   C. P. Yue, On-chip spiral inductors for silicon-based radio-frequency integrated circuits, Ph.D. dissertation, Stanford University, Department of Electrical Engineering, July 1998

[48] N. D. Arora, "Modeling and Characterization of Copper Interconnects for So
      Design", SISPAD 2003 International Conference on Simulation
      Semiconductor Processes and Devices, Boston Marriott Cambridge, Cambridg
      , MA , USA, Sept 2003. pp 1- 6.

[49] S. R. Nassif, D. Boning, and N. Hakim, "The Care and Feeding of you
      Statistical Static Timer", ICCAD-2004. IEEE/ACM International Conferenc
      on Computer Aided Design, 2004, pp. 138- 139.

[50] S. R. Nassif , "Modeling and Analysis of Manufacturing Variations
      Proceedings of the 2007 IEEE/ACM international conference on Compute
      aided design, 2001, pp.223-228.

[51] Stefan Stalf, Thomson Multimedia, Villingen, Germany, "Printed inductors
      RF   consumer applications", Vol. 47, No. 3, August 2001, pp.426-439

[52] C.K. Liu, P.L. Cheng, S.Y.Y. Leug D.C.C. Lam , Inductance Tolerance
      Analyses and Design –process Map of Embedded Planar Spiral Inductor ,
      Proceedings. 54th in Electronic Components and Technology Conference,
      2004. Vol.1,1 - 4 June 2004. pp.1108-1112.

[53] J. C. Rautio and R. F. Harrington, "An Electromagnetic Time-Harmonic
      Analysis of Shielded Microstrip Circuits," IEEE Trans. Microwave Theory
      Tech., Vol. MTT-35, pp. 726-730, Aug. 1987.

[54] H. E. Green, "The Numerical Solution of Some Important Transmission-Line
      Problems", lEEE Transactions on Microwave theory and techniques, Vol.
      MTT-13, no. 5, September, 1965, pp. 676-692.

[55] R. Garg, Analytical and computational methods in Electromagnetics, Artech

House, London, 2009, pp 212-216.

[56] .H. A. Wheeler, Formulas for the Skin Effect, Proceedings of the IRE Vol 30, Sept 1942, pp.412- 424.

[57] R. A. Pucel, J Masse and C. P Hartwig, "Losses in microstrip", IEEE Transactions on Microwave theory and techniques, Vol. MTT-16, No. June 1968, pp. 342-350.

[58] R. Garg and I. J. Bahl, "Characteristics of Coupled Microstriplines", IEEE Transactions on Microwave theory and techniques, Vol. MIT-27, no. 7, July 1979, pp.700-705.

[59] M. Danesh, Monolithic Inductors for Silicon Radio Frequency Integrated Circuits, Master Thesis, University of Toronto, Department of Electrical and Computer Engineering, 1999.

APPENDICES

Appendix A: Simulated inductors set.

Simulates inductors with nominal conductor line width w=5 micron; conductor thickness t=1 micron and nominal spacing =5 micron.

No	No. of turns (n)	Conductor Width (w μm)	Side1 Length (L1 μm)	Side2 Length (L2 μm)	Conductor thickness (t μm)	Spacing (S μm)	Description	Set .No	Total time for all frequencies (hour)
1	1	5	120	110	1	5	Nominal		0.124
2	1	4	120	110	1	6	Δw= -1 μm		0.116
3	1	3	120	110	1	7	Δw= -2 μm	Set1	0.113
4	1	6	120	110	1	4	Δw= +1 μm		0.122
5	1	8	120	110	1	2	Δw= +3 μm		0.200
6	2	5	120	110	1	5	Nominal		0.223
7	2	4	120	110	1	6	Δw= -1 μm		0.188
8	2	3	120	110	1	7	Δw= -2 μm	Set2	0.185
9	2	6	120	110	1	4	Δw= +1 μm		0.235
10	2	8	120	110	1	2	Δw= +3 μm		0.255
11	3	5	120	110	1	5	Nominal		0.403
12	3	4	120	110	1	6	Δw= -1 μm		0.312
13	3	3	120	110	1	7	Δw= -2 μm	Set3	0.333
14	3	6	120	110	1	4	Δw= +1 μm		0.423
15	3	8	120	110	1	2	Δw= +3 μm		0.471
16	4	5	120	110	1	5	Nominal		0.668
17	4	4	120	110	1	6	Δw= -1 μm		0.485
18	4	3	120	110	1	7	Δw= -2 μm	Set4	0.549
19	4	6	120	110	1	4	Δw= +1 μm		0.700
20	4	8	120	110	1	2	Δw= +3 μm		0.773

Simulated inductors with nominal conductor line width w=5 micron; conductor thickness t=2 micron and nominal spacing =5 micron.

No	No of turns (n)	Conductor Width (w μm)	Side1 Length (L1 μm)	Side2 Length (L2 μm)	Conductor thickness (t μm)	Spacing (S μm)	Description		Total time for all frequencies (hour)
21	1	5	120	110	2	5	Nominal		0.49
22	1	4	120	110	2	6	Δw= -1 μm		0.434
23	1	3	120	110	2	7	Δw= -2 μm	Set5	0.423
24	1	6	120	110	2	4	Δw= +1 μm		0.487
25	1	8	120	110	2	2	Δw= +3 μm		0.507
26	2	5	120	110	2	5	Nominal		1.10
27	2	4	120	110	2	6	Δw= -1 μm		0.89
28	2	3	120	110	2	7	Δw= -2 μm	Set6	0.921
29	2	6	120	110	2	4	Δw= +1 μm		1.133
30	2	8	120	110	2	2	Δw= +3 μm		1.2
31	3	5	120	110	2	5	Nominal		2.366
32	3	4	120	110	2	6	Δw= -1 μm		1.75
33	3	3	120	110	2	7	Δw= -2 μm	Set7	2.01
34	3	6	120	110	2	4	Δw= +1 μm		2.416
35	3	8	120	110	2	2	Δw= +3 μm		2.566
36	4	5	120	110	2	5	Nominal		6.383
37	4	4	120	110	2	6	Δw= -1 μm		4.966
38	4	3	120	110	2	7	Δw= -2 μm	Set8	5.566
39	4	6	120	110	2	4	Δw= +1 μm		6.500
40	4	8	120	110	2	2	Δw= +3 μm		6.733

Simulated inductors with nominal conductor line width w=5 micron; conductor thickness t=3 micron and spacing =5 micron.

No	No of turns (n)	Conductor Width (w μm)	Side1 Length (L1 μm)	Side2 Length (L2 μm)	Conductor thickness (t μm)	Spacing (S μm)	Description		Total time for all frequencies (hour)
41	1	5	120	110	3	5	Nominal		1.116
42	1	4	120	110	3	6	Δw= -1 μm		1
43	1	3	120	110	3	7	Δw= -2 μm	Set9	1
44	1	6	120	110	3	4	Δw= +1μm		1.15
45	1	8	120	110	3	2	Δw= +3μm		1.216
46	2	5	120	110	3	5	Nominal		3.066
47	2	4	120	110	3	6	Δw= -1μm		2.400
48	2	3	120	110	3	7	Δw= -2μm	Set10	2.583
49	2	6	120	110	3	4	Δw= +1μm		3.166
50	2	8	120	110	3	2	Δw= +3μm		3.466
51	3	5	120	110	3	5	Nominal		10.766
52	3	4	120	110	3	6	Δw= -1μm		8.566
53	3	3	120	110	3	7	Δw= -2μm	Set11	9.500
54	3	6	120	110	3	4	Δw= +1μm		10.983
55	3	8	120	110	3	2	Δw= +3μm		12.1
56	4	5	120	110	3	5	Nominal		17.750
57	4	4	120	110	3	6	Δw= -1μm		13.633
58	4	3	120	110	3	7	Δw= -2μm	Set12	15.55
59	4	6	120	110	3	4	Δw= +1μm		17.86
60	4	8	120	110	3	2	Δw= +3μm		20.366

Simulated inductors with nominal conductor line width w=10 micron; conductor thickness t=1 micron and nominal spacing =5 micron.

No	No of turns (n)	Conductor Width (w μm)	Side1 Length (L1 μm)	Side2 Length (L2 μm)	Conductor thickness (t μm)	Spacing (S μm)	Description		Total time for all frequencies (hour)
61	1	10	150	140	1	5	Nominal	Set13	15.012
62	1	9	150	140	1	6	Δw= -1μm		16.008
63	1	8	150	140	1	7	Δw= -2 μm		28.015
64	1	11	150	140	1	4	Δw= +1 μm		16.006
65	1	13	150	140	1	2	Δw= +3 μm		18.001
66	2	10	150	140	1	5	Nominal	Set14	33.316
67	2	9	150	140	1	6	Δw= -1 μm		32.002
68	2	8	150	140	1	7	Δw= -2 μm		28.015
69	2	11	150	140	1	4	Δw= +1 μm		33.005
70	2	13	150	140	1	2	Δw= +3 μm		36.003
71	3	10	150	140	1	5	Nominal	Set15	1.000
72	3	9	150	140	1	6	Δw= -1 μm		1.000
73	3	8	150	140	1	7	Δw= -2 μm		53.0116
74	3	11	150	140	1	4	Δw= +1 μm		1.000
75	3	13	150	140	1	2	Δw= +3 μm		1.003
76	4	10	150	140	1	5	Nominal	Set16	1.0127
77	4	9	150	140	1	6	Δw= -1 μm		1.0119
78	4	8	150	140	1	7	Δw= -2 μm		1.0127
79	4	11	150	140	1	4	Δw= +1 μm		1.0125
80	4	13	150	140	1	2	Δw= +3 μm		1.0155

Simulated inductors with nominal conductor line width w=10 micron; conductor thickness t=2 micron and nominal spacing =5 micron.

No	No of turns (n)	Conductor Width (w μm)	Side1 Length (L1 μm)	Side2 Length (L2 μm)	Conductor thickness (t μm)	Spacing (S μm)	Description		Total time for all frequencies (hour)
81	1	10	150	140	2	5	Nominal		59.000
82	1	9	150	140	2	6	Δw= -1 μm		1.001
83	1	8	150	140	2	7	Δw= -2 μm	Set17	1.000
84	1	11	150	140	2	4	Δw= +1 μm		1.0013
85	1	13	150	140	2	2	Δw= +3 μm		1.003
86	2	10	150	140	2	5	Nominal		2.550
87	2	9	150	140	2	6	Δw= -1 μm		2.500
88	2	8	150	140	2	7	Δw= -2 μm	Set18	2.316
89	2	11	150	140	2	4	Δw= +1 μm		2.500
90	2	13	150	140	2	2	Δw= +3 μm		2.700
91	3	10	150	140	2	5	Nominal		8.850
92	3	9	150	140	2	6	Δw= -1 μm		8.716
93	3	8	150	140	2	7	Δw= -2 μm	Set19	5.000
94	3	11	150	140	2	4	Δw= +1 μm		8.733
95	3	13	150	140	2	2	Δw= +3 μm		9.500
96	4	10	150	140	2	5	Nominal		13.650
97	4	9	150	140	2	6	Δw= -1 μm		13.833
98	4	8	150	140	2	7	Δw= -2 μm	Set20	14.266
99	4	11	150	140	2	4	Δw= +1 μm		13.633
100	4	13	150	140	2	2	Δw= +3 μm		14.650

Simulated inductors with nominal conductor line width w=10 micron; conductor thickness t=3 micron and nominal spacing =5 micron.

No	No of turns (n)	Conductor Width (w μm)	Side1 Length (L1 μm)	Side2 Length (L2 μm)	Conductor thickness (t μm)	Spacing (S μm)	Description		Total time for all frequencies (hour)
101	1	10	150	140	3	5	Nominal		2.333
102	1	9	150	140	3	6	Δw= -1 μm	Set21	2.600
103	1	8	150	140	3	7	Δw= -2 μm		2.500
104	1	11	150	140	3	4	Δw= +1 μm		2.616
105	1	13	150	140	3	2	Δw= +3 μm		2.500
106	2	10	150	140	3	5	Nominal		17.283
107	2	9	150	140	3	6	Δw= -1 μm	Set22	12.200
108	2	8	150	140	3	7	Δw= -2 μm		11.716
109	2	11	150	140	3	4	Δw= +1 μm		12.166
110	2	13	150	140	3	2	Δw= +3 μm		10.783
111	3	10	150	140	3	5	Nominal		22.400
112	3	9	150	140	3	6	Δw= -1 μm	Set23	22.016
113	3	8	150	140	3	7	Δw= -2 μm		21.166
114	3	11	150	140	3	4	Δw= +1 μm		22.000
115	3	13	150	140	3	2	Δw= +3 μm		20.300
116	4	10	150	140	3	5	Nominal		36.800
117	4	9	150	140	3	6	Δw= -1 μm	Set24	37.616
118	4	8	150	140	3	7	Δw= -2 μm		38.433
119	4	11	150	140	3	4	Δw= +1 μm		30.700
120	4	13	150	140	3	2	Δw= +3 μm		32.466

Simulated inductors with nominal conductor line width w=10 micron; conductor thickness t=2 micron and nominal spacing s=10 micron.

No	No of turns (n)	Conductor Width (w μm)	Side1 Length (L1 μm)	Side2 Length (L2 μm)	Conductor thickness (t μm)	Spacing (S μm)	Description		Total time for all frequencies (hour)
121	2	10	150	140	2	10	Nominal		1.500
122	2	9	150	140	2	11	Δw= -1 μm	Set25	1.500
123	2	8	150	140	2	12	Δw= -2 μm		1.366
124	2	11	150	140	2	9	Δw= +1 μm		1.500
125	2	13	150	140	2	7	Δw= +3 μm		1.616
126	3	10	150	140	2	10	Nominal		3.066
127	3	9	150	140	2	11	Δw= -1 μm	Set26	2.966
128	3	8	150	140	2	12	Δw= -2 μm		2.766
129	3	11	150	140	2	9	Δw= +1 μm		3.033
130	3	13	150	140	2	7	Δw= +3 μm		5.850

Simulated inductors with nominal conductor line width w=10 micron; conductor thickness t=3 micron and nominal spacing s=5 micron.

No	No of turns (n)	Conductor Width (w μm)	Side1 Length (L1 μm)	Side2 Length (L2 μm)	Conductor thickness (t μm)	Spacing (S μm)	Description		Total time for all frequencies (hour)
131	3	10	120	110	3	5	Nominal		
131	3	9	120	110	3	6	Δw= -1 μm	Set27	
132	3	8	120	110	3	7	Δw= -2 μm		
133	3	11	120	110	3	4	Δw= +1 μm		
135	3	13	120	110	3	2	Δw= +3 μm		

Table 1Simulated inductors with nominal conductor line width wn=9 micron; conductor thickness t=3 micron and nominal spacing Sn=5 micron

No	No of turns (n)	Conductor Width (w μm)	Side1 Length (L1 μm)	Side2 Length (L2 μm)	Conductor thickness (t μm)	Spacing (S μm)	Description		Total time for all frequencies (hour)
131	3	9	120	110	3	5	Nominal	Set27	
131	3	8	120	110	3	6	Δw= -1 μm		
132	3	7	120	110	3	7	Δw= -2 μm		
133	3	10	120	110	3	4	Δw= +1 μm		
135	3	12	120	110	3	2	Δw= +3 μm		

Simulated inductors with nominal conductor line width w=7 micron; conductor thickness t=3 micron and nominal spacing s=5 micron

No	No of turns (n)	Conductor Width (w μm)	Side1 Length (L1 μm)	Side2 Length (L2 μm)	Conductor thickness (t μm)	Spacing (S μm)	Description		Total time for all frequencies (hour)
131	3	7	120	110	3	5	Nominal	Set27	
131	3	6	120	110	3	6	Δw= -1 μm		
132	3	5	120	110	3	7	Δw= -2 μm		
133	3	8	120	110	3	4	Δw= +1 μm		
135	3	10	120	110	3	2	Δw= +3 μm		

Simulated inductors with nominal conductor line width w=10 micron; conductor thickness t=2 micron and nominal spacing s=7 micron

No	No of turns (n)	Conductor Width (w μm)	Side1 Length (L1 μm)	Side2 Length (L2 μm)	Conductor thickness (t μm)	Spacing (S μm)	Description		Total time for all frequencies (hour)
131	3	10	150	140	3	7	Nominal	Set27	
131	3	11	150	140	3	6	Δw= -1 μm		
132	3	12	150	140	3	5	Δw= -2 μm		
133	3	9	150	140	3	8	Δw= +1 μm		
135	3	7	150	140	3	10	Δw= +3 μm		

Simulated inductors with nominal conductor line width w=10 micron; conductor thickness t=2 micron and nominal spacing s=6micron

No	No of turns (n)	Conductor Width (w μm)	Side1 Length (L1 μm)	Side2 Length (L2 μm)	Conductor thickness (t μm)	Spacing (S μm)	Description		Total time for all frequencies (hour)
131	3	10	150	140	3	6	Nominal		
131	3	11	150	140	3	5	Δw= -1 μm	Set27	
132	3	12	150	140	3	4	Δw= -2 μm		
133	3	9	150	140	3	7	Δw= +1 μm		
135	3	7	150	140	3	9	Δw= +3 μm		

Simulated inductors with nominal conductor line width w=10 micron; conductor thickness t=2 micron and nominal spacing s=8 micron

No	No of turns (n)	Conductor Width (w μm)	Side1 Length (L1 μm)	Side2 Length (L2 μm)	Conductor thickness (t μm)	Spacing (S μm)	Description		Total time for all frequencies (hour)
131	3	10	150	140	3	8	Nominal		
131	3	11	150	140	3	7	Δw= -1 μm	Set27	
132	3	12	150	140	3	6	Δw= -2 μm		
133	3	9	150	140	3	9	Δw= +1 μm		
135	3	7	150	140	3	11	Δw= +3 μm		

Appendix B : S-parameters in smith chart for 4-turns inductor having w =10µm, s= 5 µm and t= 3µm
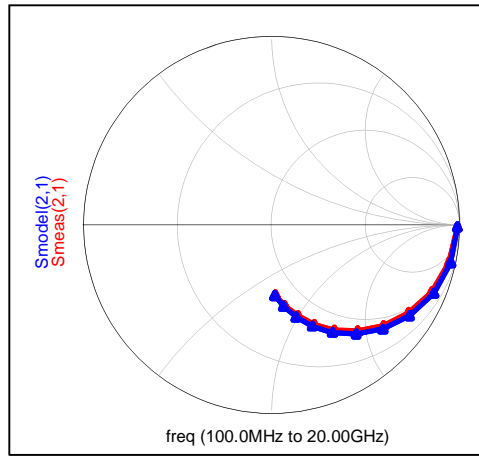
S21
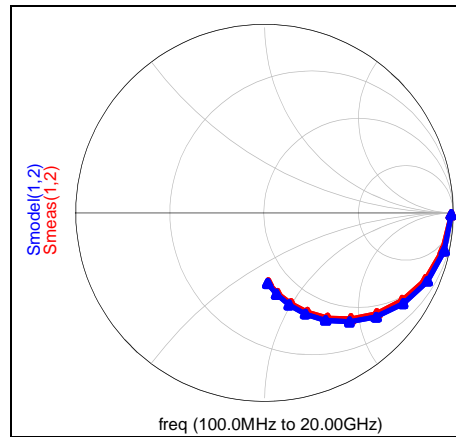
S12
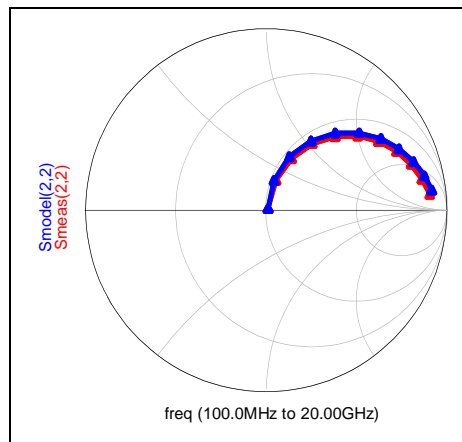
S22

Appendix C: S-parameters in dB chart for 4-turns inductor having w =10µm, s= 5 µm and t= 3µm
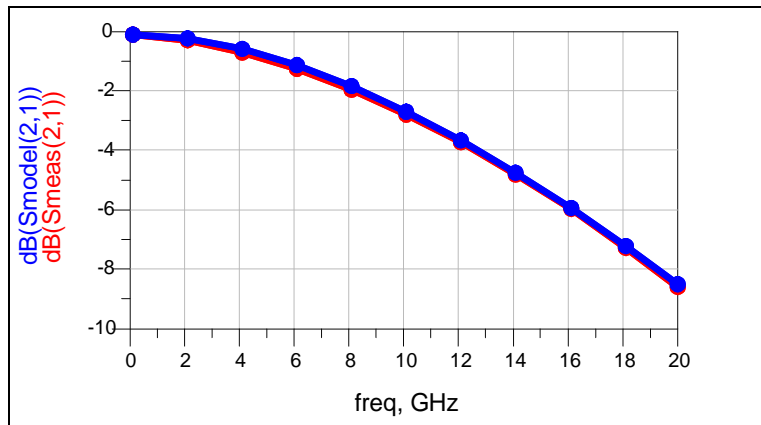
S21
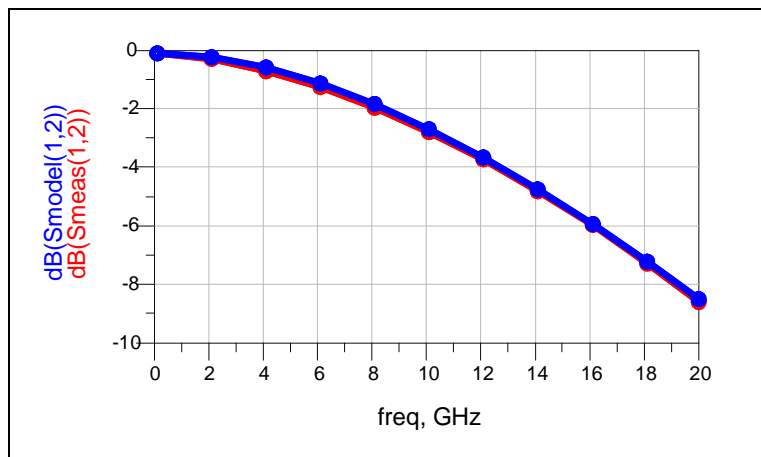
S12
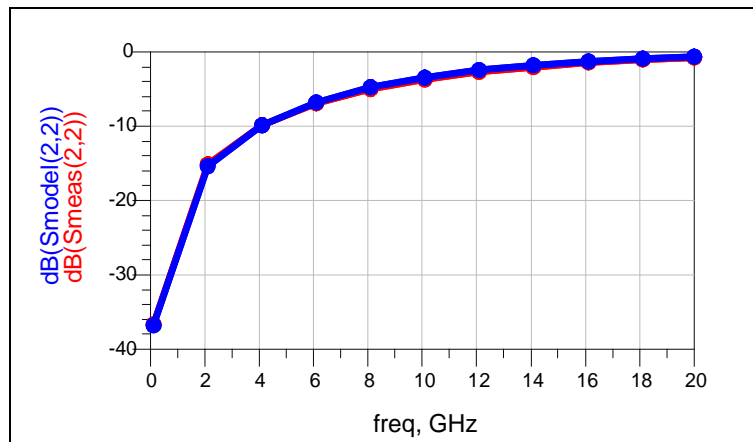
S22

Appendix D: S-parameters in phase chart for 4-turns inductor having w =10µm, s= 5 µm and t= 3µm
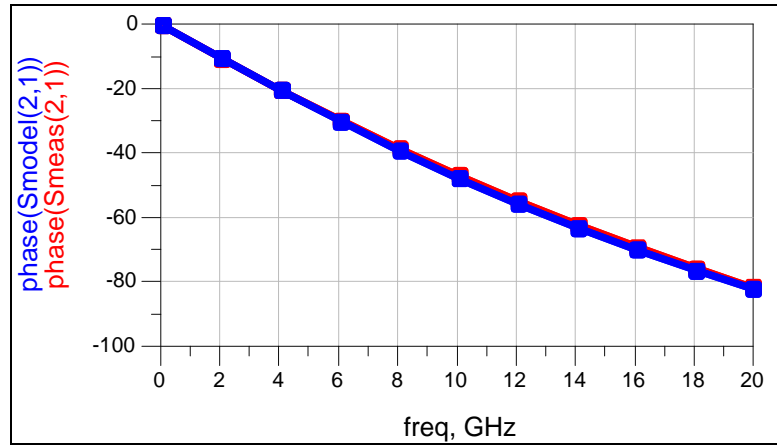
S21
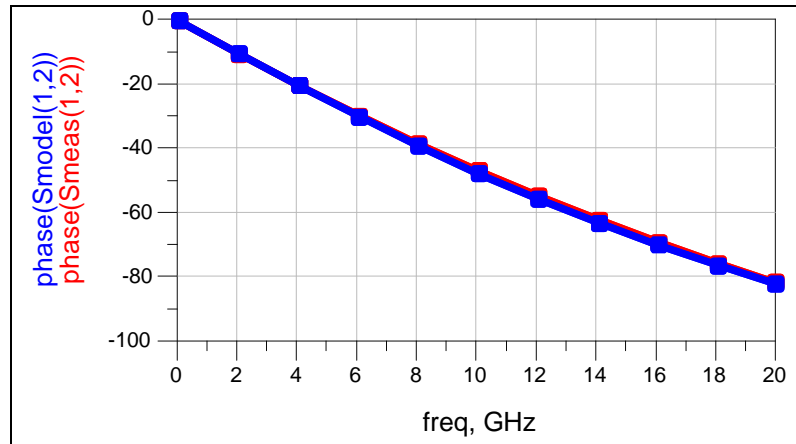
S12

S22

Appendix E: The convergence of model parameters using 2μm cell size and various number of sheets for inductor with w =10μm, s= 5 μm and t= 3μm and n=3.

2 sheet_2μm cell	
L	1.32728
R	2.9585
C	0.0104754
CG_1	0.323304
CG_2	0.0232605
4 sheet_2μm cell	
L	1.32368
R	3.00076
C	0.0103751
CG_1	0.0323192
CG_2	0.0231919
8 sheet_2μm cell	
L	1.32408
R	3.02086
C	0.0103615
CG_1	0.0323099
CG_2	0.0231802
12 sheet_2μm cell	
L	1.32476
R	3.0326
C	0.0103645
CG_1	0.0323068
CG_2	0.0231768
16 sheet_2μm cell	
L	1.32525
R	3.04171
C	0.0103664
CG_1	0.0323065
CG_2	0.0231769
20 sheet_2μm cell	
L	1.32558
R	3.0497
C	0.0103695
CG_1	0.0323084
CG_2	0.0231781

Appendix F: The convergence of model parameters using 1.5 µm cell size and various number of sheets for inductor with w =10µm, s= 5 µm and t= 3µm and n=3.

2 sheet_1.5 µm cell	
L	1.33558
R	3.07161
C	0.0100822
CG_1	0.032213
CG_2	0.0234044
4 sheet_1.5 µm cell	
L	1.33169
R	3.12833
C	0.00996258
CG_1	0.032196
CG_2	0.0233232
8 sheet_1.5 µm cell	
L	1.33238
R	3.15722
C	0.009938
CG_1	0.0321762
CG_2	0.0233002
12 sheet_1.5 µm cell	
L	1.33325
R	3.17187
C	0.00993782
CG_1	0.0321718
CG_2	0.0232965
16 sheet_1.5 µm cell	
L	1.33381
R	3.18225
C	0.009940
CG_1	0.0321699
CG_2	0.0232952
20 sheet_1.5 µm cell	
L	1.33423
R	3.1907
C	0.00994204
CG_1	0.0321697
CG_2	0.0232952

Appendix G: The convergence of model parameters using 1 µm cell size and various number of sheets for inductor with w =10µm, s= 5 µm and t= 3µm and n=3

Nominal_10um_gold_3t_t1_2sheet	
L	1.32551
R	2.94448
C	0.0107761
CG_1	0.0323958
CG_2	0.0231111
Nominal_10um_gold_3t_t1_4sheet	
L	1.31953
R	3.02644
C	0.0107745
CG_1	0.0323359
CG_2	0.0230461
Nominal_10um_gold_3t_t1_8sheet	
L	1.32016
R	3.09951
C	0.0107568
CG_1	0.0323158
CG_2	0.0230231
Nominal_10um_gold_3t_t1_12sheet	
L	1.32449
R	3.13553
C	0.0105613
CG_1	0.0322984
CG_2	0.0229497
Nominal_10um_gold_3t_t1_16sheet	
L	1.32523
R	3.10122
C	0.0105621
CG_1	0.0322989
CG_2	0.0229517
Nominal_10um_gold_3t_t1_20sheet	
L	1.322583
R	3.11068
C	0.010566
CG_1	0.0322972
CG_2	0.0229513

Appendix H: The convergence of model parameters using 0.5 μm cell size and various number of sheets for inductor with w =10μm, s= 5 μm and t= 3μm and n=3

Nominal_10um_gold_3t_t1_2sheet	
L	1.32426
R	2.9587
C	0.0109995
CG_1	0.032456
CG_2	0.0231295
Nominal_10um_gold_3t_t1_4sheet	
L	1.32574
R	3.03937
C	0.0107495
CG_1	0.0323028
CG_2	0.022931
Nominal_10um_gold_3t_t1_8sheet	
L	1.33037
R	3.07902
C	0.0107005
CG_1	0.0321604
CG_2	0.0227975
Nominal_10um_gold_3t_t1_12sheet	
L	1.33387
R	3.1187
C	0.0106686
CG_1	0.0321318
CG_2	0.0227764
Nominal_10um_gold_3t_t1_16sheet	
L	1.33539
R	3.13304
C	0.0106917
CG_1	0.0321088
CG_2	0.0227596
Nominal_10um_gold_3t_t1_20sheet	
L	1.33635
R	3.14277
C	0.017119
CG_1	0.0320987
CG_2	0.0227542

Appendix I: extracted model parameters values

w_n=5μm , s_n =5μm , t=1μm ,n=1				
Parameter	Δw= -2 μm	Δw= -2 μm	Nominal	Δw= +1 μm	Δw= +3 μm
L (nH)	0.38262	0.359281	0.3345505	0.321682	0.292724
R (ohm)	3.54372	2.65512	2.11043	1.74747	1.30366
C	6.0372E-12	8.68099E-10	0.000000025	1.02636E-10	0.000000025
C_{G1} (pF)	0.0160591	0.0166845	0.0168851	0.0174976	0.0181113
C_{G2} (pF)	0.0155004	0.016045	0.0164607	0.0169717	0.0175097

w_n=5μm , s_n =5μm , t=1μm ,n=2				
Parameter	Δw= -2 μm	Δw= -2 μm	Nominal	Δw= +1 μm	Δw= +3 μm
L (nH)	0.951095	0.902099	0.859532	0.822404	0.759044
R (ohm)	6.54599	4.88066	3.86763	3.20331	2.3768
C	0.00465377	0.00572904	0.00690103	0.00821645	0.012774
C_{G1} (pF)	0.0193209	0.0196872	0.0200033	0.0203112	0.20937
C_{G2} (pF)	0.0169494	0.017093	0.0172401	0.0173172	0.0174808

w_n=5μm , s_n =5μm , t=1μm ,n=3				
Parameter	Δw= -2 μm	Δw= -2 μm	Nominal	Δw= +1 μm	Δw= +3 μm
L (nH)	1.44456	1.41369	1.34757	1.28881	1.18532
R (ohm)	8.69703	6.60266	5.23266	4.32908	3.20287
C	0.00575796	0.00710976	0.00844592	0.00925163	0.0137213
C_{G1} (pF)	0.0212456	0.218165	0.2019357	0.0220597	0.222244
C_{G2} (pF)	0.0161689	0.0163712	0.016078	0.0158567	0.0152453

w_n=5μm , s_n =5μm , t=1μm ,n=4				
Parameter	Δw= -2 μm	Δw= -2 μm	Nominal	Δw= +1 μm	Δw= +3 μm
L (nH)	1.81967	1.78977	1.70238	1.62285	1.47527
R (ohm)	10.3198	7.85367	6.21503	5.13527	3.79471
C	0.00547157	0.006692	0.0079039	0.00914243	0.0123889
C_{G1} (pF)	0.022862	0.0234734	0.0234543	0.0234167	0.0231204
C_{G2} (pF)	0.0155707	0.0156272	0.0151627	0.0147667	0.0137106

wₙ=5μm , sₙ =5μm , t=2μm ,n=1				
Parameter	Δw= -2 μm	Δw= -2 μm	Nominal	Δw= +1 μm	Δw= +3 μm
L (nH)	0.363879	0.343586	0.320916	0.309636	0.282844
R (ohm)	1.7875	1.33926	1.06468	0.881751	0.658615
C	3.49395E-11	3.2519E-10	6.81684E-13	4.81873E-10	0.000000025
C_{G1} (pF)	0.0168447	0.0174119	0.0175421	0.01811095	0.0186476
C_{G2} (pF)	0.0160741	0.0165877	0.016975	0.0174254	0.0179168

wₙ=5μm , sₙ =5μm , t=2μm ,n=2				
Parameter	Δw= -2 μm	Δw= -2 μm	Nominal	Δw= +1 μm	Δw= +3 μm
L (nH)	0.915325	0.871941	0.832498	0.797253	0.735386
R (ohm)	3.28484	2.44719	1.93915	1.60686	1.19541
C	0.00473887	0.00572467	0.00703459	0.00863993	0.0136403
C_{G1} (pF)	0.0198048	0.201812	0.0204841	0.0207767	0.0213557
C_{G2} (pF)	0.0171718	0.0173453	0.0174873	0.0175523	0.0176495

wₙ=5μm , sₙ =5μm , t=2μm ,n=3				
Parameter	Δw= -2 μm	Δw= -2 μm	Nominal	Δw= +1 μm	Δw= +3 μm
L (nH)	1.39531	1.37002	1.30731	1.25009	1.1435
R (ohm)	4.3558	3.30405	2.61886	2.16819	1.60762
C	0.00613756	0.00753262	0.00900013	0.0106359	0.0153638
C_{G1} (pF)	0.0214519	0.220209	0.0221619	0.223103	0.0225217
C_{G2} (pF)	0.0160436	0.0162707	0.0160174	0.0158207	0.0152205

wₙ=5μm , sₙ =5μm , t=2μm ,n=4				
Parameter	Δw= -2 μm	Δw= -2 μm	Nominal	Δw= +1 μm	Δw= +3 μm
L (nH)	1.7608	1.73612	1.65143	1.57231	1.4202
R (ohm)	5.16199	3.92536	3.10719	2.56958	1.90348
C	0.00583126	0.00711789	0.00846134	0.00989983	0.0138235
C_{G1} (pF)	0.0229663	0.0235759	0.0235817	0.0235792	0.02334
C_{G2} (pF)	0.0153137	0.0154025	0.0149837	0.0146301	0.013607

	w_n=5μm , s_n =5μm , t=3μm ,n=1				
Parameter	Δw= -2 μm	Δw= -2 μm	Nominal	Δw= +1 μm	Δw= +3 μm
L (nH)	0.347887	0.329842	0.308927	0.299014	0.274215
R (ohm)	1.2004	0.899041	0.714707	0.591957	0.442421
C	0.000000025	3.47888E-11	9.0822E-14	0.000000025	2.89168E-12
C_{G1} (pF)	0.017379	0.0179032	0.0179969	0.0185506	0.0190609
C_{G2} (pF)	0.016438	0.0176927	0.0173133	0.0177363	0.0182257
	w_n=5μm , s_n =5μm , t=3μm ,n=2				
Parameter	Δw= -2 μm	Δw= -2 μm	Nominal	Δw= +1 μm	Δw= +3 μm
L (nH)	0.885312	0.843586	0.808663	0.775139	0.71536
R (ohm)	2.19596	1.63586	1.2966	1.07496	0.80089
C	0.00461119	0.00568216	0.00719721	0.00910837	0.0151894
C_{G1} (pF)	0.021902	0.0205585	0.0208526	0.0211293	0.0216872
C_{G2} (pF)	0.0173707	0.0175514	0.0176897	0.177412	0.0178042
	w_n=5μm , s_n =5μm , t=3μm ,n=3				
Parameter	Δw= -2 μm	Δw= -2 μm	Nominal	Δw= +1 μm	Δw= +3 μm
L (nH)	1.3534	1.33167	1.27173	1.21628	1.11084
R (ohm)	2.90837	2.20627	1.74962	1.44958	1.07717
C	0.00639069	0.00793633	0.0096105	0.011522	0.0171997
C_{G1} (pF)	0.0216108	0.0221716	0.0223158	0.0224649	0.0226598
C_{G2} (pF)	0.0159755	0.0162099	0.0159639	0.0157711	0.0151202
	w_n=5μm , s_n =5μm , t=3μm ,n=4				
Parameter	Δw= -2 μm	Δw= -2 μm	Nominal	Δw= +1 μm	Δw= +3 μm
L (nH)	1.71021	1.68883	1.60663	1.52866	1.3748
R (ohm)	3.44416	2.61968	2.07751	1.71766	1.2761
C	0.00613042	0.0075769	0.0091227	0.01008168	0.0155379
C_{G1} (pF)	0.0230287	0.023632	0.0236381	0.0236328	0.0233769
C_{G2} (pF)	0.0151336	0.0152326	0.0148223	0.014466	0.0133794

$w_n=10\mu m$, $s_n=5\mu m$, $t=1\mu m$,n=1					
Parameter	$\Delta w= -2$ μm	$\Delta w= -2$ μm	Nominal	$\Delta w= +1$ μm	$\Delta w= +3$ μm
L (nH)	0.396082	0.380579	0.366273	0.354804	0.332305
R (ohm)	1.6425	1.45616	1.2547	1.18703	0.998068
C	3.66598E-10	1.684E-10	7.6672E-10	5.87311E-10	4.9779E-13
C_{G1} (pF)	0.0236538	0.0241612	0.0247843	0.025106	0.0259255
C_{G2} (pF)	0.0239835	0.0238471	0.0234983	0.0242822	0.0247678
$w_n=10\mu m$, $s_n=5\mu m$, $t=1\mu m$,n=2					
Parameter	$\Delta w= -2$ μm	$\Delta w= -2$ μm	Nominal	$\Delta w= +1$ μm	$\Delta w= +3$ μm
L (nH)	0.966795	0.930206	0.898863	0.8696	0.81609
R (ohm)	2.94897	2.60099	2.32693	2.1114	1.77212
C	0.00628	0.0077224	0.0091999	0.0110444	0.0160534
C_{G1} (pF)	0.0290502	0.0292237	0.0294604	0.0296814	0.0301934
C_{G2} (pF)	0.0249842	0.0247278	0.024673	0.0246742	0.0245686
$w_n=10\mu m$, $s_n=5\mu m$, $t=1\mu m$,n=3					
Parameter	$\Delta w= -2$ μm	$\Delta w= -2$ μm	Nominal	$\Delta w= +1$ μm	$\Delta w= +3$ μm
L (nH)	1.42472	1.37209	1.3237	1.27665	1.23867
R (ohm)	3.88284	3.42776	3.06718	2.78541	2.39401
C	0.00783435	0.0091671	0.0105692	0.0121639	0.0174335
C_{G1} (pF)	0.321117	0.032214	0.0323161	0.03240089	0.0332359
C_{G2} (pF)	0.0234816	0.0231969	0.0229659	0.0227022	0.0226686
$w_n=10\mu m$, $s_n=5\mu m$, $t=1\mu m$,n=4					
Parameter	$\Delta w= -2$ μm	$\Delta w= -2$ μm	Nominal	$\Delta w= +1$ μm	$\Delta w= +3$ μm
L (nH)	1.67311	1.60364	1.53692	1.47049	1.339555
R (ohm)	4.45871	3.94446	3.51048	3.18177	2.65377
C	0.00706535	0.0084731	0.00955108	0.0110341	0.0148039
C_{G1} (pF)	0.033985	0.0338379	0.0338306	0.033711	0.0148039
C_{G2} (pF)	0.0224281	0.0225526	0.0218292	0.0215133	0.0205867

w_n=10μm , s_n =5μm , t=2μm ,n=1				
Parameter	Δw= -2 μm	Δw= -2 μm	Nominal	Δw= +1 μm	Δw= +3 μm
L (nH)	0.383246	0.368821	0.355839	0.344619	0.323355
R (ohm)	0.828364	0.734931	0.633662	0.601766	0.507058
C	7.247E-11	2.057E-11	5.622E-11	5.22943E-12	5.8099E-13
C_{G1} (pF)	0.24208	0.0246921	0.02532	0.0255912	0.0263847
C_{G2} (pF)	0.0238808	0.2024224	0.238133	0.0246355	0.0251101
w_n=10μm , s_n =5μm , t=2μm ,n=2				
Parameter	Δw= -2 μm	Δw= -2 μm	Nominal	Δw= +1 μm	Δw= +3 μm
L (nH)	0.940676	0.905424	0.874906	0.84632	0.793255
R (ohm)	1.48336	1.31021	1.173552	1.06878	0.898503
C	0.0068104	0.0085179	0.0103	0.0125527	0.0188704
C_{G1} (pF)	0.0294361	0.0295942	0.029813	0.0300111	0.0304956
C_{G2} (pF)	0.025513	0.0248529	0.024774	0.0247388	0.0245537
w_n=10μm , s_n =5μm , t=2μm ,n=3				
Parameter	Δw= -2 μm	Δw= -2 μm	Nominal	Δw= +1 μm	Δw= +3 μm
L (nH)	1.38657	1.33501	1.28656	1.23998	1.19912
R (ohm)	1.95283	1.72604	1.54625	1.40953	1.21376
C	0.00866422	0.0102114	0.0118615	0.0137775	0.0201869
C_{G1} (pF)	0.0323507	0.0324612	0.325724	0.326726	0.0334927
C_{G2} (pF)	0.0234232	0.0231414	0.229095	0.0226365	0.0224974
w_n=10μm , s_n =5μm , t=2μm ,n=4				
Parameter	Δw= -2 μm	Δw= -2 μm	Nominal	Δw= +1 μm	Δw= +3 μm
L (nH)	1.62476	1.555	1.48786	1.419885	1.28109
R (ohm)	2.2417	1.98529	1.76863	1.60865	1.34368
C	0.007906	0.0095790	0.010824	0.0125945	0.0171571
C_{G1} (pF)	0.0341707	0.0340426	0.034054	0.0339473	0.0334379
C_{G2} (pF)	0.223283	0.0224773	0.021769	0.0214521	0.020498

wₙ=10μm , sₙ =5μm , t=3μm ,n=1				
Parameter	Δw= -2 μm	Δw= -2 μm	Nominal	Δw= +1 μm	Δw= +3 μm
L (nH)	0.372235	0.35884	0.3470027	0.336048	0.315936
R (ohm)	0.55574	0.493217	0.475501	0.404884	0.341767
C	7.927E-10	4.79E-15	0.000000025	8.970E-12	1.7040E-11
C_{G1} (pF)	0.024643	0.025124	0.0257602	0.026005	0.26796
C_{G2} (pF)	0.024181	0.024526	0.0240687	0.0249432	0.0254393

wₙ=10μm , sₙ =5μm , t=3μm ,n=2				
Parameter	Δw= -2 μm	Δw= -2 μm	Nominal	Δw= +1 μm	Δw= +3 μm
L (nH)	0.917984	0.884124	0.85459	0.82692	0.774502
R (ohm)	0.993497	0.878311	0.787269	0.718488	0.604926
C	0.007542	0.009553	0.0116829	0.0143612	0.0221406
C_{G1} (pF)	0.029716	0.029865	0.0300742	0.0302634	0.0307039
C_{G2} (pF)	0.025235	0.024942	0.0248469	0.0247928	0.0245289

wₙ=10μm , sₙ =5μm , t=3μm ,n=3				
Parameter	Δw= -2 μm	Δw= -2 μm	Nominal	Δw= +1 μm	Δw= +3 μm
L (nH)	1.35398	1.3037	1.25602	1.20971	1.167
R (ohm)	1.307998	1.15705	1.03755	0.94794	0.818272
C	0.009774	0.011616	0.0136049	0.0159365	0.0237416
C_{G1} (pF)	0.032470	0.032575	0.0326788	0.0327632	0.0334812
C_{G2} (pF)	0.023314	0.023016	0.0227633	0.022455	0.0221317

wₙ=10μm , sₙ =5μm , t=3μm ,n=4				
Parameter	Δw= -2 μm	Δw= -2 μm	Nominal	Δw= +1 μm	Δw= +3 μm
L (nH)	1.58416	1.51478	1.44798	1.37931	1.23482
R (ohm)	1.50155	1.33121	1.18733	1.08269	0.907984
C	0.009075	0.011158	0.0125994	0.0147395	0.0203539
C_{G1} (pF)	0.032222	0.034073	0.0340821	0.033946	0.033357
C_{G2} (pF)	0.022146	0.022226	0.0215482	0.0211851	0.0200853

wn=10μm , sn =10μm , t=2μm ,n=2					
Parameter	Δw= -2 μm	Δw= -2 μm	Nominal	Δw= +1 μm	Δw= +3 μm
L (nH)	0.838755	0.808809	0.780745	0.754205	0.705189
R (ohm)	1.41847	1.25622	1.12672	1.02656	0.860101
C	0.003338	0.004245	0.00501657	0.0062673	0.0085644
C_{G1} (pF)	0.029951	0.030217	0.0304574	0.306854	0.0311385
C_{G2} (pF)	0.024844	0.024908	0.0249434	0.0249604	0.02497

wn=10μm , sn =10μm , t=2μm ,n=3					
Parameter	Δw= -2 μm	Δw= -2 μm	Nominal	Δw= +1 μm	Δw= +3 μm
L (nH)	1.10432	1.05922	1.01646	0.984685	0.9
R (ohm)	1.7701	1.56493	1.40089	1.27447	1.0629
C	0.003806	0.004642	0.0054936	0.00646556	0.00821528
C_{G1} (pF)	0.032931	0.033138	0.0333343	0.0335142	0.0339359
C_{G2} (pF)	0.024044	0.024041	0.0240388	0.0240266	0.0240956

wn=10μm , sn =5μm , t=3μm ,n=3, 120x110					
Parameter	Δw= -2 μm	Δw= -2 μm	Nominal	Δw= +1 μm	Δw= +3 μm
L (nH)	0.826298	0.788452	0.753967	0.714244	0.641003
R (ohm)	0.96436	0.851463	0.763793	0.695939	0.586013
C	0.0059419	0.0060785	0.00593208	0.00646045	0.00531978
CG1 (pF)	0.017527	0.0174854	0.0176356	0.0177085	0.0183052
CG2 (pF)	0.0239545	0.0243173	0.0247664	0.0251933	0.0266189

wn=7μm, sn =5μm , t=3μm ,n=3, 120x110					
Parameter	Δw= -2 μm	Δw= -2 μm	Nominal	Δw= +1 μm	Δw= +3 μm
L (nH)	1.25228	1.07876	1.03192	0.986438	0.898615
R (ohm)	2.20818	1.41678	1.21048	1.05767	0.850399
C	0.00736	0.0078287	0.0085392	0.00938826	0.0120043
CG1 (pF)	0.016184	0.0158175	0.0162085	0.0155921	0.0152357
CG2 (pF)	0.0223499	0.023116	0.0238996	0.0237938	0.024452

wn=9μm, sn =5μm , t=3μm ,n=3, 120x110					
Parameter	Δw= -2 μm	Δw= -2 μm	Nominal	Δw= +1 μm	Δw= +3 μm

r					
L (nH)	0.920229	0.880168	0.841395	0.802075	0.721771
R (ohm)	1.13901	0.992746	0.87028	0.78729	0.659247
C	0.0069565	0.0073627	0.00748875	0.00791053	0.009036
CG1 (pF)	0.017827	0.0177692	0.0173412	0.0176708	0.0178061
CG2 (pF)	0.0238886	0.0241564	0.0241926	0.0249029	0.0259416
wn=10μm, sn =6μm , t=3μm ,n=2,					
Parameter	Δw= -2 μm	Δw= -2 μm	Nominal	Δw= +1 μm	Δw= +3 μm
L (nH)	1.32123	1.27394	1.2287	1.18415	1.0975
R (ohm)	1.97434	1.74751	1.56458	1.42627	1.20141
C	0.0085032	0.0093619	0.0103003	0.0112353	0.013919
CG1 (pF)	0.0322057	0.0325035	0.0327934	0.0331506	0.0338992
CG2 (pF)	0.0235813	0.023387	0.0231862	0.0232347	0.0229922
wn=10μm, sn =7μm , t=3μm ,n=2,					
Parameter	Δw= -2 μm	Δw= -2 μm	Nominal	Δw= +1 μm	Δw= +3 μm
L (nH)	1.26113	1.21442	1.17137	1.12581	1.04351
R (ohm)	1.93435	1.71246	1.53305	1.39316	1.16792
C	0.0075538	0.0081784	0.00887657	0.00982929	0.0117499
CG1 (pF)	0.0322129	0.0325972	0.0329897	1.12581	0.03397
CG2 (pF)	0.0235828	0.0235137	0.234182	0.0232624	0.0230409
wn=10μm, sn =8μm, t=3μm, n=2,					
Parameter	Δw= -2 μm	Δw= -2 μm	Nominal	Δw= +1 μm	Δw= +3 μm
L (nH)	1.20142	1.15682	1.11361	1.07078	0.990883
R (ohm)	1.89513	1.6772	1.49977	1.36463	1.14349
C	0.0068703	0.0073919	0.00801444	0.00877084	0.010004
CG1 (pF)	0.0322711	0.0073919	0.330186	0.0333963	0.0341967
CG2 (pF)	0.0234822	0.0326921	0.0233266	0.023273	0.02328